Aus der Klinik für Neurologie
der Heinrich-Heine-Universität Düsseldorf
Direktor: Univ.-Prof. Dr. Dr. Sven G. Meuth

The Effects of Diroximel Fumarate on Ferroptotic Glial Cell Death and Demyelination

Dissertation

zur Erlangung des Grades eines Doktors der Medizin
der Medizinischen Fakultät der Heinrich-Heine-Universität Düsseldorf

vorgelegt von

Dipl.-Math. Katinka Fischer

2025

Als Inauguraldissertation gedruckt mit der Genehmigung der
Medizinischen Fakultät der Heinrich-Heine-Universität Düsseldorf

gez.:
Dekan: Univ.-Prof. Dr. Nikolaj Klöcker
Erstgutachter: Univ.-Prof. Dr. med. Orhan Aktas
Zweitgutacher: Univ.-Prof. Dr. rer. nat. Björn Stork

Abstract

Background: Ferroptosis is an iron-dependent, non-apoptotic cell death mechanism characterized by lipid peroxidation and has been implicated in the pathogenesis of multiple sclerosis (MS). A critical enzyme in preventing ferroptosis, glutathione peroxidase 4 (GPx4), is found at reduced levels in the brain tissue of MS patients. Fumarates such as diroximel fumarate (DRF) and dimethyl fumarate (DMF), which are approved for the treatment of relapsing-remitting MS (RRMS), exert their effects through activation of the nuclear factor erythroid 2-related factor 2 (Nrf2) pathway. This pathway mitigates oxidative stress by regulating the expression of antioxidant and anti-inflammatory proteins. However, the role of Nrf2 activation in protecting against neuroinflammation and axonal demyelination, particularly in the context of ferroptosis, remains inadequately understood.

Aim: The aim of this study is to evaluate the effect of fumarates on oligodendrocytes and myelin structure in relation to ferroptosis-induced damage.

Methods: The effects of DRF and its primary metabolite monomethyl fumarate (MMF) on GPx4 gene and protein expression, cell survival, lipid peroxidation, and myelin integrity were investigated in OLN-93 oligodendrocytes and organotypic cerebellar slice cultures subjected to ferroptosis induction by Erastin or iron (ammonium iron(II) sulphate, $(NH_4)_2Fe(SO_4)_2$). Additionally, GPx4 gene expression was assessed in mouse brain tissue (wild-type C57BL/6J) and peripheral blood mononuclear cells (PBMCs) from five patients with RRMS before and after one year of DMF therapy. These results were compared with those from five patients treated with ocrelizumab (OCR) over the same period and four healthy controls.

Results: OLN-93 cells exhibited sensitivity to the ferroptosis inducers Erastin and iron. Pretreatment with the fumarates MMF and DRF conferred protection against Erastin-induced cell death, but not against iron-induced cell death. The ferroptosis inhibitor liproxstatin-1 (LIP-1) effectively reduced lipid peroxidation, while a 24-hour pretreatment with fumarates did not offer the same protection. In organotypic cerebellar slice cultures, Erastin predominantly caused myelin damage, whereas iron induced both myelin and axonal damage. DRF and MMF mitigated myelin damage, similar to the effects observed with LIP-1 and the iron chelator salicylaldehyde isonicotinoyl hydrazone (SIH). In mouse brains, DMF treatment elevated GPx4 mRNA and protein levels in the white matter but not in the gray matter. In RRMS patients with an average Expanded Disability Status Scale (EDSS) score of 2 (IQR: [1,2]), GPx4 mRNA levels in PBMCs were unchanged compared to healthy controls. One year of DMF treatment resulted in a moderate increase in GPx4 gene expression in only two of the five patients (median 1.01, IQR: [0.80, 2.52]). In contrast, OCR treatment led to an average increase in GPx4 mRNA levels of 570% (IQR: [537%, 713%]) at 12 months.

Discussion and conclusion: The results suggest a detrimental role of ferroptosis in glial cells, as evidenced by the indirect induction of ferroptosis in OLN-93 cells following Erastin exposure and point the potential of fumarates to protect oligodendrocytes from ferroptotic cell death. The observed increase in expression of the anti-ferroptotic enzyme GPx4 in both OLN-93 cells and mouse brain parenchyma after fumarate treatment points to a possible underlying mechanism. However, the exact mechanism remains unclear, as a reduction in lipid peroxidation could not be demonstrated. More frequent fumarate administration (e.g., twice daily) may be necessary to reduce lipid peroxidation. The moderate elevation of GPx4 levels in PBMCs from young RRMS patients does not provide definitive conclusions regarding oligodendrocytes but may suggest that fumarates increase GPx4 levels in CNS-infiltrating monocytes and macrophages, potentially protecting resident CNS cells from excess iron. Additionally, the marked increase in GPx4 levels in ocrelizumab-treated patients may suggest a role for ocrelizumab in inhibiting ferroptosis, a potential, yet unexplored, additional aspect of its mechanism of action.

Zusammenfassung

Hintergrund: Ferroptose, ein eisenabhängiger nicht-apoptotischer Mechanismus, der über Lipidperoxidation Zelltod induziert, wird mit dem Pathomechanismus der Multiplen Sklerose (MS) in Verbindung gebracht. Glutathionperoxidase 4 (GPx4) ist ein Schlüsselenzym in der Inhibierung der Ferroptose und wird niedriger exprimiert im Hirngewebe von MS-Patienten. Die zur Behandlung der schubförmig remittierenden MS (RRMS) zugelassenen Fumarate Diroximelfumarat (DRF) und Dimethylfumarat (DMF) wirken auf den *Nuclear factor erythroid 2–related factor 2 (Nrf2*) -Signalweg, der vor oxidativen Schäden schützt, indem er die Expression von antioxidativen und entzündungshemmenden Proteinen reguliert. Die Relevanz der Nrf2-Aktivierung beim Schutz vor Neuroinflammation und axonaler Demyelinisierung im Kontext von Ferroptose ist jedoch noch unklar.

Ziel: Ziel dieser Studie ist es die Wirkung von Fumaraten auf Oligodendrozyten und die Myelinstruktur im Hinblick auf Ferroptose-induzierte Schäden zu bewerten.

Methoden: Die Auswirkungen von DRF und Monomethylfumarat (MMF, als Hauptmetabolit von DMF und DRF) auf GPx4-Gen- und Proteinexpression, Zellübereben, Lipidperoxidationsschutz und Myelinschädigung wurden in OLN-93-Oligodendrozyten und organotypischen Kleinhirnschnittkulturen unter den Ferroptose-Induktoren Erastin oder Eisen (Ammoniumeisen(II)-sulfat, $(NH_4)_2Fe(SO_4)_2$). untersucht. Des Weiteren wurde die GPx4-Genexpression in Maushirngewebe (Wildtyp C57BL/6J) sowie in peripheren mononukleären Blutzellen (PBMCs) von fünf RRMS-Patienten vor und nach einer einjährigen Behandlung mit Dimethylfumarat analysiert. Diese Ergebnisse wurden mit denen von fünf RRMS-Patienten, die über den gleichen Zeitraum eine Behandlung mit Ocrelizumab (OCR) erhielten, sowie mit den Ergebnissen von vier gesunden Probanden verglichen.

Ergebnisse: OLN-93-Zellen sind sensitiv gegenüber den Ferroptose-Induktoren Erastin und Eisen, können durch Vorbehandlung mit den Fumaraten MMF und DRF jedoch gegen Erastin-Exposition geschützt werden. Gegen Zelltod durch Eisenbehandlung schützen Fumarate jedoch nicht. Der Ferroptoseinhibitor Liproxstatin-1 (LIP-1) verminderte Lipidperoxidation, eine 24-stündige Fumarat-Vorbehandlung dagegen nicht. In den Hirnschnittkulturen schädigte Erastin hauptsächlich Myelin, während Eisen zusätzlich Axone schädigte. DRF und MMF milderten Myelinschäden ab, wie LIP-1 und der Eisenchelator Salicylaldehyd-Isonicotinoyl-Hydrazone (SIH). DMF steigerte sowohl GPx4-mRNA-, als auch -Protein-Menge in der weißen, jedoch nicht in der grauen Substanz von Mausgehirnen. Bei RRMS-Patienten mit einem durchschnittlichen EDSS (Expanded Disability Status Scale) von 2 (IQR: [1,2]) waren die GPx4-mRNA-Spiegel in PBMCs im Vergleich zu gesunden Probanden nicht verändert. Eine einjährige DMF-Behandlung führte lediglich bei zwei Patienten zu einer moderaten Erhöhung der GPx4-Genexpression (Median 1,01, IQR: [0,80, 2,52]). Im Vergleich dazu führte die OCR-Behandlung nach 12 Monaten zu einem durchschnittlichen Anstieg der GPx4-mRNA-Spiegel um 570% (IQR: [537%, 713%]).

Diskussion und Schlussfolgerung: Die Ergebnisse deuten auf eine schädliche Rolle der Ferroptose in Gliazellen hin, wie die indirekte Induktion von Ferroptose in OLN-93-Zellen nach Erastin-Exposition zeigt und weisen auf das Potenzial von Fumaraten hin, Oligodendrozyten vor ferroptotischem Zelltod zu schützen. Die beobachtete Zunahme der Expression des anti-ferroptotischen Enzyms GPx4 sowohl in OLN-93-Zellen als auch im Gehirnparenchym von Mäusen nach Fumarat-Behandlung deutet auf den möglichen zugrunde liegenden Mechanismus hin. Der genaue Mechanismus bleibt jedoch unklar, da eine Verringerung der Lipidperoxidation nicht nachgewiesen werden konnte. Eine häufigere Verabreichung von Fumarat (z. B. zweimal täglich) könnte möglicherweise erforderlich sein, um die Lipidperoxidation zu verringern. Der moderate Anstieg der GPx4-Konzentrationen in PBMCs von jungen RRMS-Patienten lässt keine endgültigen Schlussfolgerungen in Bezug auf Oligodendrozyten zu, könnte aber auf einen Schutz vor überschüssigem Eisen durch Fumarate in ZNS-infiltrierenden Monozyten und Makrophagen hindeuten. Der deutliche GPx4-Anstieg bei Ocrelizumab-Behandlung lässt eine mögliche Hemmung der Ferroptose vermuten, was einen potenziellen, noch unerforschten Aspekt seines Wirkmechanismus darstellen könnte.

List of Abbreviations

AAR	Annualized Attack Rate
ACSL4	Acyl-CoA Synthetase Long-chain family member 4
ACTB	B-actin
ARE	Antioxidant Response Element
ATP	Adenosine Triphosphate
BBB	Blood-brain barrier
BCA	Bicinchoninic Acid Assay
BSA	Bovine Serum Albumin
BW	Body Weight
Ca	Calcium
cDNA	Complementary Desoxyribonucleic Acid
CNS	Central Nervous System
CNTF	Ciliary Neurotrophic Factor
CO_2	Carbon Dioxide
CSF	Cerebrospinal Fluid
CTB	CellTiter-Blue
CVS	Central vein sign
DHODH	Dihydroorotate Dehydrogenase
DIS	Dissemination In Space
DIT	Dissemination In Time
DIV	Days In Vitro
DMEM	Dulbecco´s Modified Eagle´s Medium
DMF	Dimethyl Fumarate
DMT	Disease-modifying therapy
DMSO	Dimethyl Sulfoxide
DNA	Desoxyribonucleic Acid
DRF	Diroximel Fumarate
DTT	Dithiothreitol
EAE	Experimental Autoimmune Encephalomyelitis
EBV	Epstein-Barr Virus
EDSS	Expanded Disability Status Scale
EDTA	Ethylene Diamine Tetraacetic Acid
ESCM	Experimental Horse Serum-Free Slice Culture Medium
FACS	Fluorescence Activated Cell Sorting
FBS	Fetal Bovine Serum
Fe	Iron
FITC	Fluorescein Isothiocyanate
FPN1	Ferroportin
FSP1	Ferroptosis Suppressor Protein 1
FTL	Ligh Chain of Ferritin
FTH1	Heavy Chain of Ferritin
G	Gram
Gapdh	Glycerinaldehyd 3 Phospate Dehydrogenase
GCH-1	GTP-Cyclohydrolase 1
GCL	Glutamate Cysteine Ligase
GFAP	Glial Fibrillary Acidic Protein
GI	Gastrointestinal

GM-CSF	Granulocyte-Macrophage Colony-Stimulating Factor
GPx	Glutathione Peroxidase
GPx4	Glutathione Peroxidase 4
GRFS1	Guanine-Rich Sequence Binding Factor 1
GSH	Glutathione
GSR	Glutathione Reductase
GSSG	Glutathione Disulfide
HCAR2	Hydroxycarboxylic acid receptor 2
HEK cell	Human embryonic Kidney cell
HES	Hydroxyethyl succinimide
4-HNE	4-Hydroxynonenal
Hmox 1	Heme Oxygenase 1
IC_{50}	Half maximal inhibitory concentration
ICAM-1	Intracellular Adhesion Molecule 1
Ig G	Immunoglobulin G
IL	Interleukin
INF	Interferon
IQR	Interquartile Range
Keap1	Kelch-like ECH-associated protein 1
kDa	Kilodalton
κFLC	Kappa free light chains
kg	Kilogram
LIP-1	Liproxstatin-1
LOOH	Lipid Hydroperoxides
LPS	Lipopolysaccharide
M	Molar
MACS	Magnetic-activated cell sorting
MAG	Myelin-associated Glycoprotein
MBP	Myelin Basic Protein
MDA	Malondialdehyde
MEM	Eagle´s Minimum Essential Medium
MEP	Motor Evoked Potential
MFIS	Modified Fatigue Impact Scale
Mg	Magnesium
mg	Milligram
mg/kg	Miligram per kilogram
mg/ml	Milligram per mililiter
µg	Microgram
µg/ml	Microgram per mililiter
ml	Mililiter
µl	Microliter
mM	Milimolar
µm	micrometer
µM	micromolar
MMF	Monomethyl Fumarate
MOG	Myelin Oligodendrocyte Glycoprotein
MRI	Magnetic Resonance Imaging
mRNA	Messenger Ribonucleic Acid
MS	Multiple Sclerosis
MSFC	Multiple Sclerosis Functional Composite

NaOH	Sodium hydroxide
NAWM	Normal-Appearing White Matter
nm	Nanometer
nM	Nanomolar
NF	Neurofilament
NF-κB	Nuclear factor 'kappa-light-chain-enhancer' of activated B-cells
Nrf2	Nuclear factor erythroid 2-related factor 2
OCR	Ocrelizumab
OCT	Optical Coherence Tomography
OPC	Oligodendrocyte Progenitor Cell
OSC	Organotypic Slice Culture
PBMCs	Peripheral blood mononuclear cells
PBS	Phosphate Buffered Saline
PCR	Polymerase Chain Reaction
PFA	Paraformaldehyde
pH	Potentia hydrogenii
PI	Propidium Iodide
PLP	Proteolipid Protein
PPMS	Primary Progressive Multiple Sclerosis
PRL	Paramagnetic Rim Lesion
pTreg	Peripheral regulatory T cells
RE	Relative Expression
RFU	Relative Fluorescence Unit
P9	Postnatal day
PUFA	Polyunsaturated Fatty Acid
qPCR	Real-time quantitative Polymerase Chain Reaction
RAS	Rat Sarcoma (protooncoprotein)
RFU	Relative Fluorescence Unit
RIPA	Radioimmunoprecipitation Assay
RNA	Ribonucleic Acid
RNS	Reactive Nitrogen Species
ROS	Reactive Oxygen Species
rpm	Revolutions per minute
rRNA	Ribosomal ribonucleic acid
RMS	Relapsing Multiple Sclerosis
RRMS	Relapsing-Remitting Multiple Sclerosis
RSL3	RAS-selective lethal 3
RT	Room Temperature
SD	Standard Deviation
SDMT	Symbol Digit Modalities Test
SDS-PAGE	Sodium Dodecyl Sulfate - Polyacrylamide Gel Electrophoresis
SIH	Salicylic acid Isonicotinoyl Hydrazone
SP1	Specificity Protein 1 (transcription factor)
S1p	Sphingosine-1-Phosphate
SPMS	Secondary Progressive Multiple Sclerosis
18S rRNA	18S ribosomal Ribonucleic Acid
SSEP	Somatosensory Evoked Potential
ST	Small T (oncoprotein)

TCR	T Cell Receptor
Tf	Transferrin
TFAP2C	Transcription Factor AP-2 gamma
TfR(c)1	Transferrin Receptor 1
Tf-TfR	Transferrin-Transferrin-Receptor complex
TGF β	Transforming Growth Factor β
Th1 cell	T Helper 1 cell
Th2 cell	T Helper 2 cell
Th17 cell	T Helper 17 cell
TRAIL	TNF-related apoptosis-inducing ligand
Treg	Regulatory T cell
TNF	Tumor Necrosis Factor
Tubb3	β-III tubulin
TXNRD1	Thioredoxin Reductase 1
VEP	Visual Evoked Potential
v/v	Volume by volume
xCT	Cystine-Glutamate Antiporter
yrs	Years

Content

1 Introduction

1.1 Multiple Sclerosis

Multiple sclerosis (MS) is the most common chronic inflammatory disease of the central nervous system (CNS) in western countries (Lassmann, 2020). The main features of this autoimmune disease are inflammatory demyelination and axonal degeneration, resulting in a variety of neurological symptoms of varying severity. Although there have been significant research efforts, the etiology and pathogenesis of MS are still not fully understood and it remains an incurable disease. However, an increasing number of approved immunomodulatory and symptomatic treatments can influence the course of the disease and relieve symptoms, such as neuropathic pain and spasticity, making life easier for patients.

1.1.1 Epidemiology

According to the Atlas of MS published by the MS International Federation, there is a prevalence of approximately 2.9 million patients worldwide (Atlas of MS, 2023). Over the past decade, the number of diagnosed MS cases globally has increased by about 30%, with an incidence of 2.1 per 100,000 people per year (Walton et al., 2020).

Worldwide, the prevalence of MS is three times higher in women than in men (Jakimovski et al., 2024). With a disease onset between the ages of 20 and 40 years, MS is typically diagnosed at an average age of 32 years (Atlas of MS, 2023). In addition, there are at least 30,000 people under the age of 18 living with MS worldwide, based on data from 55 reporting countries (Atlas of MS, 2023). Higher prevalence rates are observed in Europe, North America, Australia, and Iran, while lower rates are seen in regions along the Silk Road, Africa (note: low reported rates here), and South America (Atlas of MS, 2023). In general, MS is less common in non-Caucasian than in Caucasians (Marrie, 2011). Migration studies have shown that even after moving to distant areas with different disease rates, individuals over 15 years of age retain the specific disease risk of their origin (Gale & Martyn, 1995). The reasons for the geographical distribution and the general increase in risk of developing MS are not fully understood but may involve a combination of genetic, environmental, infectious and lifestyle factors. Among the established risk factors for MS are certain genetic variants within the HLA-DRB1 gene, low blood levels of vitamin D, cigarette smoking, and a history of infection with the Epstein-Barr virus (EBV) (Cortese et al., 2020; Moutsianas et al., 2015).

In Germany, approximately 280,000 individuals are affected by MS, with a prevalence of 337 per 100,000 citizens annually. On average, 14,600 people get diagnosed every year, averaging 33 years old. In Germany, 72% of MS patients are female (Atlas of MS, 2023).

1.1.2 Pathogenesis

MS is a chronic inflammatory disease characterized by focal demyelinating lesions in the brain and spinal cord (Lassmann, 2022). In the early stages of the disease, most patients experience reversible clinical deficits due to inflammatory attacks involving a cascade of inflammation, demyelination, and remyelination in the CNS (Lassmann, 2022). The current understanding of MS pathogenesis primarily involves autoimmune mechanisms, including the activation of autoreactive T and B lymphocytes, as well as myeloid immune cells, in the peripheral immune system (Duffy et al., 2014).

This complex interplay of immune cells contributes to the initiation and perpetuation of inflammatory processes within the CNS, leading to myelin damage, axonal injury and neurodegeneration (Duffy et al., 2014).

Inflammation is initiated by the infiltration of activated autoreactive T cells from the periphery, crossing the blood-brain barrier (BBB) into the CNS. Hereby, BBB permeability is increased by cytokines released by pathogenic Th17 cells (Duarte-Silva et al., 2023). However, the reason for the activation of autoreactive T cells remains unknown (Faiss, 2020). Recent studies suggest that B cells play an additional crucial role in the pathogenesis of MS. Natural mechanisms of B cells are antibody production, antigen presentation, and the production of immunoregulatory cytokines. In MS patients, intrathecal synthesis of immunoglobulins is a well-known phenomenon (Bittner et al., 2017). However, there is currently no specific autoantibody and autoimmune reaction that has been identified as the cause of MS (Lassmann, 2022). Recent studies have identified a subtype of memory B cells that produce granulocyte macrophage colony-stimulating factor (GM-CSF), which are more prevalent and active in the blood of MS patients compared to healthy controls. These GM-CSF-producing B cells can induce a proinflammatory phenotype in myeloid cells and subsequently in T cells (Bittner et al., 2017). Proinflammatory myeloid cells sustain neuroinflammation by enhancing their phagocytic activity, generating reactive oxygen species (ROS), and secreting proinflammatory cytokines (Duarte-Silva et al., 2023). Emerging evidence suggests a synergistic relationship between the major risk factors HLA-DR15 and Epstein-Barr virus (EBV). This interplay appears to facilitate the interaction between B and T lymphocytes through antigen presentation mechanisms, specifically with CD4+ T cells recognizing EBV-infected or EBV antigen-presenting B cells (Marti et al., 2024). Overall, B cells modulate T-cell function and drive demyelinating processes within MS lesions. Furthermore, recent studies have identified the presence of meningeal lymphoid follicles containing B-cells, T-cells and antigen-presenting cells. These cells may contribute to cortical neuronal damage through ongoing inflammatory processes (Bittner et al., 2017). In addition, two-way interactions between periphery and central immune system. In addition, Blauth et al. (2015) examined the bidirectional trafficking of B lymphocytes between the CNS and the peripheral immune compartment.

MS lesions are usually located in areas with a high concentration of medium to large drainage veins, which may explain why they tend to occur in specific locations, such as the optic nerve, spinal cord (especially the cervical spinal cord), and periventricular, juxtacortical, and infratentorial white matter (Faiss, 2020). This MRI-detectable central vein inside MS lesions (central vein sign, CVS) appears to be specific for MS (La Rosa et al., 2022).

MS lesions exhibit heterogeneity in their demyelination patterns including macrophage-associated demyelination, demyelination with oligodendropathy including apoptosis of oligodendrocytes and reduced tendency for remyelination, as well as primary oligodendrocyte degeneration in the periphery of the lesion. The latter is often the cause of secondary demyelination and is particularly common in progredient forms of MS (Faiss, 2020).

Recent studies have highlighted the role of iron metabolism dysregulation in the CNS and subsequent ferroptosis in MS progression. During demyelination, iron released from oligodendrocytes accumulates extracellularly, leading to uptake by microglia and infiltrating macrophages (Duarte-Silva et al., 2023). Notably, iron plaques form in the periphery of chronically active lesions (iron rim lesions or paramagnetic rim lesions, PRL), a feature specific to MS (Clarke et al., 2024).

Axonal and neuronal degeneration, associated with permanent clinical deficits, occur in active lesions during early disease stages and in the periphery of active chronic lesions during progressive stages (Faiss, 2020).

The resolution of inflammation involves complex mechanisms, including the activation of regulatory T cells (Tregs) and the production of anti-inflammatory cytokines such as IL-10 and TGF-beta. In MS, while Treg cell numbers may not be significantly altered, their suppressive function is often impaired. Current understanding suggests that autoimmune disorders, including MS, involve a dysregulation in the balance between pro-inflammatory cells (such as Th17) and regulatory cells (such as Tregs), along with other factors affecting immune homeostasis (Duarte-Silva et al., 2023).

Remyelination failure is a key pathological process in MS. Oligodendrocyte precursor cells (OPCs) and their differentiation into mature myelinating oligodendrocytes are essential for remyelination. In MS lesions, OPCs persist with reduced numbers and uneven distribution, while mature oligodendrocytes are largely lost. Impaired oligodendrocyte differentiation contributes to remyelination failure, particularly in progressive MS resulting in neurodegeneration (Kuhlmann et al., 2023). Early stages of MS exhibit incomplete remyelination, resulting in thinner myelin sheaths and reduced nerve conduction velocity (Faiss, 2020).

However, the precise mechanisms of neuroinflammatory demyelination and their contribution to neurodegeneration remain unclear. This is an area of ongoing research.

1.1.3 Forms and Symptoms

MS typically presents in three clinical courses: relapsing-remitting (RRMS), primary progressive (PPMS), and secondary progressive (SPMS). RMS encompasses both RRMS and active SPMS with relapses.

The most prevalent form of MS is the RRMS, which is diagnosed in 85% of cases (Atlas of MS, 2023) and typically begins before the age of 30 (Hufschmidt, 2020). This form is characterized by well-defined relapses with either new or worsening neurological symptoms that resolve completely or incompletely. A relapse is defined as an episode of subjective or objective symptoms lasting at least 24 hours, with a latency period of at least 30 days from the last relapse. Between relapses, the disease is stable (Hufschmidt, 2020).

Longitudinal cohort studies indicate that the majority of RRMS-patients progress to SPMS over time, typically in the 5th decade of life (Hufschmidt, 2020). A transition to SPMS is usually characterized by a gradual increase in clinician-assessed neurological dysfunction, that persists for a specified period, typically twelve months, and is not related to relapse activity. However, a precise definition is still lacking (Ziemssen et al., 2023). Additionally, SPMS can have active episodes (relapses with or without full remission or MRI activity), and stable episodes (Lublin, 2014).

10-15% of MS patients have PPMS, which is characterized by a progressive course from the beginning without early relapses or remissions (Atlas of MS, 2023). Typically, the onset of the disease is around the age of 40 (Hufschmidt, 2020).

Neurological symptoms can be varied and typically correspond to the affected areas of damage. Early symptoms of the disease often include sensory disturbances (30-40%) such as paraesthesia and a positive Lhermitte´s sign, retrobulbar neuritis, typically associated with visual disturbances and pain on movement of the affected eye (20-30%). Other common issues in the course of the

disease include motor disorders such as spastic paresis and internuclear ophthalmoplegia, cerebellar disorders such as ataxia and intention tremor, as well as fatigue (affect up to 90% of MS-patients during the course of the disease), and sensory, bladder/gastrointestinal, and cognitive disorders. 20-50% of patients suffer from neuropathic or other forms of pain (Faiss, 2020). Clinical assessment is typically conducted using the Expanded Disability Status Scale (EDSS) to evaluate the level of disability, the Symbol Digit Modalities Test (SDMT) to assess cognitive impairment, and the Modified Fatigue Impact Scale (MFIS) to determine the impact of fatigue on the patient's life (Hufschmidt, 2020).

1.1.4 Diagnostic

Due to the lack of pathognomonic biomarkers, MS remains a disease that can only be diagnosed by exclusion of other diagnoses. This means that no alternative explanation for symptoms or paraclinical findings can be identified (Thompson et al., 2018).

Since 2001, the McDonald criteria (last updated in 2017) have been used to diagnose MS. They require typical clinical symptoms and evidence of dissemination in time (DIT) and dissemination in space (DIS) of inflammatory demyelinating lesions in the CNS (McDonald et al., 2001). The revised McDonald criteria for multiple sclerosis diagnosis, presented by Xavier Montalban at ECTRIMS 2024, are expected to be published in early 2025, introducing significant updates to improve diagnostic accuracy and early detection.

Demyelinating lesions can be detected with a high degree of sensitivity by means of MRI. MRI criteria for dissemination in space include the four typical MS regions for CNS lesions: periventricular, cortical or juxtacortical, infratentorial, and spinal cord. The upcoming Montalban criteria will likely include the optic nerve as the fifth typical MS region. If two of these regions are involved, a dissemination in space can be assumed. The distinction between old and new active demyelinating lesions, e.g. based on their different contrast agent uptake behavior due to a disrupted blood-brain barrier, serves as evidence of dissemination in time (Faiss, 2020).

Cerebrospinal fluid (CSF) analysis is a crucial diagnostic tool for MS, particularly when MRI findings are inconclusive. Key diagnostic markers in CSF include the presence of oligoclonal bands (OCBs) and the MRZ reaction, which measures the intrathecal, polyspecific humoral immune response against measles, rubella, and varicella zoster viruses. Oligoclonal bands are detected in over 95% of MS patients and represent antibodies produced intrathecally by plasma cell clones. While OCBs are highly sensitive for MS diagnosis, they are not entirely specific to the disease. The positive MRZ reaction is more specific but less sensitive than OCBs, making it a valuable complement in the diagnostic process (Faiss, 2020). The 2017 McDonald criteria for MS diagnosis allow for OCBs to replace for MRI-based evidence of dissemination in time (Thompson et al., 2018). Key CSF findings also include an increased cell count and total protein levels, although these are often within normal limits (Faiss, 2020).

The upcoming Montalban criteria for MS diagnosis are expected to incorporate the central vein sign (CVS) and paramagnetic rim lesions (PRL) as additional MRI markers for DIS. According to the proposed changes, DIS criteria may be fulfilled if either at least six CVS or one PRL is detected on MRI, in combination with MS-typical symptoms and a single lesion in a characteristic MS location.

Furthermore, the revised criteria are likely to consider elevated kappa free light chains (KFLCs) in the CSF as an alternative to OCBs for demonstrating DIT. KFLCs are essential components of antibodies and their presence in CSF can indicate intrathecal immunoglobulin synthesis. This modification would allow KFLCs to substitute for the current requirement of simultaneous detection of contrast-enhancing and non-enhancing lesions on MRI for establishing DIT (Fagnart et al., 1988; Levraut et al., 2023).

In addition to MRI and the CSF examination, there are other important paraclinical methods that can contribute to the diagnosis of MS. Measurements of visual, motor, or somatosensory evoked potentials (VEP, MEP, SSEP) are valuable in detecting subclinical or past manifestations. The measurement of retinal fiber layer thickness by optical coherence tomography (OCT) is an appropriate tool to assess the extent of neuroaxonal damage after acute optic neuritis and, thus, to detect advanced neurodegenerative changes in the anterior segment of the visual pathway (Faiss, 2020).

1.1.5 Therapy

The treatment of MS can be divided into three categories: acute relapse therapy, chronic disease-modifying therapy and symptomatic/supportive therapy.

The acute treatment of MS relapses with methylprednisolone is widely accepted as the standard of care. In cases where therapy escalation is necessary, plasmapheresis or immunoadsorption may be considered (Faiss, 2020).

Disease-modifying therapies (DMTs) aim to prevent MS relapses and slow progression. The two main treatment strategies for active MS are: The escalation approach which starts with lower-efficacy DMTs and escalate if disease activity persists. The early high-efficacy intervention which begins with high-efficacy DMTs at diagnosis, especially for patients with poor prognostic factors, i.e. young age, severe initial relapse, polysymptomatic onset, incomplete remission, high lesion load, infratentorial/spinal lesions (Wiendl et al., 2021). Recent studies suggest that early high-efficacy intervention is associated with less disability progression (He et al., 2020; Pipek et al., 2023; Spelman et al., 2021). A systematic review and meta-analysis found a 30% reduction in EDSS worsening at 5 years with early high-efficacy therapy compared to escalation (Pipek et al., 2023). A Scandinavian study showed that initiating high-efficacy DMTs within 2 years of disease onset reduced the risk of disability progression by 29% compared to escalation (Spelman et al., 2021).

Current DMTs target multiple inflammatory processes, including immune cell depletion, reduced cell proliferation, migration blockade, and pleiotropic effects. These treatments affect the peripheral immune system, the blood-brain barrier, and the CNS and can be divided into monoclonal antibodies and pharmacological agents (Bierhansl et al., 2022). In addition, DMTs are classified based on their efficacy observed in clinical trials. Low to moderate efficacy DMTs for mild to moderate RRMS, including beta-interferons, glatirameroids, teriflunomide, and fumarates, demonstrate a 20-50% relative reduction in relapse rate compared to placebo (Singer et al., 2024). Beta-interferons, and glatirameroids are immunomodulators with incompletely understood modes of action. Fumarates modulate cytokine expression and activate the Nrf2 pathway, though their precise mechanism remains still unclear. Teriflunomide exerts immunosuppression by inhibiting the proliferation of activated immune cells (Wiendl et al., 2021). Advancements in the understanding of MS pathogenesis have led to more effective and targeted therapies, including substances with higher

efficacy. These DMTs for highly active RRMS, including Cladribine, S1P receptor modulators, Natalizumab, anti-CD20 antibodies, and Alemtuzumab, demonstrate a relative reduction in annualized relapse rate exceeding 50% compared to placebo (Singer et al., 2024). Cladribine suppresses the immune system by disrupting DNA synthesis, reducing circulating lymphocytes (Warnke et al., 2012). S1P receptor modulators Fingolimod, Ozanimod, and Ponesimod bind to S1P1 receptors, inhibiting lymphocyte migration from lymphoid tissues, thus preventing their entry into the CNS (Aktas et al., 2010; Ingwersen et al., 2012; Wiendl et al., 2021). Alemtuzumab, Natalizumab, and the anti-CD20 antibodies are monoclonal antibodies selectively suppress the immune system. Alemtuzumab, a CD52 antibody, eliminates primarily T cells and, for a short time, B cells from circulation (Hartung et al., 2015). Natalizumab, an alpha4 integrin inhibitor, hinders T-cell migration across the blood-brain barrier (Wiendl et al., 2021). Anti-CD20 antibodies, including Ocrelizumab, Ofatumumab, Ublituximab, and off-label Rituximab, deplete circulating CD20+ B cells (Graf et al., 2020).

Approved treatments for active SPMS include beta-interferons, Cladribine, the S1P receptor modulator Siponimod (Wiendl et al., 2021). For PPMS, the anti-CD20 antibody Ocelizumab alone is approved (Graf et al., 2020; Wiendl et al., 2021).

Symptomatic therapy in MS aims to alleviate specific symptoms and enhance quality of life. It includes drug-based and non-medication approaches such as physiotherapy, ergotherapy, and neuropsychological interventions. (Faiss, 2020)

1.2 Ferroptosis

Recent research has linked ferroptosis to the development of various neurodegenerative diseases, such as Parkinson's disease, Alzheimer's disease, and ischemic stroke (Ou et al., 2022; Ren et al., 2020). In addition, its role in the pathogenesis and, in particular, the progression of MS is an area of growing interest (Van San et al., 2023).

Ferroptosis is a distinct form of regulated cell death that differs from apoptosis, necrosis, necroptosis, or autophagy in its morphology, biochemistry, and genetics (Dixon et al., 2012). Ferroptosis is characterized by the accumulation of lipid peroxidation products in cell membranes. These products result from the iron-catalyzed oxidation of polyunsaturated fatty acids (PUFA), which are the most susceptible fatty acids to ferroptosis. These modifications result in noticeable changes in cellular morphology, including damaged mitochondria with condensed membrane density, reduced or absent cristae, and a ruptured outer membrane (Hu et al., 2019).

Certain genes and proteins have been observed to be overexpressed and have been suggested as biomarkers for ferroptosis. Notably, in neurons, the upregulation of acyl-CoA synthetase long-chain family member 4 (ACSL4) promotes the esterification of PUFAs. This increases neuronal vulnerability to ferroptosis (Tang et al., 2021).

However, our current understanding of the mechanisms that control ferroptosis remains incomplete. Recent evidence suggests that mitochondria-mediated production of reactive nitrogen and oxygen species (RNS and ROS), including hydrogen peroxide (H_2O_2), as well as DNA stress and metabolic reprogramming, play a critical role in triggering lipid peroxidation and ferroptosis. In addition,

ferroptosis is closely related to iron accumulation and an imbalance of cellular oxidant-antioxidant mechanisms, resulting in an unstable cellular redox state (Tang et al., 2021).

In the subsequent process, the redox-active ferrous iron Fe^{2+} reacts with hydrogen peroxide in the Fenton reaction, resulting in the creation of hydroxyl radicals. These radicals then react with lipids, initiating a chain reaction that produces numerous toxic lipid peroxides, such as initial lipid hydroperoxides (LOOH) and subsequent reactive aldehydes (e.g., malondialdehyde (MDA) and 4-hydroxynonenal (4-HNE)) until the reaction is complete (Girotti, 1985; Tang et al., 2021).

Physiologically, the prevention of lipid peroxide accumulation is primarily achieved through the activity of the intracellular antioxidant enzyme GPx4 and the cellular homeostasis of its substrate glutathione (GSH). GSH homeostasis is maintained through both the regulation of the GSH redox state, achieved by the reduction of glutathione disulfide (GSSG) to GSH mediated by glutathione reductase (GSR), and de novo synthesis (Harvey et al., 2009). GSH is a tripeptide composed of glutamic acid, cysteine, and glycine. It is synthesized through glutamate cysteine ligase (GCL) and depends on the intracellular availability of cysteine derived from cystine. The xCT antiporter maintains adequate cystine levels by exchanging extracellular cystine for intracellular glutamate (Tang et al., 2021). Thus, xCT , GCL and GSR are essential for maintaining normal GSH levels and work together with GPx4 to efficiently reduce harmful hydroperoxides and, thus, inhibit ferroptosis. However, it is important to note that under physiological conditions, intracellular GSH concentrations are at least 1,000 times higher than peroxide levels. In situations where peroxides accumulate, a reduction in GPx4 has a greater impact on the oxidative/antioxidative balance than a reduction in glutathione (Hu et al., 2019). GPx4 utilizes GSH as an electron donor to convert peroxidized phospholipids in biological membranes into their respective alcohols. (Hu et al., 2019). In addition to GPx4, several other enzymes play a role in regulating ferroptosis, including GTP cyclohydrolase 1 (GCH1), ferroptosis suppressor protein (FSP1), and dihydroorotate dehydrogenase (DHODH). These enzymes can partially compensate for the decrease in GPx4 activity (Van San et al., 2023). Nonetheless, the importance of GPx4 for neuronal survival is supported by several studies. Seiler et al. (2008) demonstrated that neuron-specific GPx4-knockout mice show relevant degeneration of neurons in the hippocampal CA3 region and the cerebral cortex. Yoo et al. (2012) showed that the ablation of the GPx4 gene in adult mice resulted in profound neurodegeneration. Thus, ferroptotic cell death is mainly regulated by GPx4 and inhibition of its enzymatic activity induces ferroptosis (Yang et al., 2014).

Specifically, the Nrf2 transcriptional pathway regulates a relevant number of essential endogenous components that suppress ferroptosis (see Chapter 1.4) (Dodson et al., 2019).

In general, ferroptosis can be induced by direct inhibition of GPx4 or indirectly by reducing GSH levels through blockade of the cystine-glutamate-antiporter xCT or iron overload. Erastin, an acronym for eradicator of RAS and ST-expressing cells, is a small molecule inhibitor that induces ferroptosis via the inhibition of cystine uptake by the xCT-antiporter (Dixon et al., 2012). The small molecule RAS-selective lethal 3 (RSL3) was initially developed by Yang and Stockwell (2008) for potential anti-cancer applications. It was thought to directly inhibit selenoprotein GPx4 and protect against ferroptotic cell death. However, recent studies have shown that RSL3 may have additional targets, particularly other selenoproteins such as thioredoxin reductase 1 (TXNRD1), and mechanisms of action beyond GPx4 inhibition, such as the activation of the NF-κB pathway (Cheff et al., 2023; Li et al., 2021).

LIP-1 has been found as a potent inhibitor of ferroptotic cell death in oligodendrocytes (Fan et al., 2021). LIP-1 prevents cell death by decreasing mitochondrial lipid peroxidation, featuring restored GSH production, and the expression of Glutathione peroxidase 4 (GPX4) and glutathione-independent FSP1. By this, LIP-1 exhibits immunomodulatory effects (through decreasing microglia activation and reducing secretion levels of proinflammatory cytokines IL-6, IL-1β, and TNF-α (Cao et al., 2021; Fan et al., 2021). Additionally, the radical scavenger Ferrostatin-1 (Fer-1) acts as a potent inhibitor of ferroptosis (Dixon et al., 2012). In the presence of added iron, iron chelators, such as deferoxamine and SIH, also inhibit ferroptosis (Berndt et al., 2010; Yan et al., 2021).

1.3 Ferroptosis as a Possible Part of Pathogenesis in Multiple Sclerosis

1.3.1 Demyelination and Neurodegeneration in Multiple Sclerosis

Inflammatory demyelination and neurodegeneration are key processes in the pathogenesis of multiple sclerosis. Multifactorial mechanisms can lead to their onset. These include activation of immune cells, chronic oxidative damage, accumulation of mitochondrial damage in axons, and dysbalanced iron homeostasis in neurons and oligodendrocytes, which are also associated with ferroptosis (Mahad et al., 2015; Van San et al., 2023). However, the detailed process from the development of inflammatory demyelination to neurodegeneration as well as the exact role of ferroptosis in the pathogenesis of MS has not yet been fully elucidated.

1.3.2 Activated Microglia Promote Oxidative Stress in the Central Nervous System

Activated pro-inflammatory microglia and Lipopolysaccharide (LPS) have been found in close proximity to neurons (Lucchinetti et al., 2011) in both active and chronic MS lesions (Gray et al., 2008; Jack et al., 2005). According to Fischer et al. (2012) these cells largely produce reactive oxygen and nitrogen species in early MS lesions. Furthermore, oxidized phospholipids accumulate in the cytoplasm of degenerating neurons, axons, and myelin sheaths in cortical areas with high levels of microglial activation (Fischer et al., 2013; Mahad et al., 2015). Therefore, it is postulated that oxidative damage, particularly through the action of microglia, may enhance inflammatory responses by activating signaling pathways that lead to the production of proinflammatory cytokines, which are associated with axonal degeneration and neuronal and oligodendrocyte cell death (Fischer et al., 2013). In comparison to other inflammatory diseases of the CNS, microglia activation and oxidative damage of tissue are significantly more apparent in active lesions in multiple sclerosis (Mahad et al., 2015).

1.3.3 Oxidative and Mitochondrial Damage in Multiple Sclerosis

In addition to microglia activation and oxidative damage, molecular studies have revealed an accumulation of axonal mitochondrial damage in MS lesions (Lassmann, 2022). Excessive accumulation of mitochondrial injury results in ATP deficiency, leading to axonal and neuronal degeneration, and tissue destruction (Mahad et al., 2009). In addition, dysfunction in the respiratory chain may also produce reactive oxygen species, intensifying oxidative damage and contributing to further tissue destruction (Mahad et al., 2015).

Severe oxidative and mitochondrial damage can cause the loss of cell processes, disrupting cell-cell interactions and ultimately leading to cell death (Lassmann & van Horssen, 2016). Lassmann (2022) describes the consequences for each cell type in detail: The distal processes of oligodendrocytes are particularly affected, leading to their cell death and demyelination. In neurons, synapses are

primarily damaged, followed by axonal and dendritic damage and severing, resulting in a loss of signal transmission and subsequent neuronal and axonal degeneration. In demyelinated MS lesions, it has been observed that the few surviving oligodendrocyte precursor cells do not differentiate into mature oligodendrocytes, which may be due in part to the loss of their cellular processes, thereby hindering the remyelination process (Lassmann & van Horssen, 2016).

The accumulation of mitochondrial damage promotes demyelination and neurodegeneration in MS, which leads to the progression of the disease (Mahad et al., 2015).

1.3.4 Susceptibility of Oligodendrocytes to Ferroptosis

The most relevant oxidative damage in active MS lesions is found in myelin and oligodendrocytes (Lassmann & van Horssen, 2016).

Oligodendrocytes are the cells in the CNS with the highest iron content (Connor & Menzies, 1996). To form myelin sheaths, they need enough iron to produce essential myelin components such as cholesterol and phospholipids (Stephenson et al., 2014). In addition, iron is a co-factor for several enzymes that are involved in the proliferation of OPC and their differentiation into mature oligodendrocytes (Cheli et al., 2020). Several proteins collaborate to maintain cellular iron homeostasis by controlling the uptake and storage of iron. Transferrin (Tf) is the primary transporter of iron. After binding to its receptor (TfR) situated on the cell surface, the ligand-receptor (Tf-TfR) complex undergoes internalization through receptor-mediated endocytosis (Cheli et al., 2020). Significant levels of transferrin stimulate the production of myelin constituents (Saleh et al., 2003) and facilitates OPC differentiation into mature oligodendrocytes (Paez et al., 2002).
Recent studies have identified the Transferrin receptor 1 (TfR1) as a reliable marker for ferroptosis. Feng et al. (2020) reported notable TfR1 accumulation on the cell surface in ferroptosis within the HT-1080 fibrosarcoma cell line, and anti-TfR1 antibodies could distinguish ferroptosis from apoptosis in these cells. However, the exact reason for the upregulation in the ferroptotic cells has not yet been clarified.
Zhang et al. (2006) demonstrated that ferritin, secreted by ferritin-positive-microglia, acts as a primary iron delivery protein to mature oligodendrocytes, in addition to its ability as an intracellular iron storage and regulatory protein with ferroxidase activity. The results of their cell culture experiments showed that conditioned media containing ferritin enhances the survival of oligodendrocytes. Additionally, Schulz et al. (2012) showed that the efflux of iron from astrocytes, facilitated by the iron exporter ferroportin, is involved in OPC maturation and myelination and remyelination. Consequently, proper iron supply is essential for optimal oligodendrocyte maturation, particularly in the first postnatal weeks, but also for efficient adult brain remyelination (Cheli et al., 2018; Stephenson et al., 2014) and preservation of myelin (Zhang et al., 2006).
Physiologically, most intracellular iron is bound to ferritin in its trivalent form (Fe^{3+}) to minimize the amount of free iron, as free trivalent iron is constantly in dynamic equilibrium with its oxidizing bivalent form (Fe^{2+}) (Lassmann & van Horssen, 2016). Zhang et al. (2005) demonstrated that a dysbalance in iron homeostasis, such as a deficiency in ferritin, can result in a high concentration of free redox-active ferrous iron (Fe^{2+}), which increases the susceptibility of oligodendrocytes to oxidative stress and cytokine toxicity. The susceptibility mentioned is intensified by the relatively low levels of antioxidants, particularly Glutathione (GSH), in oligodendrocytes (Lassmann & van Horssen, 2016; van Horssen et al., 2011).

Oligodendrocytes produce huge amounts of their plasma membrane and ensheathe axons in multiple layers within the CNS, known as myelin sheaths (Aggarwal et al., 2011). In addition, these myelin sheaths are mainly composed of lipids (about 80%), including polyunsaturated fatty acids (PUFA)(Barnes-Velez et al., 2023). The increased susceptibility to oxidative stress and the high concentration of fatty acids make oligodendrocytes susceptible to lipid peroxidation, which facilitates membrane permeabilization and ultimately ferroptotic cell death and axon demyelination in the CNS (Li et al., 2023). Compared to mature oligodendrocytes, oligodendrocyte precursor cells are more susceptible to oxidative stress and ferroptosis (Baud et al., 2004; Wu et al., 2024). Additionally, Lepka et al. (2017) demonstrated that treatment with ferroptosis inducer Erastin causes cell death in primary mouse oligodendroglial progenitor cells. Furthermore, the death of oligodendrocyte progenitor cells due to ferroptosis may impede the process of remyelination.

1.3.5 Ferroptosis and T Cells in the Pathogenesis of Experimental RRMS Models

During the acute phase, the pathogenesis of MS is a complex process involving intricate interactions between peripheral and central immune cells. It is established that peripheral leukocytes, including T cells, B cells, and myeloid cells, play a pivotal role in the pathogenesis of MS (Charabati et al., 2023). Upon migration into the CNS, these immune cells can activate resident cells, such as microglia and astrocytes, and interact with myelin and other antigens, resulting in damage to oligodendrocytes and neurons (Charabati et al., 2023; Hohlfeld et al., 2016). Murphy et al. (2010) demonstrated that autoreactive T lymphocytes, especially Th1 and Th17 cells, are significantly associated with acute episodes of MS. Th1 cells contribute to the disease process in a number of ways, including the stimulation of macrophages and microglia through the release of factors such as granulocyte-macrophage colony-stimulating factor (GM-CSF) and the impairment of the survival and differentiation of oligodendrocyte progenitor cells. Th17 cells exacerbate the condition by disrupting the blood-brain barrier, promoting the infiltration of inflammatory phagocytes, and altering glial cell functions (Charabati et al., 2023). Additionally, autoreactive B lymphocytes in MS promote the proliferation of Th1 and Th17 cells recruited from the CNS (Jelcic et al., 2018).

Autoreactive lymphocytes are typically eliminated in the thymus during negative selection or later in blood circulation through death ligand pathways. These pathways are crucial for immune homeostasis and apoptosis regulation and appear dysregulated in MS. The Fas-Fas ligand (FasL) pathway, extensively studied, mediates apoptosis of autoreactive lymphocytes during negative selection, activation-induced cell death of repeatedly stimulated T cells, elimination of autoreactive B cells, and regulation of B cell somatic hypermutation. In MS and experimental autoimmune encephalomyelitis (EAE), dysregulation of this pathway is evident. Th17 cells in MS exhibit low FasL expression, potentially enabling persistent inflammation, while FasL-deficient mice develop prolonged EAE symptoms (Volpe et al., 2016). Other relevant factors include increased expression of anti-apoptotic Bcl-X(L) in MS patients' PBMCs and elevated soluble TNF-related apoptosis-inducing ligand (TRAIL) levels (Waiczies et al., 2002; Wandinger et al., 2003). In the context of neuroinflammation TRAIL emerges as a significant mediator of neuronal injury. In EAE, Aktas et al. (2005) demonstrates that TRAIL blockade leads to a marked reduction in neuronal damage and clinical severity. Conversely, intracerebral TRAIL administration in EAE-affected subjects resulted in an exacerbation of clinical deficits. These findings collectively suggest a pivotal role for TRAIL in the pathogenesis of inflammatory neurological conditions. Notably, interferon-beta responders in MS treatment can be identified by early and persistent expression of soluble TRAIL, highlighting its potential as a biomarker for treatment efficacy (Wandinger et al., 2003).

While T cells are initially activated in the periphery during an acute attack and subsequently migrate into the CNS, CD4+ T cells can also be activated within the CNS. In EAE, ferroptosis has been demonstrated to be a pivotal mechanism underlying T cell-mediated neurodegeneration (Luoqian et al., 2022; White, 2023). EAE specifically stimulates an upregulation of ACSL4 expression, which is a biomarker for ferroptosis (Dodson et al., 2019; Luoqian et al., 2022). The enzyme ACSL4 facilitates the esterification of PUFAs in neurons, rendering them susceptible to ferroptosis (Tuo et al., 2022). The supernatant obtained from ferroptotic neurons increases T cell receptor (TCR) signaling, resulting in the activation of CD4+ T cells and their differentiation into Th1 and Th17 cells. These cells cause demyelination and neurodegeneration via the secretion of cytokines like interleukin 2 (IL-2) and Interferon gamma (IFN-ϒ) (Luoqian et al., 2022).

In support of this, Lucchinetti et al. (2011) discovered that T cells are in the proximity of oligodendrocytes within early demyelinating lesions. Van San et al. (2023) also demonstrated in an experimental RRMS model in Biozzi ABH mice that inflammation during a disease attack is primarily mediated by macrophages, microglia and T cells, while B cell infiltration is observed during the chronic course of the disease.

Luoqian et al. (2022) revealed that ferroptosis inhibitors, such as LIP-1, ameliorated neuroinflammation by regulating T-cell activation in the CNS of EAE-mice. This provides further support for the implication of ferroptosis in immune process regulation.

Van San et al. (2023) identified fluctuating alterations in the levels of distinct antioxidant proteins throughout the progression of EAE disease in spinal cord segments of mice. During the acute phase, decreased levels of the primary inhibitor of ferroptosis, GPx4, were observed in conjunction with the upregulation of Hmox1 and, as a potential feedback mechanism for GPx4 deficiency, two additional ferroptosis antagonists: FSP1 and GCH1 (Carvalho et al., 2014; Kraft et al., 2020; Van San et al., 2023).

Furthermore, the expression of TFR1 was found to increase during the pre-acute phase of EAE, but it decreases significantly as the disease progresses until the first attack occurs. In EAE, during the remission phase, a significant increase in GPx4 was reported (Van San et al., 2023). Van San et al. (2023) also have shown that administering ferroptosis inhibitor UAMC-3203, a third-generation synthetic lipophilic radical trap compound, protects against the early progressive disease course in experimental RRMS in Biozzi ABH mice. The evaluation of the demyelinated region revealed a significant decrease in damage observed in the lumbar spinal cords. Iron chelators, such as deferoxamine (Pedchenko & LeVine, 1998) and deferiprone (Mitchell et al., 2007), have been shown to suppress the disease activity of EAE. As far as is currently known, no agents that significantly increase GPx4 activity have been discovered.

1.3.6 Oxidative Stress, Iron Accumulation and Ferroptosis in Multiple Sclerosis

The pathogenesis of MS appears to be decisively influenced by oxidative stress, imbalance of iron homeostasis and ferroptotic cell death, as several clinical and basic scientific studies have shown.

One of the main biochemical characteristics of ferroptosis is the accumulation of iron alongside lipid peroxidation (Tang et al., 2021). Recent neuropathological and magnetic resonance imaging (MRI) studies provide evidence that progressive iron accumulation is a central factor in the CNS tissue damage associated with MS (Absinta et al., 2019; Dal-Bianco et al., 2021; Lassmann, 2022). Iron accumulation was mainly found in lesions with chronically active but low-grade inflammation,

such as in progressive MS, e.g. smoldering lesions, but also in lesions with acute inflammation, such as in relapsing-remitting MS (Dal-Bianco et al., 2017; Dal-Bianco et al., 2021).

High levels of ferrous iron were observed in active MS lesions from postmortem samples, compared to normal-appearing white matter (NAWM) and non-MS control samples (Van San et al., 2023). In addition, Van San et al. (2023) recently reported a significant increase in the ratio of redoxactive ferrous to ferric iron (Fe^{2+}/Fe^{3+}) in the cerebrospinal fluid (CSF) of MS patients. In contrast, the total iron content and ferritin-bound iron were comparable in the CSF of MS and non-MS patients.

Some white matter lesions that are chronically active are surrounded by a rim composed of activated microglia and macrophages. These lesions expand slowly and are referred to as smoldering lesions (Lassmann, 2022). Iron accumulation in chronically active lesions is primarily located in their rim (Dal-Bianco et al., 2017; Ropele et al., 2017). The process of iron uptake by microglia and macrophages, as well as the development of iron rim lesions, was described by Mahad et al. (2015). Iron is released from compromised myelin and oligodendrocytes during inflammatory demyelination. It enters the extracellular space where it transforms into bier ferrous form, potentially increasing the toxicity of reactive oxygen species. To prevent further damage, released iron is primarily absorbed by activated microglia and macrophages. It accumulates within the cells at the periphery of the lesion and in the perivascular space, forming the rim lesion as described by Lassmann (2022).

The histopathological findings are consistent with the imaging observations of iron rim lesions in high-field MRI utilizing iron-sensitive sequences in postmortem patients (Dal-Bianco et al., 2017). The dynamics of iron accumulation in lesions can also be observed through live imaging (Lassmann, 2022). In a seven-year prospective longitudinal MRI-study, Dal-Bianco et al. (2021) discovered that chronically active lesions with iron rims grow slowly after their initial formation, over a period of more than five years, eventually merging with adjacent rim lesions. In comparison, non-iron rim lesions shrink over a three-year period before stabilizing in size (Lassmann, 2022). Iron-rim lesions typically develop in the later stages of RRMS but persist after the disease has converted into a progressive form (Dal-Bianco et al., 2021). They seem to contribute to the gradual progression of neurodegeneration and are associated with a more severe disease course, as well as a higher likelihood of conversion to a progressive form of MS (Dal-Bianco et al., 2021; Lassmann, 2022). This is supported by the results from Hametner et al. (2013). Iron-containing microglia and macrophages show signs of dystrophy and deterioration, leading to secondary iron release and uptake by neurons, oligodendrocytes, and other microglia and macrophages. This process, in combination with ROS released from other activated microglia and macrophages (Fischer et al., 2012), can lead to lipid peroxidation in these cells (Hametner et al., 2013; Van San et al., 2023), further demyelination, and subsequently, lesion growth. These findings suggest that ferroptosis may be involved in MS progression.

This concept is supported by studies of post-mortem samples and cerebrospinal fluid (CSF) from MS-patients. These studies have demonstrated lipid peroxidation and other features of ferroptosis in both active and chronic lesions (Van San et al., 2023). According to Hu et al. (2019), mRNA levels of major ferroptosis inhibitor GPx4 are reduced in the MS brain, while GPx4 protein levels in MS are still unclear. Bizzozero et al. (2005) demonstrated reduced levels of GPx4-substrate GSH and increased lipid peroxidation in the gray matter of individuals with MS. Furthermore, Van San et al. (2023) demonstrated accumulation of lipid degradation products, such as 4-HNE, particularly within

active lesions and the peripheral area of chronically active lesions. Mahad et al. (2009) found structural changes in neuronal mitochondria in MS, including the disappearance of cristae and damage to the outer membrane, resulting in impaired cellular respiration, leading to energy failure, accumulation of oxidative stress, ferroptotic cell death, further demyelination and neurodegeneration (Mahad et al., 2015). In addition, in the CSF of MS patients, the activity of GPx and the levels of its substrate GSH were significantly lower than in control subjects. This contributes to an altered detoxification of reactive oxidants in the CNS (Calabrese et al., 1994; Calabrese et al., 2002; Carvalho et al., 2014). However, the available evidence on GPx activity in peripheral blood mononuclear cells (PBMCs) and erythrocytes of MS patients is still inconclusive (Carvalho et al., 2014).

These observations indicate that ferroptosis plays an important role in the pathology of MS. To date, there is no known therapy in humans that specifically targets ferroptosis. However, these findings suggest that a therapy that prevents ferroptosis in the CNS may be a promising new treatment for the active and progressive form of MS.

1.4 Fumarates in Multiple Sclerosis: Mode of Action and its Effects on Demyelination

Fumarates are a natural compound found in every cell of every organism and are produced by metabolic pathways such as the citrate and urea cycles, as well as the purine biosynthesis (Papadopoulou et al., 2010). Dimethyl fumarate (DMF), a fumaric acid ester, has been approved for the treatment of psoriasis vulgaris since 1994 and for the treatment of RRMS in adult patients since 2013 (Corazza et al., 2021; Wicks et al., 2016). Since 2021, another fumaric acid ester, DRF, has been approved in Europe for the treatment of RRMS in adults. DMF and its successor DRF are low to moderate efficacy DMTs for mild to moderate RRMS.

The most common adverse events observed with both DMF and DRF include flushing and gastrointestinal symptoms such as abdominal pain, diarrhea, and nausea. However, the EVOLVE-MS-2 trial investigated the gastrointestinal tolerability of DMF and DRF and demonstrated superior gastrointestinal tolerability of DRF compared to DMF. This was evidenced by a reduction in self-rated symptom days and a lower discontinuation rate due to gastrointestinal issues (Naismith et al., 2020). DRF's superiority is explained by its molecular and pharmacokinetic characteristics. Upon oral ingestion, intestinal esterases promptly hydrolyze both fumaric acid esters into the active metabolite, Monomethyl fumarate (MMF) (Linker & Gold, 2013). DMF and DRF provide bioequivalent MMF exposure, indicating similar efficacy and safety profiles (Naismith et al., 2020). MMF reaches peak serum concentrations of approximately 20 µM, distributing uniformly in organs, including the CNS, and undergoes subsequent metabolism in the citrate cycle (Linker & Gold, 2013). However, the hydrolysis of DMF and DRF produces several metabolites, including methanol in the case of DMF and hydroxyethyl succinimide (HES) in the case of DRF. Small amounts of methanol are also produced in the latter. Methanol is a known gastrointestinal irritant. DMF produces higher levels of methanol, resulting in more severe gastrointestinal adverse effects. Furthermore, DMF may have more off-target interactions with GI receptors or microbiota/proteins due its larger molecular size, higher electrophilicity with greater reactivity, and longer half-life (Palte et al., 2019).

The mode of action of fumaric acid esters in MS remains incompletely understood. DMF studies have reported multiple anti-inflammatory, immunomodulatory, and neuroprotective effects. DMF treatment reduces lymphocyte counts in MS patients' PBMCs by approximately 30% after six

months, primarily affecting CD4+ and CD8+ memory T cells. This reduction preferentially targets memory T cells over naive T cells, with a decrease in TH1 cells and an increase in TH2 cells (Gross et al., 2016). This shift has an impact on cytokine expression, such as a decrease in the production of pro-inflammatory Th1 cytokines (such as IL-22, GM-CSF, TNF-α, IFN-γ) (Gross et al., 2016). Ex vivo incubation of healthy donor PBMCs with MMF increased production of anti-inflammatory Th2 cytokines (such as IL-4, IL-10) (Moharregh-Khiabani et al., 2009). However, IL-4 levels remained stable in PBMCs from DMF-treated MS patients (Gross et al., 2016). In addition, fumarate incubation in endothelial cell culture experiments decreased adhesion molecules like ICAM-1 and E-selectin, which is partly mediated by the observed inhibition of the NF-κB pathway and causes a reduction in the migration of immune cells across the blood-brain barrier into the CNS . In addition, DMF treatment increases the proportion of peripheral regulatory T cells (pTreg) in PBMCs of MS patients, whose function is often compromised in patients with MS (Gross et al., 2016). Microglial culture and EAE studies demonstrated microglia polarization from M1 pro-inflammatory to M2 anti-inflammatory phenotype via hydroxycarboxylic acid receptor 2 (HCAR2) activation. The observed anti-inflammatory effect in the brain was partially Nrf2-dependent (Parodi et al., 2015; Satoh & Lipton, 2017).

The main mechanism of action is explained through the activation of the Nrf2 signaling pathway, which helps maintain intracellular redox homeostasis, particularly during periods of increased oxidative or metabolic stress (Linker et al., 2011; Wang et al., 2024). Nrf2 is regulated by Kelch-like ECH-associated protein 1 (Keap1). Keap1 functions as a sensor for the cellular redox state through its reactive thiol groups, due to its high cysteine content. This regulatory mechanism relies on Keap1's ability to detect changes in the cellular redox state (Lu et al., 2016). Keap1 modulates the ubiquitination level of Nrf2 in response to the redox state, thereby influencing its overall activity. Under normal conditions, Keap1 binds to Nrf2 and facilitates its degradation, but in the presence of oxidative stress or cellular insults, Nrf2 stabilizes, escapes Keap1-mediated degradation, and translocates to the nucleus. In the nucleus, Nrf2 binds to the antioxidant response element (ARE) in regulatory DNA regions and activates transcription of genes, resulting in the expression of over 100 antioxidant proteins (Lu et al., 2016). For example, Nrf2 plays a central role in maintaining GSH homeostasis by regulating the cystine-glutamate antiporter xCT, which influences de novo GSH synthesis, and by regulating glutathione reductase (GSR), which modulates the redox state of GSH (Harvey et al., 2009). Furthermore, Nrf2 regulates key metabolic pathways, including lipid and iron metabolism (via expression of Hmox1, light chain and heavy chain of ferritin (FTL/FTH1), ferroportin (FPN1)), and apoptosis (Dodson et al., 2019). Additionally, the key enzyme that inhibits ferroptosis, GPx4, seems to be a target gene of Nrf2 (Dodson et al., 2019; Osburn et al., 2006; Salazar et al., 2006). However, some authors question whether the Nrf2 pathway regulates GPx4, as the promoter region of GPx4 lacks the necessary structural cis-elements (Berndt et al., 2024). Specifically, during embryonic brain development, the expression of GPx4 seems to be upregulated by guanine-rich sequence binding factor 1 (GRFS1) (Ufer et al., 2008). Nevertheless, the regulatory mechanisms governing GPx4 expression in oligodendrocytes remain an area of ongoing investigation.
Moreover, the Nrf2 and the pro-inflammatory NF-κB pathways act as antagonists and work together to maintain cellular homeostasis and respond appropriately to stressors (Gao et al., 2021). Thus, proper Nrf2 function is critical for cell survival and may mediate neuroprotective effects in the CNS (Gross et al., 2016; Lu et al., 2016).

After MMF incubation of rodent astrocyte cultures, the Keap1 protein was found to be covalently modified at cysteine residue 151, thereby stabilizing Nrf2 (Wang et al., 2024). Elevated levels of Nrf2 were found in the CNS of DMF-treated mice (Linker et al., 2011). In addition, Linker et al. (2011) demonstrated the protective effect of DMF treatment as a result of stimulation of the Nrf2 pathway on neurons, oligodendrocytes, myelin, and axons in MOG-EAE. They observed a reduction in protein nitrosylation, a marker of oxidative stress. Conversely, the absence of this protective effect in Nrf2 knockout mice supports the dependency of the functional impact of DMF on Nrf2. Additionally, Linker et al. (2011) showed that mice with an Nrf2 knockout developed a more severe form of MOG-EAE compared to mice with wild-type Nrf2. This exacerbation was associated with increased oxidative damage in the CNS. This ultimately led to more extensive demyelination and axonal loss. Scannevin et al. (2012) confirmed that DMF and its primary MMF exert cytoprotective effects on primary CNS cells against oxidative stress-induced injury. However, Schulze-Topphoff et al. (2016) demonstrated that DMF exhibits potent anti-inflammatory and immunomodulatory activity in CNS autoimmunity that may not require Nrf2 for many of its beneficial effects. They showed that DMF protected both wild-type and Nrf2-deficient mice equally well from acute EAE, reducing Th1 and Th17 cells and inducing anti-inflammatory M2 monocytes. This suggests that DMF's therapeutic effects in EAE can also occur through Nrf2-independent pathways.

1.5 Research Question and Aim of this Thesis

Ferroptosis has been implicated in the pathomechanism of MS. However, it remains unclear whether and how ferroptosis contributes to death of oligodendrocytes and the demyelination process in MS. Luoqian et al. (2022) demonstrated in EAE mice that ferroptosis primarily triggers neuronal cell death directly, while demyelination occurs indirectly through activated T cells (Figure 1).

As oligodendrocytes are particularly susceptible to ferroptosis, it is thought that they may undergo direct ferroptotic cell death without the influence of T cells, leading to demyelination (Figure 1). One objective of this thesis is to investigate whether oligodendrocytes are susceptible to ferroptotic cell death by exposing them to various concentrations of known ferroptosis inducers, specifically Erastin and iron. To investigate whether the death of oligodendrocytes is indeed ferroptotic, the level of lipid peroxidation is measured. Subsequently, it will be investigated whether ferroptosis can trigger demyelination in organotypic cerebellar slice cultures (OSCs).

Fumarates have been used in the treatment of RRMS for 10 years. The mechanism of action involves the Nrf2 signaling pathway, a cellular signaling mechanism that protects against oxidative damage by regulating gene expression of antioxidant and anti-inflammatory proteins and that is downregulated in MS patients, among others (Maldonado et al., 2022). The extent to which activation of this physiological protective mechanism is involved in protection against further neuroinflammation and axonal demyelination remains unclear. Considering that ferroptosis, triggered by oxidative stress and iron accumulation, can lead to cell death, and potentially contribute to demyelination, this study aims to contribute to the existing body of knowledge by exploring the potential protective effects of fumarates, with a particular focus on DRF and its active substance MMF, against increased lipid peroxidation and subsequent ferroptotic cell death in oligodendrocytes.

Figure 1 A Potential Role of Ferroptotic Cell Death in Demyelination and Neurodegeneration

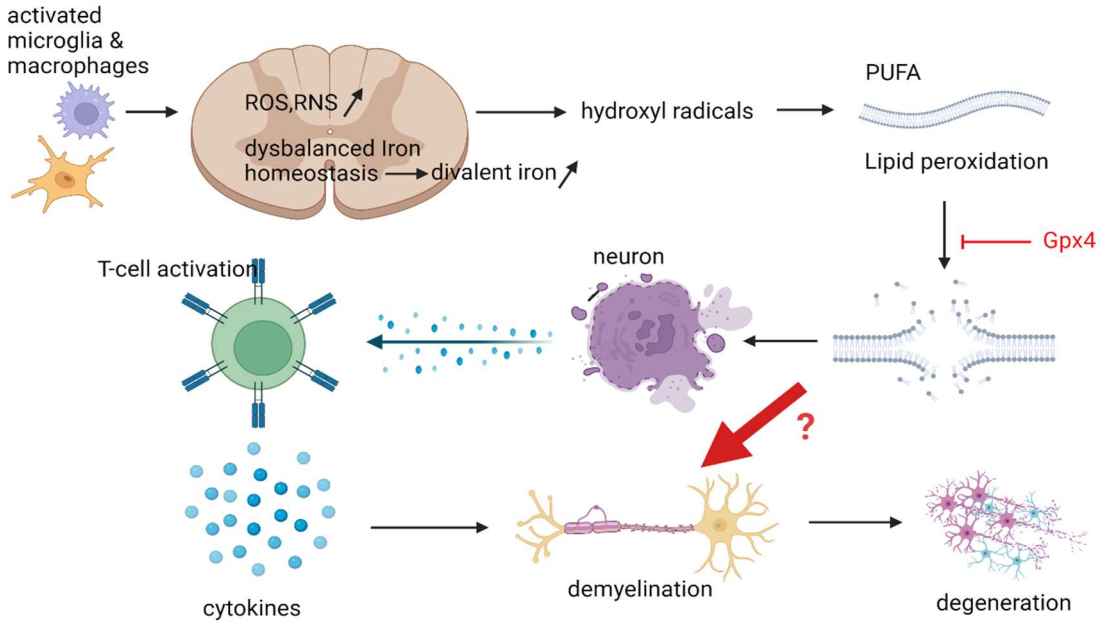

Fig. 1: According to Luoqian et al. (2022), autoimmune neuroinflammation is induced by activated microglia and macrophages, which triggers the accumulation of reactive species and iron dysbalance in favor of toxic divalent iron. This process induces lipid peroxidation through the Fenton reaction, which particularly affects neurons and leads to their death. The supernatant of ferroptotic neurons triggers T cell activation, resulting in cytokine-induced demyelination and neurodegeneration. The aim of this study is to demonstrate the direct relationship between ferroptosis and oligodendrial cell death, leading to demyelination. Created with BioRender.com; GPx4: Glutathione Peroxidase 4, PUFA: Polyunsaturated Fatty Acid, RNS: Reactive nitrogen species, ROS: Reactive oxygen species.

Furthermore, it will be investigated whether diroximel fumarate modulates the effect of iron accumulation. In addition, the ability of fumarates to protect against ferroptosis-induced demyelination will be tested in cerebellar OSCs.

Given that the key enzyme that protects against ferroptosis, GPx4, is discussed as a gene product within the Nrf2 signaling pathway, this study will investigate whether and to what extent GPx4 is upregulated in oligodendrocytes as well as in brain tissue after fumarate treatment.

To investigate the potential ferroptosis inhibition by fumarates in a more clinically relevant manner, the study was extended to in vivo experiments using blood samples from MS patients. However, due to the significant physiological heterogeneity among humans and the limited sample size in this study, the results can, at best, indicate a potential trend rather than definitive conclusions. Considering the previously identified GPx4 deficiency in the postmortem brain tissue of MS patients, an additional investigation will assess the existence of an in vivo deficiency in GPx4 gene expression. Furthermore, the research aims to determine if cellular GPx4 gene expression increases in MS patients after one year of DMF treatment.

Assuming that GPx4 is expressed in all nucleated cells, PBMCs will be used for this study. Since the CNS is enveloped by CSF, cells from CSF would reflect CNS processes more accurately than PBMCs. However, due to the retrospective nature of the study, the decision to utilize PBMCs instead of CSF

was primarily influenced by the availability of materials. No CSF puncture was performed at the specified time points immediately before and 12 months after switching to the new drug. Furthermore, in their gene expression analysis, Brynedal et al. (2010) found in their gene expression analysis that the stage of the disease determines the level of gene expression. Generally, most differences in gene activity between MS patients and healthy individuals are found in the CSF. For instance, it has been found that the activity of glutathione peroxidase (GPx) and the amount of its substrate GSH are significantly lower in the CSF of MS patients compared to control subjects. In contrast, the available findings on GPx activity in the PBMCs and erythrocytes of MS patients are not yet conclusive (Carvalho et al., 2014). However, disease relapses can only be recognized based on PBMCs, suggesting a peripheral genesis of relapses. Consequently, the study of gene expression profiles in PBMCs represents a useful starting point for further investigations

Fumarate-induced increase in GPx4 levels in CNS cells may inhibit ferroptotic cell death, potentially contributing to its therapeutic mechanism in MS. However, whether the current dosing regimen of DMF and DRF achieves sufficient CNS concentrations for this effect requires further investigation.

2 Materials and Methods

2.1 Cell Culture Experiments

The OLN-93 cell line (RRID: CVCL_5850) (Richter-Landsberg & Heinrich, 1996) was maintained in low glucose Dulbecco's modified Eagle's medium (DMEM) supplemented with 10% fetal bovine serum (FBS) and a mixture of 100 µg/ml penicillin and 100 µg/ml streptomycin in a humidified incubator with 5% CO_2 at 37°C. In experimental conditions, serum-free DMEM/F-12 media was used. Cell dissociation and passaging were performed using 1 ml of Trypsin/EDTA solution prepared in PBS (without Ca^{2+}, Mg^{2+}) following an incubation period at 37°C for 1-3 minutes. The cells underwent testing for mycoplasma infection utilizing the MycoStrip™ mycoplasma detection kit. All cell culture procedures were consistently conducted under as sterile conditions as feasibly achievable.

16 hours prior to treatment, cells were seeded in 96-well plates (3 000 cells/well), 24-well plates (40 000 cells/well), 6-well plates (120 000 cells/well) or 60-mm dishes (1 000 000 cells/dish).

2.2 Treatments

Monomethyl fumarate (MMF) and dimethyl fumerate (DMF) were purchased from Sigma-Aldrich and dissolved in 100% dimethyl sulfoxide (DMSO). 500 mM aliquots were stored at -20°C until use. Diroximel fumarate (DRF; Vumerity®) was provided as a promotional sample by Biogen. To prepare the DRF solution, the spheroids from one capsule, 240 mg of the fumarate, were initially soaked with 200 µl of water and subsequently solubilized by the addition of 800 µl of 100% DMSO. The resulting 480 mM aliquots were stored at -20°C. Unless otherwise stated, OLN-93 cells were treated with 2 µM and 10 µM concentrations of MMF and DRF after 16 hours of cultivation, with untreated cells as controls. Following 24 hours of incubation at 37°C and 5% CO_2, the treatment media were removed, and cells were further processed as required by the specific experiment.

Erastin, an acronym for eradicator of RAS and ST-expressing cells, is a small molecule inhibitor that induces ferroptosis via several mechanism (Zhao et al., 2020). One of these mechanisms is the inhibition of cystine uptake by the cystine-glutamate antiporter (system Xc−) by Erastin (Dixon et al., 2012). This leads to a loss of cysteine access (cystine availability) and subsequent inability to produce the antioxidant GSH in Erastin-treated cells. This process depletes the intracellular antioxidant defenses, leading to the accumulation of reactive species and an excessive amount of lipid peroxidation. Ultimately, this results in iron-dependent oxidative non-apoptotic cell death.
Ferrous ammonium sulphate $(NH_4)_2Fe(SO_4)_2$ was utilised as an iron-dependent cell death inducer. This compound is a double salt consisting of ferrous sulphate and ammonium sulphate $(NH_4)_2Fe(SO_4)_2$.
Lipopolysaccharide (LPS) is an endotoxin derived from the outer membrane of Gram-negative bacteria. It is a potent inducer of neuroinflammation through the activation of microglia (Skrzypczak-Wiercioch & Salat, 2022).
LIP-1 is a highly potent radical-trapping antioxidant in lipid bilayers, which reduces lipid peroxidation of mitochondrial and cellular membranes (Fan et al., 2021; Shah et al., 2017; Zilka et al., 2017). In more detail, it blocks directly mitochondrial lipid ROS, stimulates the production of reduced glutathione (GSH) and the expression of GPx4 and the glutathione-independent FSP1 (Fan et al., 2021). Moreover, LIP-1 exhibits immunomodulatory effects (through decreasing microglia activation and

reducing secretion levels of proinflammatory cytokines IL-6, IL-1β, and TNF-α (Cao et al., 2021; Fan et al., 2021).
Erastin, LPS and LIP-1 were dissolved in 100% DMSO and stored at -20°C in 6 mM, 10µM and 0.1 mM aliquots, respectively. Given the observed variability in sensitivity to Erastin-induced ferroptosis across the maturation states of oligodendrocytes (Hoshino et al., 2020), the dosages (IC_{50}) were determined on a cell-by-cell basis for cultured OLN-93 cells and myelinated slice cultures. LIP-1 was employed at 100 nM and 200 nM concentrations for cell culture and slice culture experiments, respectively (Fan et al., 2021; Lepka et al., 2017).
A 10mM water solution of iron salt (ferrous ammonium sulphate) was prepared immediately prior to use. During the incubation period, cultures treated with the iron salt were continuously shaken on a rotating platform to ensure uniform distribution. The optimal concentrations of iron salt chosen for treatment were determined based on intracellular iron concentrations observed in oligodendrocytes of adult rat brain (Reinert et al., 2019).
SIH is an orally active lipophilic iron chelator (Hofer et al., 2014). Accumulating evidence demonstrates its antiproliferative effect due to its ability to inhibit iron uptake in various types of transformed cells (Wang et al., 2019), including the human neuroblastoma cell line SK-N-MC (Wu et al., 2020). Subsequently, SIH was shown to inhibit membrane lipid peroxidation and oxidative damage (Hofer et al., 2014; Wu et al., 2020). The iron chelator SIH was purchased from Cayman Chemicals and dissolved in 100% DMSO. 1 mM aliquots were stored at -20°C. 100 µM was used to chelate iron in cultured cells according to (Berndt et al., 2010).

2.3 Cell viability assay

Cell viability was assessed using a variety of methods. The resazurin-resorufin-based assay (the CellTiter-Blue® CTB Cell Viability Assay) is based on the ability of living cells to metabolize a redox-sensitive dye. Metabolic activity and the resulting cell health are measured using this method. In brief, the assay contains the redox dye resazurin, which is irreversibly reduced to the fluorescent dye resorufin in viable cells. Unlike the dark blue resazurin, the pink resorufin emits high fluorescence (excitation 579 nm/ emission 584 nm). For this reason, together with the immediate loss of metabolic capacity after death, non-vital cells do not produce a fluorescent signal. The quantity of fluorescence is thus directly proportional to the number of viable cells (Promega, 2023) serving as an indirect measure of cell viability.

The second method involve the propidium iodide (PI)-based assessment of membrane integrity. PI can only enter a cell through a damaged plasma membrane and only emits fluorescence when it binds to nucleic acids (excitation 535nm/emission 612nm). Therefore, there is no fluorescence signal in viable cells with an intact plasma membrane, and conversely, the higher the fluorescence signal, the more affected cells are present. For clarity and comparability with the CTB cell viability plots, the fluorescence signal data has been converted to its counter-event and presented in the PI cell viability plots.

OLN-93 cells were seeded in a 96-well plate and pre-treated for 24 hours with fumarates (DRF or MMF) at various concentrations. Subsequently, the medium was replaced with serum-free DMEM/F-12 media supplemented with Erastin (at a final concentration of < 0.35% v/v DMSO; Sigma Aldrich) or iron salt (ferrous ammonium sulphate dissolved in media), along with the concentrations of fumarates used in the pre-treatment period. The cells were then cultured for a further 24 hours.

The control group was treated with the corresponding concentrations of DMSO (< 0.35 % DMSO). The viability of the cells was evaluated using a resazurin-resorufin-based assay (the CellTiter-Blue® Cell Viability Assay) or a propidium iodide (PI)-based assessment of membrane integrity for the Erastin- or iron-treated groups, respectively. Depending on the assay, a CellTiter-Blue® (CTB) solution prepared by dilution 1:6 in DMEM culture medium or a 5 µg/mL PI solution was applied for incubation periods of 2 hours or 5 minutes, respectively, in a light-protected environment. Following incubation, the fluorescence signals of the PI samples were measured after washing, while the CTB samples were measured directly without washing. Fluorescence measurements of resorufin were conducted using a microplate reader (TECAN GENios Pro) at a wavelength of 590 nm (for the CTB assay) and excitation 535nm/emission 612nm (for the PI-based assay). The relative fluorescence unit (RFU) was determined by normalizing the fluorescence level to that of the control groups. The maximal fluorescence of PI was determined in cultures treated with 0.02% Triton X-100. Three independent experiments were conducted for each treatment, with three replicates per experiment.

2.4 Lipid Peroxidation Detection (Flow Cytometry Analysis)

The processes of intra- and extracellular lipid peroxidation can result in potential damage to the plasma membrane and mitochondrial membranes, and potentially lead to cell death. Lipid peroxidation was measured by flow cytometry using the redox-sensitive fluorescent dye BODIPY™ 581/591 C11. Cells were loaded with the fatty acid BODIPY™ (boron-dipyrromethene), which can pass through the cell membrane. Lipid peroxides catalyze the oxidation of the dye, leading to a shift in the fluorescence emission peak from around 590 nm (red) to around 510 nm (green) (Thermo Fisher Invitrogen™, 2012). Measuring fluorescence levels via the FITC channel (peak emission at 525 nm) in flow cytometry enables quantification of the amount of lipid peroxides present in individual cells (Martinez et al., 2020).

BODIPY™ 581/591 C11 was dissolved in 100% ethanol to form a 1mM stock solution. Aliquots were stored at -20°C until use. Lipid peroxidation was indirectly induced in OLN-93 cells using Erastin.

In a pharmacokinetic study conducted by Tim Prozorovski, a researcher in our laboratory research group, the protein expression of GPx4 was investigated in OLN-93 cells over incubation periods ranging from 0 to 48 hours. The results showed that GPx4 expression peaked after three hours of incubation (data unpublished). Cells plated in six-well plates were pretreated with 2 µM DRF, 2 µM MMF, or 100 nM Liproxstatin for three or 24 hours, followed by a 6-hour incubation with Erastin at its IC_{50} (2x IC_{50} , 4x IC_{50}) concentration along with the respective pretreatment substance.

DMSO concentration was standardized to 0.165% v/v across all experimental groups. After 6 hours, cells were washed with PBS and loaded with 1 µM of the redox-sensitive fluorescent dye C11-BODIPY prepared from a 1 mM stock in 100% DMSO, as described by (Martinez et al., 2020). Following 15 minutes of incubation, adherent cells were washed with PBS (without Ca2+, Mg2+), trypsinized, and resuspended in 250 µl of MACS buffer (10% FCS, 2 mM EDTA in PBS). Fluorescence was measured using a 488 nm laser for excitation, with green fluorescence (oxidized dye) detected using an FL1 filter (533/30 nm) and red fluorescence (non-oxidized dye) using an FL2 filter (585/40 nm). A total of 10,000 gated events were collected.

Table 1 Cell Culture Media and MACS Buffer for Flow Cytometry Analysis

Culture Medium	Experimental Medium	MACS-Buffer
DMEM low glucose*	DMEM/F-12 low glucose*	PBS*
10% FCS**		10% FCS
		2mM EDTA

1% penicillin G/streptomycin sulphate (100µg/ml // 100µg/ml), sterile filtered was supplemented,
****** Fetal calf serum, heat inactivated, sterile filtered. DMEM: Dulbecco's modified eagle medium, EDTA: Ethylene diamine tetraacetic acid, FCS: Fetal calf serum, PBS: phosphate buffered saline, MACS: Magnetic-activated cell sorting, mM: millimolar, µg/ml: microgram per milliliter.***

2.5 Mouse Treatment with DMF in Vivo and Brain Dissection

Brain tissue from C57BL/6 wild-type mice (female, six weeks old, 20-25 g BW) exposed to DMF or to 10% DMSO (as vehicle control) was kindly provided by Michael Dietrich, a former researcher in our department. The tissue originates from a previous neuroophthalmological experiment published in 2020 (Dietrich et al., 2020). The animal experiments were conducted in accordance with protocols approved by the Ministry for Environment, Agriculture, Conservation and Consumer Protection of the State of North Rhine-Westphalia (animal protocols: AZ 8402.4.2014.A059 and AZ 84-02.04.2016.A137).

In brief, 15 mg/kg or 30 mg/kg body weight of DMF (20 mg/ml stock solution prepared in 10% DMSO) was administered daily in drinking water. To ensure precise dosing, the DMF concentrations in the water were adjusted to match the estimated daily drinking volume of mice. After seven days of treatment mice were anaesthetized and intracardially perfused with PBS. The whole brains were dissected, snap-frozen and stored at -80°C freezer for further sub-dissection, RNA isolation, or protein analyses.

After thawing, brain tissue from three and eight mice treated with 15 mg/kg BW and 30 mg DMF/kg BW, respectively, and from seven control mice was dissected into white and gray matter. White matter was obtained from the cerebellum and gray matter from the occipital cortex.

2.6 Gene Expression Analysis in OLN-93 Cells and Brain Parenchyma

Real-time quantitative PCR was employed to measure the expression levels of GPx4 and Hmox1 mRNA obtained from cultured cells, murine brain tissue, and PBMCs from human blood samples.

For RNA isolation, OLN-93 cells and dissected mouse brain tissue were stored at -80°C in 1 ml Trizol solution. Phenol/chloroform-based RNA extraction was performed according to the manufacturer's protocol for Trizol RNA isolation. Human blood samples stored in PaxGene tubes were thawed at 4°C and RNA isolation was performed using the Qiagen PaxGene RNA Blood Kit according to the manufacturer's protocol.

The NanoDrop™ 2000 spectrophotometer was utilized to determine the total RNA quantity in every sample. Purity assessments were carried out on RNA samples for any phenol/chloroform or protein contamination utilizing the NanoDrop™ 2000 tool. The RNA purification manuals were followed during the process. 2 µg of total RNA was used for cDNA synthesis using the High-Capacity cDNA

Reverse Transcription Kit. The cDNA obtained was diluted at a ratio of 1:5 in nuclease-free water and stored at +4°C. qPCR measurements were performed during the following 1-2 weeks.

qPCR analysis was performed on an Applied Biosystems 7000 instrument. Briefly, specific primer pairs (synthesized by Eurofins) were used to amplify genes of interest using SYBRGreen Master Mix. Gapdh (used as a housekeeping gene) was amplified using Taqman Master Mix and Gapdh-Fam/Tamra probe.
Duplicates of 15 µl of the mixtures and 5 µl of cDNA from each sample were added to an optical 96-well plate (suitable for the Applied Biosystems 7000 instrument), ensuring that it was protected from light. The plate was sealed using an optic membrane. Subsequently, qPCR was conducted utilizing a standard amplification protocol on the Applied Biosystems 7000 instrument with a program of 45 cycles. Ct values were used to quantify relative expression (RE) for each gene, normalized to the RE of Gapdh.

For human specimens collected at baseline and after a 12-month follow-up period, gene expression data were normalized using either 18S rRNA or β-actin as reference genes. The mRNA expression levels were then standardized relative to the median expression levels observed in healthy controls. For better comparability, the ratios of the gene expression values after 12 months of follow-up to the values before the start of the therapy are presents. In addition, the individual progressions are shown in line plots.

2.7 Bicinchoninic Acid Assay

To ensure equitability in protein concentration among each sample, a bicinchoninic acid assay (BCA) was performed. The BCA is a colorimetric method for quantifying proteins which is based on the reduction of protein-bound bivalent copper ions to monovalent ones under alkaline pH. The protein concentration in the sample can be measured via an absorbance plate reader using the absorbance at 562 nm, which is proportionate to the protein amount. Standard protein reference curve was employed for determining protein concentrations.

In this study, the BC Assay Protein Quantitation Kit from Interchim and bovine serum albumin (BSA) with a stock solution of 2 mg/mL were used as the standard protein. BSA standards were prepared by serial dilution of the stock with deionized water (dH_2O) to concentrations ranging from 6.25 µg/mL to 1000 µg/mL. 3 µl of each sample were diluted 1:10 in dH_2O. Duplicates were plated in a 96-well plate. Next, 10 µl of BSA standards and samples were added to a 96-well plate, followed by the addition of 150 µl of BCA assay reagent (50 parts solution A and 1 part solution B) to each well. The plate was incubated for 30 minutes at 37°C according to the standard protocol for plate assays (Interchim, 2023). The absorbance was measured at 562 nm using a TECAN reader. Interpolation of the protein concentrations in the samples was performed automatically using the reference curve for standard BSA. The protein concentration in each sample was generally normalized to 1 mg/ml with water.

2.8 Western Blotting

Western blotting was performed to analyze GPx4 expression levels in OLN-93 cells and brain tissues. Briefly, proteins were separated by gel electrophoresis based on their molecular weight by loading

onto an SDS-PAGE gradient gel and electrophoresing under denaturing (SDS) conditions. The proteins were then transferred to a nitrocellulose membrane. The separated protein bands were detected by immunostaining with specific primary and fluorescence-labelled (secondary) antibodies.

OLN-93 cells were seeded in each well of a six-well plate. After pretreatment with MMF or DMF for 24 hours, the cells were harvested using 100µl of trypsin (2x) and transferred to a 1.5ml Eppendorf tube using additional 900µl of ice-cold PBS. The supernatant was aspirated after centrifugation at 1500xg for 5 minutes at 4°C. Cells were washed 2 times to remove trypsin. For cell lysis, the pellet was resuspended in ice-cold (40 µl) radioimmunoprecipitation assay buffer (RIPA buffer) with the addition of a cocktail of protease and phosphatase inhibitors from Promega. Lysates were stored at -80°C (up to three months).

Prior to Western blotting, BCA (2.7) was performed to measure the total protein concentration in each sample. Total protein levels were then adjusted to 20 µg/100 µl using 10 µl 1M DTT, 25 µl 4X loading buffer and nuclease-free water. Each well of BioRad TransPlotGel (20 µl) was loaded with 15 µl of protein mixture. Additionally, one of the pockets was loaded with 5 µl of VWR Life Science's peqGOLD Protein Marker IV to run alongside the samples.
Gel electrophoresis was performed using the Bio-Rad Mini-Protean® Tetra System and the Biometra Standard Power Pack P25T at 120V for approximately 2 hours until the running front reached the black line at the end of the gel. Running buffer consisted of 10% TRIS-glycin-SDS buffer in water.
For protein blotting, proteins were transferred from the gel to a 0.2µm nitrocellulose membrane using the Trans-Blot Turbo™ Transfer System (Bio-Rad Laboratories). The membranes were then turbo-blotted for 10 minutes at 1.3 A and 25 V. To avoid non-specific antibody binding, the membranes were incubated in Bio-Rad EveryBlot Blocking Buffer for 1 hour at RT.
The membranes were immunostained with specific primary antibodies and IR-Dye secondary antibodies: rabbit anti-GPx4 (1:1000) and mouse anti-β-actin (1:5000). Mouse anti-β-actin served as loading controls for normalization. IR-Dye secondary antibodies (680 or 800) were used at a 1:15000 dilution. All antibodies were diluted in 2.5% BSA in PBS-T. Proteins on the membrane were simultaneously incubated with two primary antibodies (10 ml solution) overnight at 4ºC on a shaker. The membranes were washed three times in PBS-T (five minutes each) and then incubated with the appropriate fluorescence-labelled secondary antibodies) for 1-2 hours at room temperature on a shaker, protected from light. While the primary antibodies were reused up to five times, the secondary antibodies were always freshly prepared in their concentrations and protected from light.
Membranes were scanned using the ChemiDoc™ MP imaging system, and specific immunoreactive bands were quantified by densitometry using ImageJ software (RRID:SCR_003070).

2.9 Organotypic Cerebellar Slice Culture

To assess the protective effects of DRF and MMF against ferroptosis-induced demyelination, organotypic cerebellar slice cultures derived from C57BL/6 wild-type mouse brains (P9-P11) were isolated and cultured.

Organotypic cerebellar slice culture (OSC) is a well-established in vitro model that accurately represents all major cell types of the CNS and their physiological cell-to-cell interactions. In particular, cerebellar slices prepared from sagittal slices retain myelinated axons that can be propagated in

culture over long periods of time. Therefore, it is a valuable alternative to in vivo animal models such as EAE for drug screening and investigation of pathological mechanisms.

Figure 2 Procedure of Cerebellar Slice Preparation, Cultivation, Treatment, and Staining

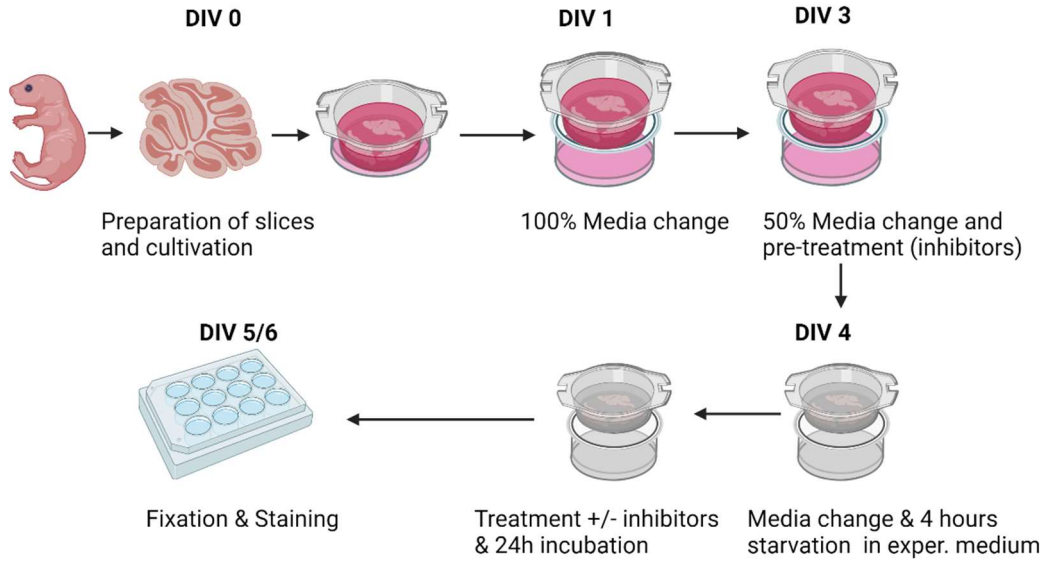

Fig. 2: Created with BioRender.com; DIV: Days in vitro.

To ensure the best possible outcome in terms of survival of the slices and their treatment a slightly modified protocol for slice preparation and culture from Kocur et al. (2015) based on Stoppini et al. (1991) and a slightly modified protocol for experimental manipulations from O'Sullivan and Dev (2017) were used here (see Figure 2). C57BL/6 wild-type mice (P9-P11) were sacrificed by decapitation. The cerebellum (see Figure 3) was dissected, carefully extracted and sectioned into 400µm thick sagittal slices using a McIlwain Tissue Chopper. Undamaged slices were collected in ice-cold dissection medium (see Figure 3, Table 2), separated and the remaining meninges removed under a Leica binocular microscope.

Figure 3 Schematic of the Mouse Brain and an Image of a Cerebellar Slice

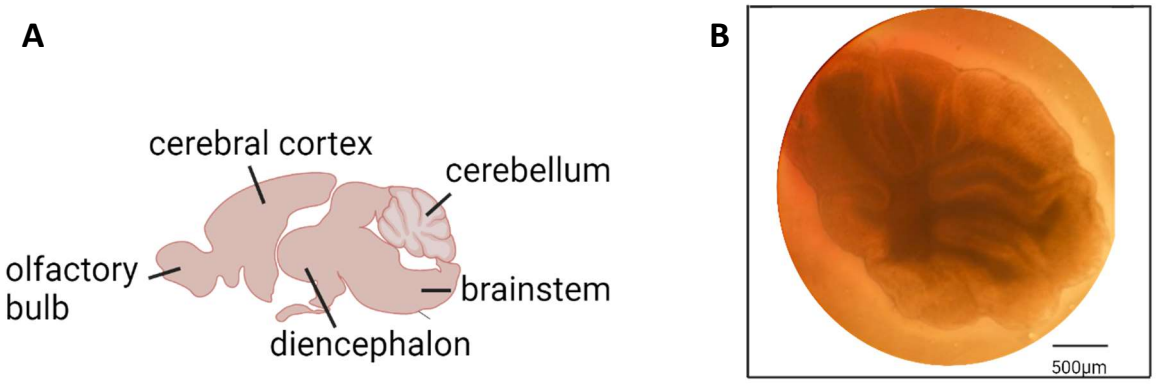

Fig. 3: A) Mouse brain, midline sagittal slice, created with BioRender.com. B) Undamaged sagittal cerebellar slice under light microscope, DIV 2 (used for culture). DIV: Days in vitro, µm: micrometer.

After washing in ice-cold washing medium (see Table 2) for 10 minutes, four slices from four different mice were transferred to the porous membrane of a cell culture insert (Millicell; pore size 0.2µm). 1 ml of tissue culture medium (see Table 2) was pipetted into each well below the insert.

All media mentioned have been optimized to contain the necessary nutrients to maintain cell viability.

Table 2 Media for Organotypic Slice Cultures

Dissection medium (pH=7,4)**	Washing medium	Slice culture medium	Experimental slice culture medium
100% HBSS* (with Ca2+, Mg2+)	50% **MEM*** (no glutamine)	50% **MEM*** (no glutamine)	75% **Opti-MEM Medium**
1mM kynurenic acid (dissolved in 2ml NaOH)	50% **HBSS*** (with Ca2+, Mg2+)	25% **HBSS*** (with Ca2+, Mg2+)	25% **HBSS** (with Ca2+, Mg2+)
1.1% glucose 45%	2.5% **HEPES** 25mM	25% **Horse serum** (heat inactivated)	1.1% **glucose** 45%
		1,1% **glucose** 45%	
		1% **Glutamax** (2mM L-glutamine)	

All media were supplemented with 1% penicillin G/streptomycin sulphate (100µg/ml // 100µg/ml) and sterile filtered, **pH adjustment for dissection media was made by bad buffering.
Ca: Calcium, HBSS: Hanks' balanced salt solution, MEM: Mg: Magnesium, NaOH: Sodium hydroxide, mM: millimolar, µg/ml: microgram per mililiter, pH: potentia hydrogenii.

In addition, culture conditions were adapted to physiological conditions to ensure optimal cell viability. The slices were cultured at 37°C, 5% carbon dioxide and 80% relative humidity. After 24 hours, the culture medium was completely replaced to remove toxic waste products. From the third day, 50% (0.5 ml) of the medium was replaced with fresh medium every other day to ensure the continued presence of factors produced that are important for myelin maintenance (e.g. CNTF from astrocytes, see Sendtner et al. (1994)).

After three days in vitro (DIV3), the slices were pretreated with potential (fumarates) or known (LIP-1) inhibitors of lipid peroxidation and incubated under the same physiological conditions as before. After 24 hours, the entire medium was replaced with experimental horse serum-free slice culture medium (ESCM), which did not contain serum-derived antioxidants. After 4 hours of starvation to increase potential myelin damage by ferroptosis inducers and to elucidate the role of intrinsic antioxidant enzymes in the absence of plasma antioxidants, slices were treated with the ferroptosis inducers Erastin and iron (in the form of ammonium ferrous sulphate $(NH_4)_2Fe(SO_4)_2$ and incubated at 37°C for 24 hours. In the case of slices pretreated with fumarate or LIP-1, the corresponding substances were again added to the ESC medium. To avoid the formation of precipitates of ferrous ammonium sulphate, which would damage the section, the slices were incubated on a horizontal shaker at 37°C, 10 rpm.

After 24 hours, the slices were fixed with 4% paraformaldehyde (PFA) for 30 minutes on a shaker at room temperature (RT). After three washes with PBS, the slices were stored in PBS at 4°C.

2.10 Immunohistochemistry

To sufficiently enable antibodies to access intracellular target antigens, fixed slices were incubated with 1.5% TritonX-100 in PBS (v/v) for 45 minutes at RT to effectively permeabilize the tissue and cellular membranes. After washing the insert membranes three times with PBS, the individual tissue sections were cut out and transferred en bloc into a 12-well plate with 500 µL blocking buffer (or a 48-well plate with 100 µL blocking buffer) (see Table 3). To avoid any non-specific binding of antibodies to undesired antigens and to reduce background staining, samples were treated with blocking buffer for 45 minutes at room temperature. Primary antibodies anti-MBP and anti-NF200 were then applied in an antibody solution (see Table 3) and incubated overnight at 4°C on a shaker, 10 rpm. Myelin basic protein (MBP) is an essential protein of the myelin sheath and provides an excellent target for the detection of myelin and myelin debris. Neurofilament component 200k (NF200) is primarily located in large, myelinated axons and functions as a marker for evaluating axon morphology, distribution, and density.

After three washes (the first with 0.1% Triton X-100, followed by PBS), the slices were incubated with secondary antibodies (see Table 3) for 2 hours at RT, protected from light.

After three additional washes, a nuclear acid stain (Hoechst 33342) was applied in the initial wash at a 1:1000 dilution to stain the nuclei. The membrane with the slices were mounted onto a microscope slide with objective glass, placing the membrane side on the glass and using ImmuMount for adherence. A cover slip with a thickness of 0.17mm was used to cover the slide. The slides with slices were dried at RT for 24 hours, stored (upright) at 4C and analyzed by fluorescence microscopy (Olympus BX51).

Table 3 Blocking Buffer, Antibodies and Antibody Solution for Immunohistochemistry

Blocking buffer	Antibody solution	Primary antibodies	Secondary antibodies
94.75% PBS*	50% blocking buffer	Anti-MBP (rat) 1:500	Goat ag. rat Cy3® 1:500
5% Goat serum**	50% PBS*	Anti-NF200 (rabbit) 1:500	Goat ag. Rabbit Cy2® 1:500
0.25% Triton-X 100			Hoechst 1:1000

supplemented with 1% penicillin G/streptomycin sulphate (100µg/ml // 100µg/ml), sterile filtered, ** sterile filtered; ag.: against, MBP: Myelin basic protein, NF: Neurofilament, PBS: Phosphate buffered saline.

2.11 Analysis of Myelin and Axonal Damage in Organotypic Slice Culture

The evaluation process was completely blinded. The cerebellar slice treatments' descriptions were masked on microscope slides and arranged in random order. Two independent assessors visually classified the demyelinated areas and axonal damage in each cerebellar branch by using fluorescence microscopy (Olympus, BX51).

Specifically, myelin damage/demyelination was assessed by evaluating a reduced MBP fluorescence signal, myelin conglomerates away from axons, and myelin debris (based on the shape of MBP

staining). Axonal damage was assessed by reduction in NF200 fluorescence, axonal bulges and fragmentation. The degree of damage for each branch was classified into one of five classes ranging from 0% (complete destruction) to 100% (complete preservation). The mean value across all cerebellar branches was calculated for every slice. The interrater reliability of these means was analyzed utilizing the Pearson correlation coefficient. Any coefficient exceeding 0.8 was deemed almost perfect, and the outcomes were employed for experimental analysis.

2.12 Animal Experiment Approval

Tissue collection for cerebellar slice cultures was conducted in compliance with approved animal experimentation protocol number O47/08. This protocol authorized the harvesting of organs for research purposes. All experiments were conducted in accordance with the ARRIVE criteria (https://arriveguidelines.org/). The mice were bred under conditions that were specifically pathogen-free and kept in individually ventilated cages for the experiments.

2.13 Patients and ethical vote

Blood samples were taken from the biobank of the Department of Neurology at Düsseldorf University Hospital (Registration Number: 2017044238, Study Number 5951R, date of ethics vote: 28.06.2018) from patients with RRMS who had undergone a change in immunotherapy. The samples were taken both before the start of treatment and 12 months afterwards. The study cohort comprised six RRMS patients taking an oral dose of 240 mg DMF (Tecfidera®) twice daily. A comparative control group consisted of six MS patients who received intravenous infusions of 600 mg OCR (Ocrevus®) bi-annually, without prior administration of DMF. In addition, a second control group of four healthy donors was formed. The healthy blood donors willingly contributed their blood samples and had no reported auto-immune diseases or diseases affecting the CNS, heart, kidneys and liver. They were in good overall health at the time of sample collection.

Patients in all cohorts were carefully selected and matched by age and sex. In addition, patients within the RRMS groups were matched for disease duration EDSS scores (see Table 4). Due to insufficient mRNA concentration in a sample obtained from one DMF-treated patient, both this patient and her matched partner were excluded from the study. This implies that each patient group comprised five individuals, while the healthy donor group consisted of four individuals (Table 4).

The blood samples from the DMF group were stored at -20°C for an average duration of 4.9 years ± 7.6 months prior to therapy initiation and 3.9 years ± 7.1 months after the 12-month follow-up period. Similarly, for the OCR group, the samples were stored for an average of 4.8 years ± 5.7 months prior to therapy initiation and 4 years ± 1 month after the 12-month follow-up period. In contrast, samples from the healthy control group were stored for an average of 5 days ± 1 day.

Regarding age and sex, all three groups are comparable: 40.2 years ± 10.9 years with two males in the DMF group, 40.7 years ± 10.2 years with two males in the OCR group, and 39.5 years ± 9.6 years with two males among the healthy donors.

The disease duration differed between treatment groups, with DMF patients having a shorter duration (median: 7.6 months, IQR: [5.8 months, 1.3 years]) compared to the OCR group (median: 4.84 years, IQR: [3.8 years, 7.8 years]) (Figure 4). In the DMF group, four out of five patients were

treatment-naïve at therapy initiation, while one patient had concluded their last immunotherapy 12 months prior (Figure 4). In contrast, only two out of five patients in the OCR group were treatment-naïve. The remaining three OCR patients had previously received highly effective immunotherapies, such as natalizumab and daclizumab, which were discontinued due to increased risk factors despite their efficacy. Specifically, natalizumab was discontinued due to an elevated JC virus antibody index, while daclizumab was withdrawn in 2018.

Figure 4 Disease Courses and Individualized Maintenance Immunotherapy in 10 RRMS Patients

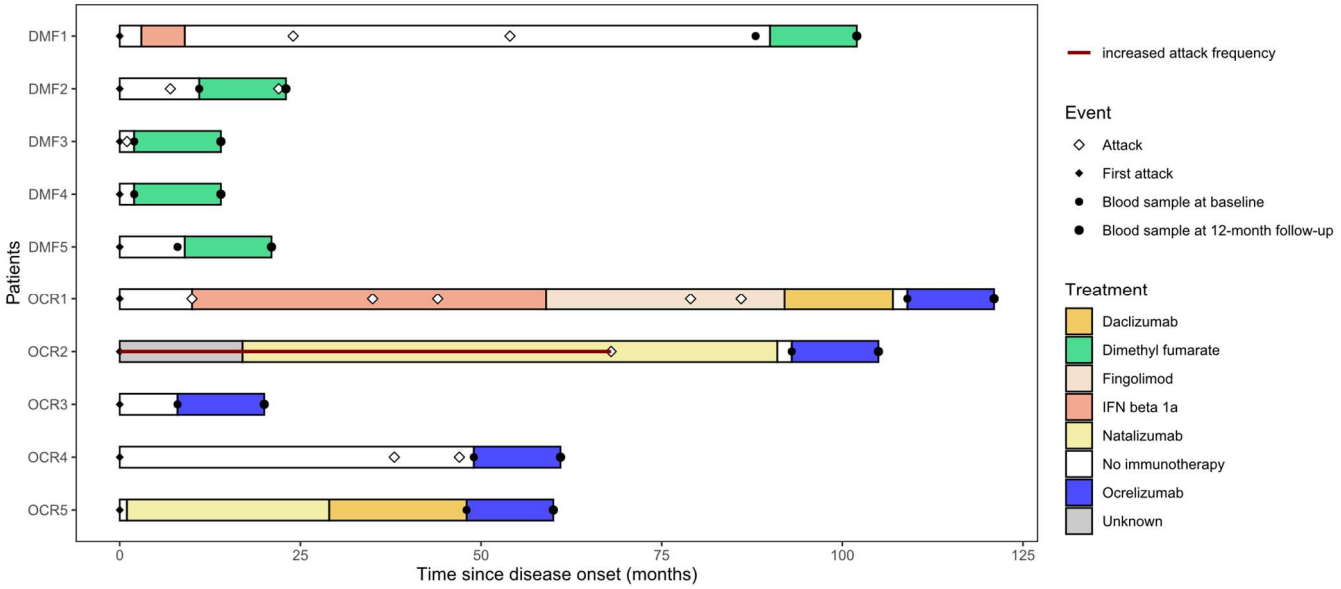

Fig. 4: 5 DMF-patients were matched with 5 OCR-patients regarding age and sex. First attacks are shown as black diamonds and subsequent attacks as white diamonds. Blood sampling times are shown as black circles. For OCR2, the exact number of attacks before 2016 is unknown; DMF: Dimethyl fumarate, IFN: Interferone, OCR: Ocrelizumab.

At baseline, the median EDSS was lower in the DMF group (2.0, IQR: [1.5, 2.0]) than in the OCR group (3.0, IQR: [1.0,5.0]). EDSS values remained stable over 12 months of treatment, with a slight decrease observed (DMF: median 1.0, IQR: [1.0,2.0]; OCR: median 3, IQR: [0, 4.5]). Baseline annualized attack rates (AAR) for the two years prior to treatment were comparable (DMF: 0.5, IQR: [0,1.0]; OCR: 0.5, IQR: [0,0.5]). The low baseline AAR in the OCR group was attributed to prior highly effective immunotherapies. After 12 months of treatment, AAR decreased to 0 (IQR: [0,0]) in both groups, with one attack occurring in the DMF group at 10 months.

Table 4 Detailed Information of the 10 RRMS Patients and 4 Blood Donors

Patient	Age at DMF/ OCR start	Sex	Pre-immunotherapies	EDSS at DMF/OCR start	AAR two years prior DMF/OCR start	Attacks under DMF/OCR	Side effects
DMF1	30 yrs	m	IFN beta	2	0.5	No	Flush
DMF2	26 yrs	f	None	1.5	1	Yes	Flush, gastro-intesti-nal complaints
DMF3	51 yrs	m	None	2	1	No	Lymphopenia
DMF4	45 yrs	f	None	2	0.5	No	None
DMF5	48 yrs	f	None	1	0.5	No	None
OCR1	32 yrs	m	IFN beta, Fingolimod, Daclizumab	1	0.5	No	None
OCR2	49 yrs	f	Natalizumab	6.5	0	No	None
OCR3	51 yrs	m	None	5	0.5	No	None
OCR4	27 yrs	f	None	1	1	No	None
OCR5	44 yrs	f	Natalizumab, Daclizumab	3	0	No	None
Healthy1	44 yrs	f	None				
Healthy2	50 yrs	m	None				
Healthy3	30 yrs	f	None				
Healthy4	32 yrs	m	None				

Blood samples were extracted from both patients treated with DMF or OCR, as well as from matched healthy control individuals, in order to measure the levels of expression of GPX4 and Hmox1 mRNA , OCR: Ocrelizumab, DMF: Dimethyl fumarate, IFN beta: Interferon beta, AAR: annualized attack rate, EDSS: Expanded Disability Status Scale, m: male, f: female, yrs: years.

2.14 Data Analysis

Statistical analysis was performed using version 4.0.5 of the R statistics package. The results of the experiments were expressed as mean or median and standard deviation (SD) or interquartile range (IQR). In contrast to the actual definition, the IQR is presented as an interval from the 1st quartile to the 3rd quartile, rather than as their distance, to provide a clearer representation of the data dispersion, especially when the sample sizes were very small. Depending on the data dispersion and the nature of the variables being analyzed, either the Spearman correlation coefficient ρ or the Pearson correlation coefficient r was determined. Likewise, depending on the data situation, the data was visualized using bar plot with error bars, dot plots with or without box plots and scatter plots as well as a swimmer plot to illustrate individual disease progressions. The Wilcoxon rank-sum test was employed to compare two independent groups (e.g., two different treatments), assessing whether the distributions of their observations differ significantly. The Wilcoxon signed-rank test was used for paired data, such as pre- and post-therapy results, to evaluate whether there was a significant difference between paired observations within the same group. For analyses involving more than two groups, the Kruskal-Wallis test with the Dunn post hoc test and Dunn-Bonferroni correction was applied.

The R package 'drc' (Ritz et al., 2015) was utilized to analyze cell viability and dose-response curves. For slice culture experiments, interrater reliability of scores was analyzed using Pearson's correlation coefficient. A coefficient greater than 0.8 was considered near perfect and the results were used for experimental analysis. Results of statistical tests are presented as p-values with a significance level of alpha=0.05. Statistical tests were performed, and p-values were determined only when appropriate.

ImageJ (www.imagej.net) was used to measure optical densities on Western blots. Kaluza analysis software (Beckman Coulter, Version 2.1) was used for analysis of FACS data.

2.15 Cell Line and Mouse Strain

Name	Reference	Supplier, order number
OLN-93 cell line	C. Richter-Landsberg, 1996	Glow-Biologics, USA, GBTC-0366H
C57BL/6J wildtype		Internal breeding, project number O74/08

2.16 Chemicals

Product Name	Reference	Order number
BSA Standard	Interchim, France	UP36859A
BODIPY™ 581/591 C11	Invitrogen, USA	2362423
CellTiter-Blue®	Promega, USA	G8082

Dimethyl fumarate (DMF)	Sigma-Aldrich, USA	242926
Diroxymel fumarate (DRF)	Biogen, Germany	promotional product
Dimethyl sulfoxide (DMSO)	Sigma-Aldrich, USA	SHBM0176
Dithiothreitol (DTT)	Bio-Rad Laboratories, Germany	1610611
Dulbecco's modified eagle medium (DMEM)	Thermo Fisher Scientific, USA	2436378
Dulbecco's modified eagle medium (DMEM)/F-12	Invitrogen, USA	31330038
Dulbecco's phosphate buffered saline (DPBS)	Thermo Fisher Scientific, USA	2375288
Ethylene diamine tetraacetic acid (EDTA)	Sigma-Aldrich, USA	E6758
Erastin	Sigma-Aldrich, USA	E7781
70% Ethanol	AppliChem, Germany	A2192
Ferrous ammonium sulphate	Sigma-Aldrich, USA	1037920500
Fetal Bovine Serum (FBS) (=FCS)	Thermo Fisher Scientific, USA	10500064
20% Glucose	Thermo Fisher Scientific, USA	2390221
GlutaMAX™ (100x)	Thermo Fisher Scientific, USA	2401813
Normal Goat serum	Invitrogen, USA	31873
Hanks' balanced salt solution (HBSS) $+Ca^{2+}$,$+Mg^{2+}$)	Thermo Fisher Scientific, USA	2131865
Hoechst 33342	Thermo Fisher Scientific, USA	15831459
(N-2-hydroxyethylpiperazine-N-2- ethane sulfonic acid) (HEPES 1M)	Thermo Fisher Scientific, USA	2193374
Horse serum	Thermo Fisher Scientific, USA	16050130
Immu Mount	Fisher Scientific, USA	9990402
Kynurenic acid	Sigma-Aldrich, USA	K3375
Lipopolysaccharide	Sigma-Aldrich, USA	L8274

Liproxstatin-1	Sigma-Aldrich, USA	SML1414
Monomethyl fumarate	Sigma-Aldrich, USA	651419
Minimal essential medium (MEM) (no glutamine)	Thermo Fisher Scientific, USA	2192687
Sodium hydroxide solution 2mol/l	Carl Roth, Germany	T135.1
Nuclease-free water	Invitrogen, USA	AM9937
Opti-MEM	Thermo Fisher Scientific, USA	31985062
4%- Paraformaldehyde solution in PBS	Thermo Fisher Scientific, USA	j61899.AK
Penicillin/ Streptomycin	Thermo Fisher Scientific, USA	2441409
Propidium iodide	Thermo Fisher Scientific, USA	P1304MP
Protease/phosphatase inhibitors	Thermo Fisher Scientific, USA	78429
Protein loading buffer (4x)	LI-COR Bioscience, USA	928-40004
Radioimmunoprecipitation assay buffer (RIPA)	Sigma-Aldrich, USA	R0278
Salicylaldehyde isonicotinoyl hydrazine (SIH)	Cayman Chemicals, USA	33314
10x TRIS/Glycin/SDS	Bio-Rad Laboratories, Germany	1610772
Trypan Blue 0.4% solution	Thermo Fisher Scientific, USA	15250061
10% Triton X-100	Sigma-Aldrich, USA	93443
TRIzol	Thermo Fisher Scientific, USA	15596026
0.5 % Trypsin-EDTA (10x)	Thermo Fisher Scientific, USA	2511568
VWR Life Science´s pegGOLD protein marker IV	VWR Life Science, USA	27-2110

2.17 Antibodies

Antibody (host)	**Reference**	**Order number**
Anti-α-tubulin (rat)	Abcam, UK	ab7291
Anti-β-actin (mouse)	Abcam, UK	ab8226

Anti-GPx4 (rabbit)	Abcam, UK	ab231174
Anti-MBP (rat)	Sigma-Aldrich, USA	MAB386
Anti NF200 (rabbit)	Sigma-Aldrich, USA	N4142
IR680 anti mouse IgG	Invitrogen, USA	35519
IR800 anti rabbit IgG	Invitrogen, USA	SA5-10036
IR800 anti rat IgG	Invitrogen, USA	SA5-10024
Goat against rabbit Cy2®	Millipore, USA	AP202J
Goat against rat Cy3®	Millipore, USA	AP136C

2.18 Primers and Probes

Product name	**Reference**	**Order number/ Oligonucleotides 5´->3´**
SYBR™ Green Master Mix	Thermo Fisher Scientific, USA	A46109
TaqMan® Fast Advanced Master Mix	Thermo Fisher Scientific, USA	4444557
mrhHmox1 F1	Eurofins, Germany	GCCGAGAATGCTGAGTTCATG
mrhHmox1 R1	Eurofins, Germany	TGCAGCTCCTCAGGGAAGTAGA
mrhGPx4 F1	Eurofins, Germany	CCGATACGCTGAGTGTGGTT
mrhGPx4 R1	Eurofins, Germany	TCACCACGCAGCCGTTCT
mrhMbp F1	Tim Prozorovski	CACAGAGACACGGGCATCCT
mrhMbp R1	Tim Prozorovski	TCTGCTTTAGCCAGGGTACCTT
mrhMbp probe(Fam/TAMRA)	Tim Prozorovski	CATCCTTGACTCCATCGGGCGC
mrTubb3 F1	Tim Prozorovski	GCCAAGTTCTGGGAGGTCATC
mrTubb3 R1	Tim Prozorovski	CCGAGTCCCCCACATAGTTG
mGfap F1	Tim Prozorovski	AACCGCATCACCATTCCTGTA
mGfap R1	Tim Prozorovski	TGGTGTCCAGGCTGGTTTC
hTfrc F1	Tim Prozorovski	TCAAGCCAGATCAGCATTCTCTAA

hTfrc R1	Tim Prozorovski	TCCACATGACTGTTATCTCCATCTACTT
hTfrc1 Probe (Fam/TAMRA)	Tim Prozorovski	TCATACACCCGGTTTAGCCTTGCTCG
h18S rRNA F1	Tim Prozorovski	CGGCTACCACATCCAAGGAA
h18S rRNA R1	Tim Prozorovski	TGCTGGCACCAGACTTGCCCTC
h18S rRNA probe (Fam/TAMRA)	Tim Prozorovski	GCTGGAATTACCGCGGCT
mGapdh F1	Tim Prozorovski	CCAGCCTCGTCCCGTAGAC
mGapdh R1	Tim Prozorovski	CCATTCTCGGCCTTGACTGT
mGapdh probe (Fam/TAMRA)	Tim Prozorovski	CGGATTTGGCCGTATTGGGCG
rGapdh F1	Tim Prozorovski	*AGATGGTGAAGGTCGGTGTGA*
rGapdh R1	Tim Prozorovski	TGCCGTGGGTAGAGTCATACTG
rGapdh Probe (Fam/TAMRA)	Tim Prozorovski	CGGACGCCTGGTTACCAGGGC
rActb (β-actin) F1	Tim Prozorovski	CCCGCGAGTACAACCTTCTTG
rActb (β-actin) R1	Tim Prozorovski	AAGCCGGCCTTGCACAT
mhActb (β-actin) F1	Tim Prozorovski	GGCACCCAGCACAATGAAG
mhActb (β-actin) R1	Tim Prozorovski	GCCGATCCACACGGAGTACT

h: human, m: mouse, r: rat, F: forward, R: reverse, Actb: β-actin, Tubb3: β-III tubulin, Gfap: Glial fibrillary acidic protein, Gapdh: Glyceraldehyde 3-phosphate dehydrogenase, Gpx4: Glutathione peroxidase 4, Hmox1: Heme oxygenase 1, Mbp: Myelin basic protein, rRNA: ribosomal ribonucleic assay, Tfrc: Transferrin receptor

2.19 Kits

Product name	**Reference**	**Order number**
BC Assay Protein Quantification Kit	Interchim, France	UP40840A
High-Capacity cDNA Reverse Transcription Kit	Thermo Fisher Scientific, USA	4368814
MycoStrip™ mycoplasma detection kit	InvivoGen, France	rep-mys-10
Qiagen PaxGene RNA Blood Kit	Qiagen, Germany	762164

2.20 Material

Product name	Reference	Order number
Bio-Rad Mini-Protean TGX Stain-Free Gels	Bio-Rad Laboratories, Germany	4568096
Bio-Rad Every Blot Blocking Buffer	Bio-Rad Laboratories, Germany	12010020
Cell culture flask, 175 cm2	Greiner Bio-One, Germany	660160
Counting Slides	Bio-Rad Laboratories, Germany	1450016
Cryo Vials (2ml)	Greiner Bio-One, Germany	122261
Disposal bag 700x1100mm	VWR Life Science, USA	129-9714
Eppendorf tube, 0.5ml	Sigma-Aldrich, Germany	EP0030124537
Eppendorf tube, 1.5ml	Sigma-Aldrich, Germany	HS4323
Eppendorf tube, 2ml	Sigma-Aldrich, Germany	Z628034
Falcon, 15ml	Greiner Bio-One, Germany	T1943
Falcon, 50ml	Greiner Bio-One, Germany	T2318
Filter, 0.2µm	Sigma-Aldrich, Germany	CLS431231
Filtropur 500ml	Sarstedt, Germany	22-2489CR
Glass coverslips, 24 x 50mm	VWR Life Science, USA	630-2603
Greiner Cellstar dish	Greiner Bio-One, Germany	639160
INTEGRA inserts	INTEGRA Biosciences, Germany	6318
Microscope slide 76x26mm	Engelbrecht Medizin-&Labortechnik, Germany	11102
Millipore-Millicel-CM culture inserts	Sigma-Aldrich, Germany	PICM03050
Original Perfusor Syringe 50ml	Braun, Germany	21G09D8008
PaxGene blood RNA tubes	Qiagen, Germany	762165
Safeshield scalpel No.15	PFM Medical AG	23050452

Stripettes (2ml-25ml)	Sigma-Aldrich, Germany	CLS4486, CLS4487, CLS4488, CLS4489
Pipette tips (20µl-1000µl)	Starlab, Germany	S1111-3200, S1113-1716, S1111-6001
Syringe Omnifix® Luer Lock Solo 20ml	Braun, Germany	24E20C8
6-well plate	Greiner Bio-One, Germany	657160
24-well plate	Greiner Bio-One, Germany	662160
48-well plate	Greiner Bio-One, Germany	677180
96-well plate (U)	Greiner Bio-One, Germany	650180
96-well plate (Flat-bottom)	Greiner Bio-One, Germany	655180

2.21 Equipment

Product name	**Producer**
Applied Biosystems 7000 instrument	Applied Biosystems, USA
TC10 Automated Cell Counter	Bio-Rad Laboratories, USA
Binocular	Leica, Germany
Biometra Standard Power Pack P25T	Biometra, Germany
HI221 Calibration Check Microprocessor pH Meter	HANNA instruments, USA
Centifuge Rotanda 460R	Hettich AG, Switzerland
Centrifuge 5417R	Eppendorf, Germany
Centrifuge 5418	Eppendorf, Germany
ChemiDoc™MP imaging System	Bio-Rad Laboratories, USA
Chirurgical instruments	Fine Science Tools, Canada
CytoFLEX S	Beckman Coulter, USA
Eppendorf mastercycler	Eppendorf, Germany

Eppendorf pipettes (0.5µl-1000µl)	Eppendorf, Germany
Eppendorf thermomixer comfort 1.5ml	Eppendorf, Germany
Fluorescence microscopy BX51	Olympus K.K., Japan
F-View CCD Camera	Olympus K.K., Japan
Incubator Heracell 240i	Thermo Scientific , USA
INTEGRA pipetboy 2	Integra Biosciences, Germany
McIlwain Tissue Chopper	Mickle Laboratory Engineering Co. Ltd., USA
Microscope Osram 644275	Hund Wetzlar, Germany
Multichannel pipette	Eppendorf, Germany
NanoDrop™ 2000 spectrophotometer	Thermo Scientific, USA
Olympus U-RFL-T Burner	Olympus K.K., Japan
3D Rocking Shaker	Starlab smart instruments, Germany
TECAN GENios Microplate Reader	TECAN, Switzerland
Vortexer	VWR International, USA

2.22 Software

Software name	**Software-Repository/ Publisher**	**Version**
BioRender	Shiz Aoki, Canada, https://app.bioren-der.com/	2024
EndNote™	Clarivate Analytics, USA	21.2.0.17387
ImageJ	Wayne Rasband, USA, https://imagej.net/	1.51
Kaluza	Beckman coulter, USA	2.1
Microsoft Office 365	Microsoft Corporation; USA	2024
R statistics package	CRAN team, https://cran.r-project.org/	4.0.5

3 Results

First, the susceptibility of oligodendrocytes to ferroptotic cell death following exposure to varying concentrations of established ferroptosis inducers such as Erastin and iron is presented. To determine the ferroptotic nature of oligodendrocyte death, lipid peroxidation levels were quantified. These cell culture experiments were performed with OLN-93 cells. Furthermore, ferroptosis is shown to induce demyelination in cerebellar OSCs. Simultaneously, the potential of fumarates, particularly DRF and its active component MMF, to protect oligodendrocytes from accumulation of lipid peroxidation, subsequent ferroptotic cell death and demyelination is demonstrated.

Next, the extent of upregulation of GPx4 compared to the established Nrf2 gene Hmox1 after fumarate treatment in OLN-93 cells is shown. To translate the cell culture results to animal and patient samples, brain tissue from DMF-treated mice and PBMCs from DMF-treated patients were examined for upregulation of GPx4. For the latter, the mRNA expression levels of GPx4, Hmox1 and TfR1 were measured in PBMCs from RRMS patients at baseline and after 12 months of treatment with DMF and compared to a group of healthy controls and RRMS patients receiving ocrelizumab.

3.1 Ferroptotic Susceptibility of OLN-93 Cells and Protective Effects of Fumarate Treatment

The susceptibility of oligodendrocytes to ferroptosis was assessed by exposing them to different concentrations of the known ferroptosis inducers Erastin and iron. Subsequently, the ability of fumarates to attenuate ferroptotic death of oligodendrocytes was analyzed. For this reason, cell survival assays were performed on the OLN-93 cell line.

OLN-93 cells were exposed to increasing concentrations of Erastin (0, 0.1, 0.32, 1, 3.2, 10 µM) and iron (0, 1, 3.2, 10, 32, 100, 320, 1000 µM). The IC_{50} values for Erastin and iron were 2.3 ± 0.5 µM and 362.5 µM, respectively (Fig. 5A,D). To determine the appropriate doses for OLN-93-cell protection by MMF and DRF, OLN-93 cells were pretreated with increasing concentrations of MMF and DRF (0, 0.1, 0.32, 1, 3.2, 10, 32, 100 µM) and incubated for 24 hours. The cells were then treated with Erastin at the mean IC_{50} concentration of 2.3 µM and additionally with the corresponding concentrations of MMF or DRF as before. A plateau was observed in the cell survival curve at a concentration of 2µM DRF (Fig. 5C). While a minimum of 50% of the cells survived at 10 µM MMF, cytotoxicity exhibited a tendency to increase in OLN-93 cells at 10 µM DRF. Therefore, concentrations of 2µM and 10µM MMF/DRF were used for further experiments.

To analyze whether DRF and MMF can enhance the survival rate of oligodendrocytes against ferroptotic cell death, OLN-93 cells were exposed to increasing concentrations of Erastin or iron, as described before. The IC_{50} values in untreated control cells and in cells treated with 2 or 10 µM DRF or MMF were determined.

Figure 5 Cell Survival in OLN-93 Cells after Treatment with Ferroptosis Inducers and Fumarates

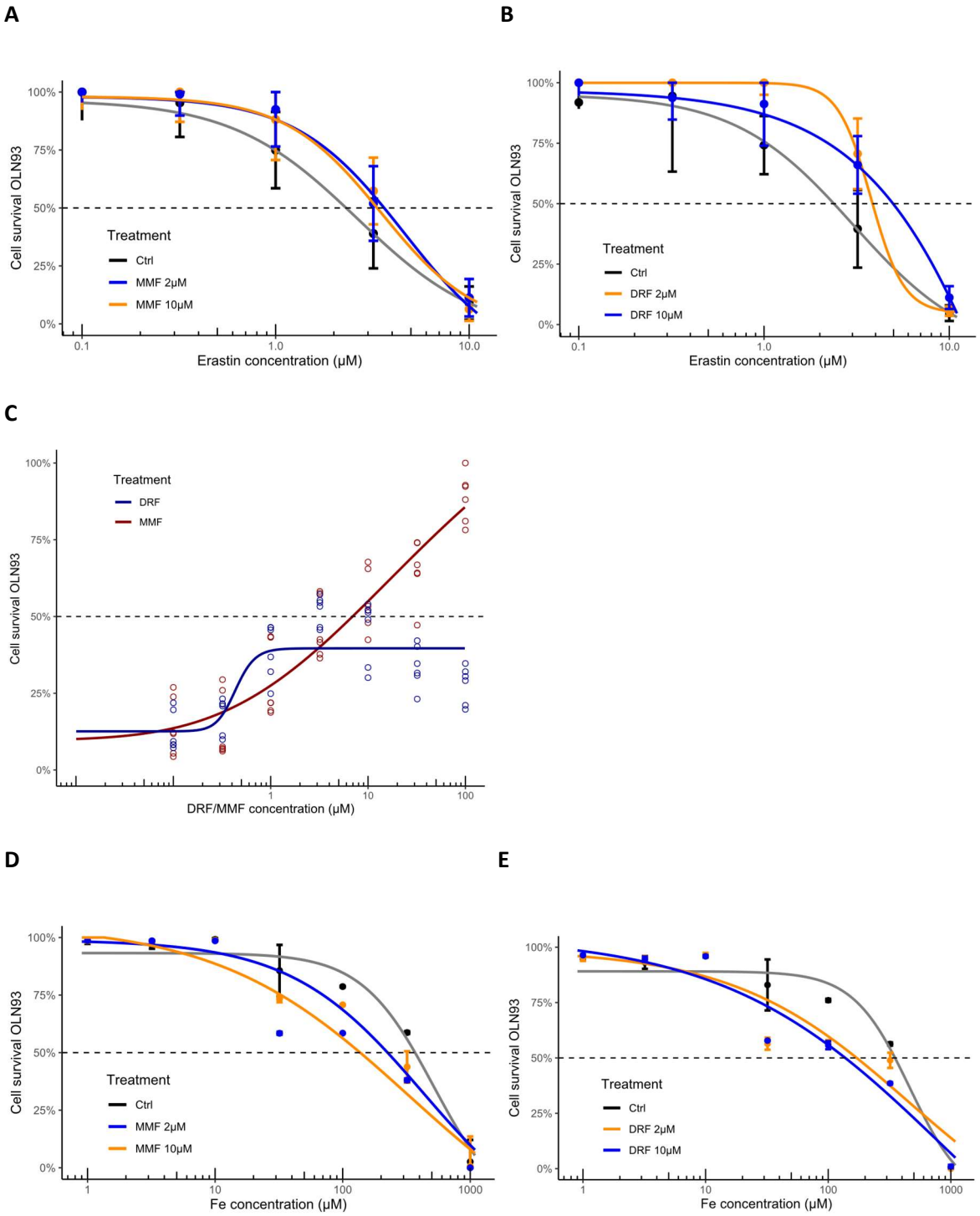

Fig. 5: Cell survival curves: A,B) OLN-93 cells were exposed to increasing concentrations of Erastin after a 24-hour pretreatment with MMF or DRF. Cell survival was assessed by CTB assay, n=3 experiments, 2 replicates each. C) Dose-response curve for increasing concentrations of MMF or DRF, OLN-93 cells were treated with Erastin (Erastin concentration corresponded to the mean IC_{50} concentration 2.3μM), n=3 experiments. D,E) OLN-93 cells were exposed to increasing concentrations of iron after a 24-hour pretreatment with MMF or DRF. Cell survival was assessed by PI assay, n=1 experiment, 2 replicates each; Ctrl: Control, DRF: Diroximel fumarate, Fe: Iron, MMF: Monomethyl fumarate, μM: micromolar.

For cells treated with Erastin, the IC_{50} values increased from 2.3 ± 0.5 µM in control cells to 3.6 ± 0.7 µM (2 µM DRF), 4.4 ± 2.2 µM (10 µM DRF), 3.7 ± 1.0 µM (2 µM MMF), and 3.6 ± 1.2 µM (10 µM MMF) (Fig. 5A,B). In cells treated with iron, the IC_{50} values decreased from 362.5 µM in control cells to 173 µM (2 µM DRF), 138 µM (10 µM DRF), 225 µM (2 µM MMF), and 135 µM (10 µM MMF) (Fig. 5D,E).

For OLN-93 cells treated with Erastin, cell survival analyses were performed three times with two replicates each. However, survival analysis for OLN-93 cells treated with iron was only performed once, resulting in n=1 with two replicates each.

In summary, the survival rate of OLN-93 cells decreased with increasing concentrations of ferroptosis inducers Erastin and iron. However, pretreatment with the fumarates MMF and DRF increased cell survival rates when exposed to Erastin. It is important to note that fumarates did not protect against cell death when cells were exposed to iron. In fact, the viability of the fumarate pre-treated cells was even lower than the control cells that were not pre-treated.

3.2 Fumarate Treatment Does Not Significantly Reduce Lipid Peroxidation in OLN-93 Cells

It was analyzed whether the cell death of the oligodendrocytes was indeed preceded by an accumulation of lipid peroxidation, suggesting that the cells died by ferroptotic cell death. It was further investigated whether DRF and MMF are able to protect the cells by reducing lipid peroxidation, suggesting that fumarates can indeed protect the cells from ferroptotic cell death.

Therefore, the extent of lipid peroxidation after Erastin-induced ferroptosis in OLN-93 cells was investigated by flow cytometry. The lipid peroxidation values after fumarate pretreatment were compared to the values after pretreatment with the established ferroptosis inhibitor LIP-1. LIP-1 at concentrations of 100nM was utilized to inhibit Erastin-induced ferroptosis. Cell survival was observed at 2 µM DRF and MMF in the cell viability assay, and no significant difference was observed compared to 10 µM. Therefore, the cells were only treated at the low concentration here.

Following an incubation period of between three or 24 hours with potential ferroptosis inhibitors, Erastin was added at a concentration corresponding to the IC_{50} (one-fold to four-fold) in the cell viability assay (2.5 µM-10 µM) in combination with the corresponding ferroptosis inhibitor (2 µM DRF, 2 µM MMF, 10 µM or 100 nM LIP-1). After a 6-hour incubation period, the cells were stained with the redox-sensitive fluorescent dye BODIPY™ 581/591 C11. The level of lipid peroxidation in cell membranes was quantified as fluorescence intensity via flow cytometry using the FITC-channel and analyzed employing an appropriate gating strategy within the Kaluza software. The distribution of fluorescence intensities is shown in histograms, with a rightward shift indicating an increased degree of lipid peroxidation.

Figure 6 Lipid Peroxidation Levels in OLN-93 cells after Treatment with Ferroptosis Inducers and Potential Inhibitors

A

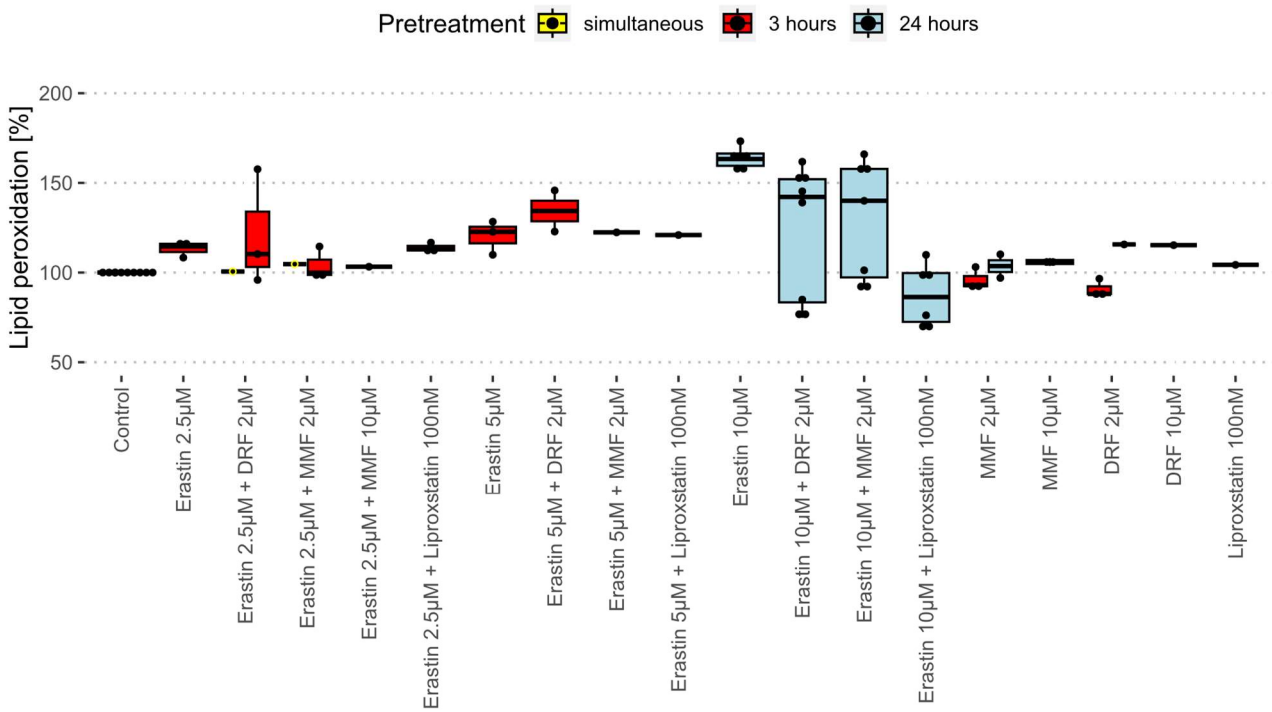

B

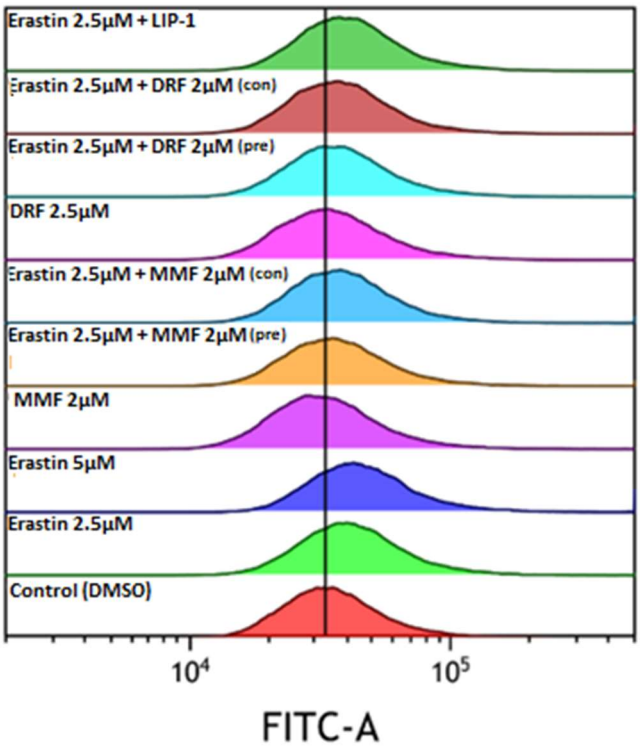

Fig. 6: Lipid peroxidation levels in OLN-93 cells after 6 hours of treatment with the ferroptosis inducer Erastin. Cells were pretreated with 2µM MMF, 10µM, 2µM DRF or 100nM Liproxstatin (=LIP-1) for 3, 24 hours or simultaneously with Erastin, except control cells. A) Mean fluorescence intensities expressed as a percentage of the untreated control group, with standard deviation indicated, n=1-7 (depending on the case). B) The histograms illustrate the distribution of fluorescence intensities, with a rightward shift indicating an increased degree of lipid peroxidation; pre=3 hours pretreatment, con=simultaneous treatment; DMSO: Dimethyl sulfoxide, DRF: Diroximel fumarate, FITC-A: Fluorescein isothiocyanate-Area, LIP-1: Liproxstatin 1, µM: micromolar, MMF: Monomethyl fumarate.

Median fluorescence intensities and their interquartile ranges for all treatments relative to untreated control cells are presented in box plots (Figure 6A). The cells treated with 10 µM Erastin without a ferroptosis inhibitor showed a 163.3 (IQR: [154.5,166.3]) increase of lipid peroxidation compared to untreated cells [2.5µM Erastin: 114.5% (IQR: [111.4%,115.3%]), 5µM Erastin: 119.1% (IQR: [114.5%,123.7%])].

Initially, cells were pretreated for 24 hours as in in the cells survival assays and treated with 10µM Erastin. In these cases, treatment with LIP-1 resulted in a median reduction of lipid peroxidation to 86.3% (IQR: [72.5%,99.7%]). However, neither 2 µM DRF (median 142.1% (IQR: [83.4%,152%]) nor 2 µM MMF (median 140% (IQR: [97.3%,157.8%]) was observed to reduce Erastin-induced lipid peroxidation.

In the case of a three-hour pretreatment with fumarates and a 2.5µM Erastin treatment, a median reduction of Erastin-induced lipid peroxidation to 110.3% (IQR: [103.1%,134%]) for 2 µM DRF and 99.9% (IQR: [98.7%,107.2%]) for 2 µM MMF was observed.

In summary, the findings indicated a decline in lipid peroxidation in cells treated with the validated ferroptosis inhibitor LIP-1. Nevertheless, the protective effect against lipid peroxidation observed after 24 hours of fumarate pretreatment could not be demonstrated in OLN-93 cells. In the case of a three-hour pretreatment and a concentration of 2.5 µM Erastin, a slight protective effect against lipid peroxidation was observed, particularly in the presence of 2 µM MMF.

3.3 Erastin-Induced Demyelination and Fumarate Protection in Organotypic Slice Culture

Next, the impact of ferroptosis on demyelination and axonal degeneration was analyzed. Furthermore, the effectiveness of DRF and MMF in protecting against ferroptosis-induced demyelination was evaluated.

For this thesis in vitro treated mouse cerebellar OSCs to investigate myelin/oligodendrocyte and axonal/neuronal damage following treatment with various ferroptosis inducers and inhibitors were used. To induce myelin and axonal damage, the slices were treated with Erastin, iron or LPS. In a first experiment, the optimal concentrations of Erastin, iron and LPS were determined with respect to demyelination and axonal damage of about 50 % (relative to controls) in OSCs. The percentages of healthy myelin and axons were directly compared with the corresponding control slices treated only with the respective solvent (DMSO for Erastin and LPS, deionized water for iron) (Figure 7). For each case, n=3 independent experiments with up to 3 slices each were performed.

The percentages of healthy myelin and healthy axons in control slices were 54% (median, IQR: [49.3%,54.7]) and 80.5% (median, IQR: [77.1%,83.9]) respectively. For better comparability, the percentages of healthy myelin and axons were set to 100% for the controls in each experiment separately. The percentages of myelin and axonal damage are given in relation to their corresponding controls in the experiment (Figure 8A, 9A). Then, healthy myelin was reduced to 65.9% (median, IQR: [60.5%,73.2]) and 46.8% (median, IQR: [36.0%,66.4%]) with 30 and 60 µM Erastin, respectively. 1 and 3 mM iron decreased healthy myelin to 57.5% (median, IQR: [56.0%,59.0%]) and 46.7% (median, IQR: [43.8%,46.7%]) respectively. 1 µM LPS reduced healthy myelin to 77.8% (median, IQR: [74.7%,79.8%]). The percentages of healthy axons were reduced to 88.5% (median, IQR: [75%,93.8%]) and 101.6% (median, IQR: [96.5%,102.2%]) with 30 and 60 µM Erastin, respectively. 1 and 3 mM iron decreased

healthy axons to 64.6% (median, IQR: [60.4%,68.7%]) and 49.0% (median, IQR: [44.5%,52.3%]), respectively. 1 µM LPS reduced healthy axons to 74.8% (median, IQR: [69.7%,83.9%]). The quality of the axons was evaluated in relation to the presence of healthy myelin.

The protective effect of the multiple sclerosis drug DRF and its active metabolite MMF against the ferroptosis-induced damage to myelin and axons caused by Erastin and iron was then investigated (Figure 8,9 B-E). In addition, the protective effects of the known ferroptosis inhibitor LIP-1 and the iron chelator SIH were compared with that of fumarates (Figure 8,9 D-E).

Slices treated with DRF (4 µM: 102.7% (median, IQR: [75%,105.5%]), 20 µM: 90.9% (median, IQR: [73.0%,93.4%])) and high-dose MMF (20 µM: 97.1% (median, IQR: [93.7%,124.9%])) showed comparable levels of healthy myelin compared to controls. Treatment with low-dose MMF (118.9% (median, IQR: [112.9%,136.6%]) resulted in a slight increase in myelin protection.

In slices treated with 60µM Erastin, DRF (4 µM: 90.9% (median, IQR: [76.7.1%,104.0%]); 20 µM: 87.1% (median, IQR: [75.4%,100.8%]), $p<0.01$), low-dose MMF (4 µM: 84.4% (median, IQR: [83.3%,114.5%]), $p<0.01$), and 200nM LIP-1 (median: 93.7, IQR: [88.5%,104.1%])) effectively attenuated induced myelin damage (Figure 8B). Treatment with high-dose MMF (20 µM: 75.8% (median, IQR: [66.3%,77.7%])) had a weaker effect. After treatment with 1 mM iron, only SIH and low-dose DRF were able to significantly mitigate the decrease of healthy myelin (SIH: median: 87.1%, IQR: [82.4%,90.9%]; 4µM DRF: median: 90.9%, IQR: [90.9%,98.5%]). Lower concentrations MMF provided some level of protection (4 µM MMF: median: 77.7%, IQR: [76.8%,78.6%])). However, high-dose DRF and MMF were unable to maintain myelin protection (20 µM DRF: median: 45.5%, IQR: [45.5%,68.2%]), 20 µM MMF: median: 60.6%, IQR: [42.6%,76.8%]). The administration of a higher dose of iron (3 mM) did not result in the protection of myelin loss when combined with either DRF or MMF (Figure 9D, E).

Axonal integrity was largely preserved in slices exposed to DRF at concentrations of 4 µM (median: 83.3%, IQR: [80.4%,86.7%] and 20 µM (median: 70.0%, IQR: [61.9%-78.1%], as well as in slices treated with LIP-1 (median: 86.5%, IQR: [84.5%,90.3%]. These results were comparable to the minimal axonal damage observed in control slices. Additionally, there was minimal axonal damage observed in slices treated with 60 µM Erastin (median: 101.6%, IQR: [96.5,102.2]). Similar results were observed in fumarate-treated slices (4 µM DRF: median: 85.25, IQR: [70.3%,102.3%]; 20 µM: median: 94.8%, IQR: [84.9%,104.7%]; 4 µM MMF: median: 84.4%, IQR: [83.3%,114.5%]; 20 µM: median: 75.8%, IQR: [66.3%,77.7%]) (Figure 9).

In contrast to this, treatment with iron results in significant axonal damage (Figure 9). After treatment with 1 mM iron, only SIH was able to mitigate the decrease of healthy axons to 96.9% (median, IQR: [92.5,100.4]). Lower concentrations of DRF and MMF as well as high dose MMF provided some level of protection (4 µM DRF: median: 72.9%, IQR: [70.8%,75.5%]; 4 µM MMF: median: 80.8%, IQR: [79.4%,82.1%], 20 µM DRF: median: 67.7%, IQR: [52.6%,69.0%]; 20 µM MMF: median: 82.0%, IQR: [76.8%,91.8%]). After treatment with 3 mM iron, only 200 nM LIP-1 and 4 µM MMF provided some level of protection (200nM LIP-1: median: 85.2%, IQR: [76.1%,86.5%]; 4 µM MMF: median: 74.3%, IQR: [68.1%,78.5%]). However, DRF and high-dose MMF were unable to maintain myelin protection (4 µM DRF: median: 49.0%, IQR: [38.7%,60.0%]; 20 µM DRF: median: 53.7%, IQR: [51.1%,57.3%]; 20 µM MMF: median: 55.8%, IQR: [48.8%,61.9%]).

In summary, the ferroptosis-inducing agent Erastin primarily affected myelin, whereas iron affected both myelin and axons. In Erastin-treated slices, LIP-1, DRF, and MMF were equally effective in attenuating the induced myelin damage. In slices treated with iron, the iron chelator SIH provided the best protection against demyelination and axonal damage.

Figure 7 Immunochemical Images of Myelin and Axonal Damage in Cerebellar Slices.

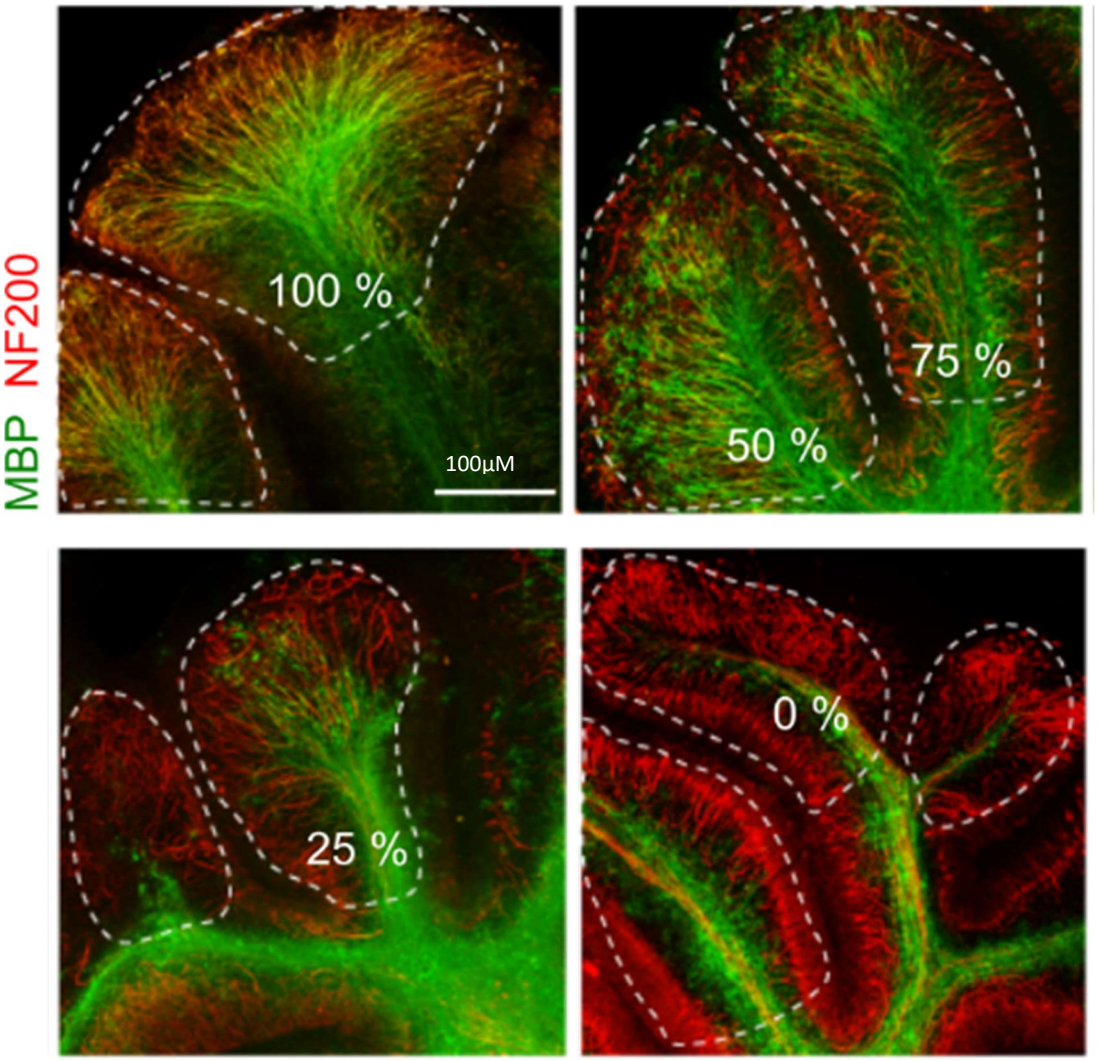

Fig.7: Myelin (anti-MBP) and axonal (anti-Neurofilament 200, anti-NF200) damage were analyzed using immunohistochemistry. The images demonstrate the quantification of healthy myelin. Classification of myelin damage for each branch is categorized into five classes, ranging from 0% (complete destruction) to 100% (complete preservation); MBP: Myelin basic protein, NF: Neurofilament.

Figure 8 Demyelination in Cerebellar Slices

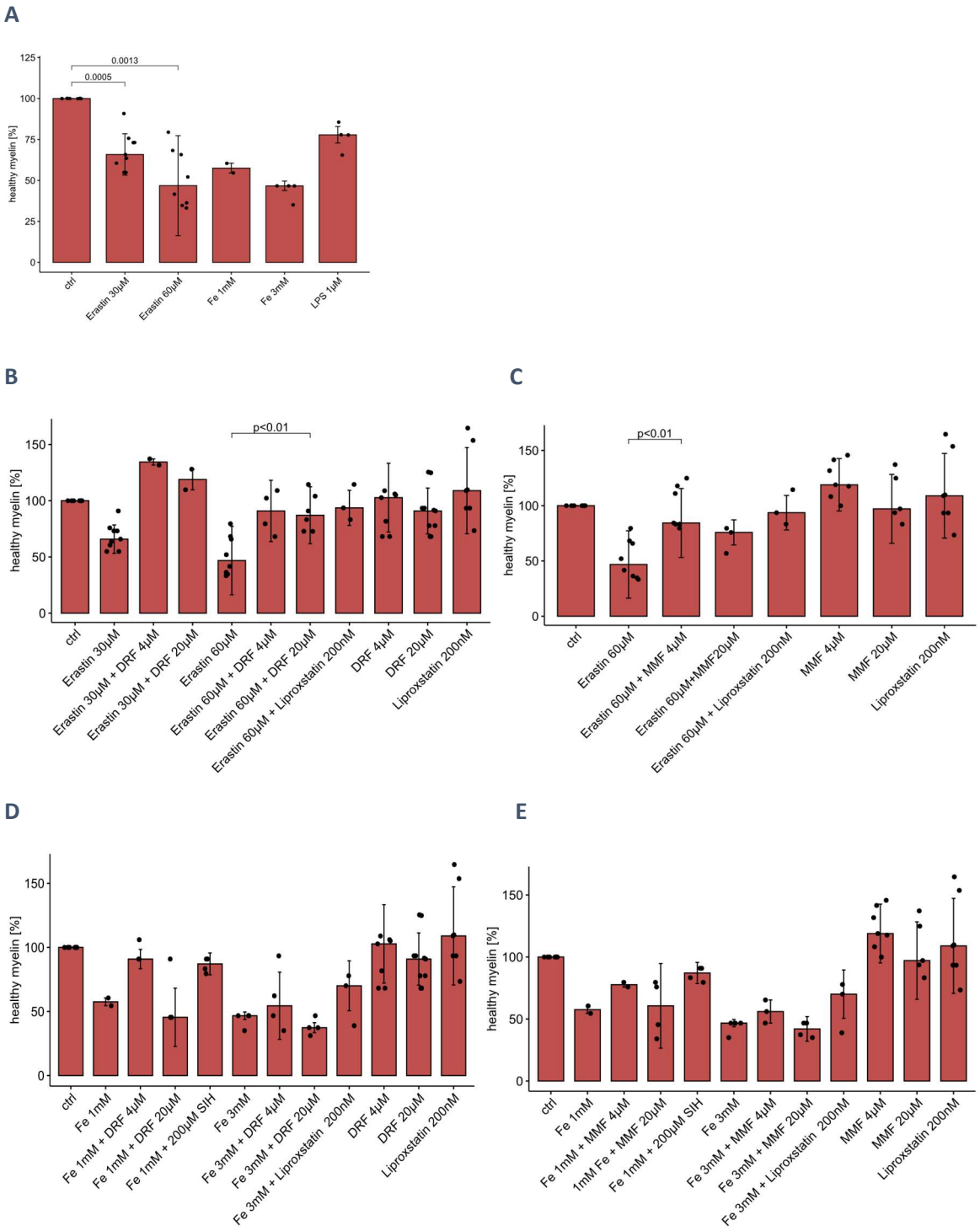

Fig. 8: Percentages (median, IQR) of healthy myelin structure in cerebellar slices for different treatments (incubated for 24 hours), standardized to those of the corresponding control slice treated with DMSO, n=3 with up to 3 replicates each. Damaged and poorly stained slices were not analyzed. A) Comparison of the proportion of myelin damage after treatment with the ferroptosis inducers Erastin and iron and the neuroinflammation activator LPS. B,C) Proportion of myelin damage in Erastin-treated slices after pretreatment with fumarates compared to Liproxstatin (LIP-1). D,E) Proportion of myelin damage in iron-treated slices after pretreatment with fumarates compared to the iron chelator SIH and Liproxstatin; Ctrl: Control, DMSO: Dimethyl sulfoxide, DRF: Diroximel fumarate, Fe: Iron, LPS: Lipopolysaccharide, µM: micromolar, mM: millimolar, MMF: Monomethyl fumarate, SIH: Salicylic acid isonicotinoyl hydrazone.

Figure 9 Axonal Damage in Cerebellar Slices

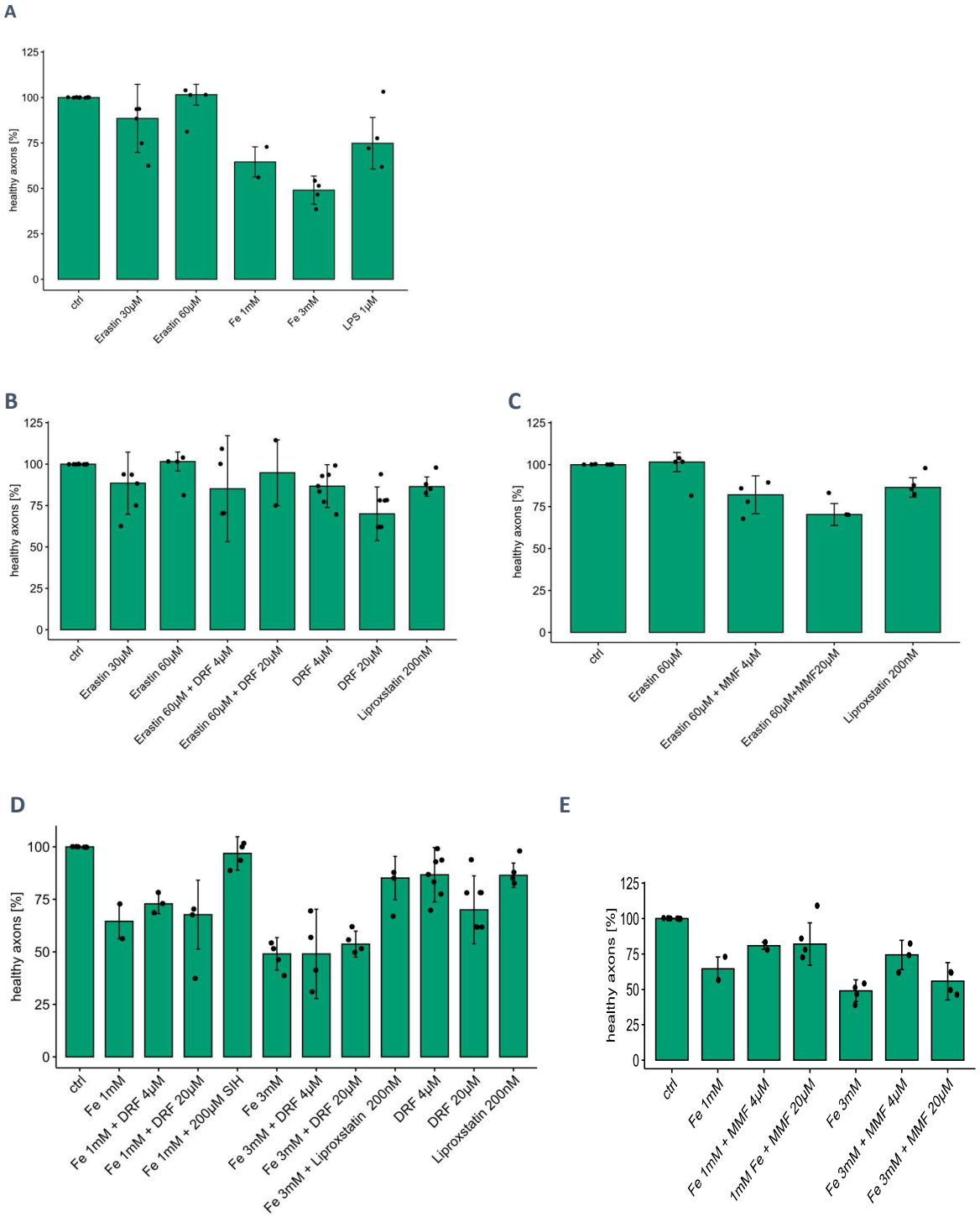

Fig. 9: Percentages (median, IQR) of healthy axonal structure in cerebellar slices for different treatments (incubated for 24 hours), standardized to those of the corresponding control slice treated with DMSO, n=3 with up to 3 replicates each. Damaged and poorly stained slices were not analyzed. A) Comparison of the proportion of axonal damage after treatment with the ferroptosis inducers Erastin, iron or LPS. B,C) Proportion of axonal damage in Erastin-treated slices after pretreatment with fumarates compared to Liproxstatin (LIP-1). D,E) Proportion of axonal damage in iron-treated slices after pretreatment with fumarates compared to the iron chelator SIH and Liproxstatin; Ctrl: Control, DMSO: Dimethyl sulfoxide, DRF: Diroximel fumarate, Fe: Iron, LPS: Lipopolysaccharide, µM: micromolar, mM: millimolar, MMF: Monomethyl fumarate, SIH: **Salicylic acid *i*sonicotinoyl *h*ydrazone.**

3.4 Upregulation of GPx4 Expression in OLN-93 Cells Following Fumarate Treatment

To investigate the upregulation of GPx4 in oligodendrocytes following DRF and MMF treatment, GPx4 gene expression was measured in OLN-93 cells after 24 hours of exposure to these compounds using qPCR. In addition, to confirm that the observed gene upregulation was a result of Nrf2 pathway activation, the expression of Hmox1, a well-established Nrf2 target gene, was assessed.

Figure 10A shows that GPx4 mRNA expression is upregulated after 24 hours of treatment with DRF and MMF. Compared to the untreated control cells (median 100%, IQR: [65%,126%]) treatment with 2 µM (median 198%, IQR: [174%,244%]), p=0.0093) and 10 µM MMF (median 217%, IQR: [163%,283%], p=0.0147) significantly increased GPx4 mRNA levels. Similarly, treatment with 2 µM (median 217%, IQR: [163%,283%]) and 10 µM DRF (median 127%, IQR: [127%,171%]) also elevated GPx4 mRNA levels. Figure 10B demonstrates that treatment with 10 µM MMF significantly increased Hmox1 mRNA levels (median 225%, IQR: [216%,317%]), p=0.0065) while treatment with 2 µM MMF resulted in a moderate increase in Hmox1 mRNA levels (median 125%, IQR: [104%,146%]) compared to untreated cells (median 100%, IQR: [75%,169%]). Similarly, treatment with 2µM and 10 µM DRF also resulted in elevated Hmox1 mRNA levels (median 187%, IQR: [176%,213%]; median 190%, IQR: [175%,208%], respectively). These results further support the conclusion that both DRF and MMF treatment enhance Hmox1 and GPx4 protein expression in OLN-93 cells.

These findings were further validated at the protein level through Western Blotting (Figure 10C,D). Treatment with 2 µM DRF resulted in a GPx4 protein level of median 122% (IQR: [108%,138%], while 10 µM DRF treatment led to a level of median 160% (IQR: [128%,189%]. Similarly, treatment with 2 µM MMF resulted in a GPx4 protein level of median 148% (IQR: [126%,182%] and treatment with 10 µM MMF led to a level of median 162% (IQR: [138%,216%].

In summary, the results confirm the upregulation of the key ferroptosis enzyme GPx4 in OLN-93 cells following the administration of DRF and MMF.

Figure 10 GPx4 and Hmox1 Gene and Protein Induction in OLN-93 Cells

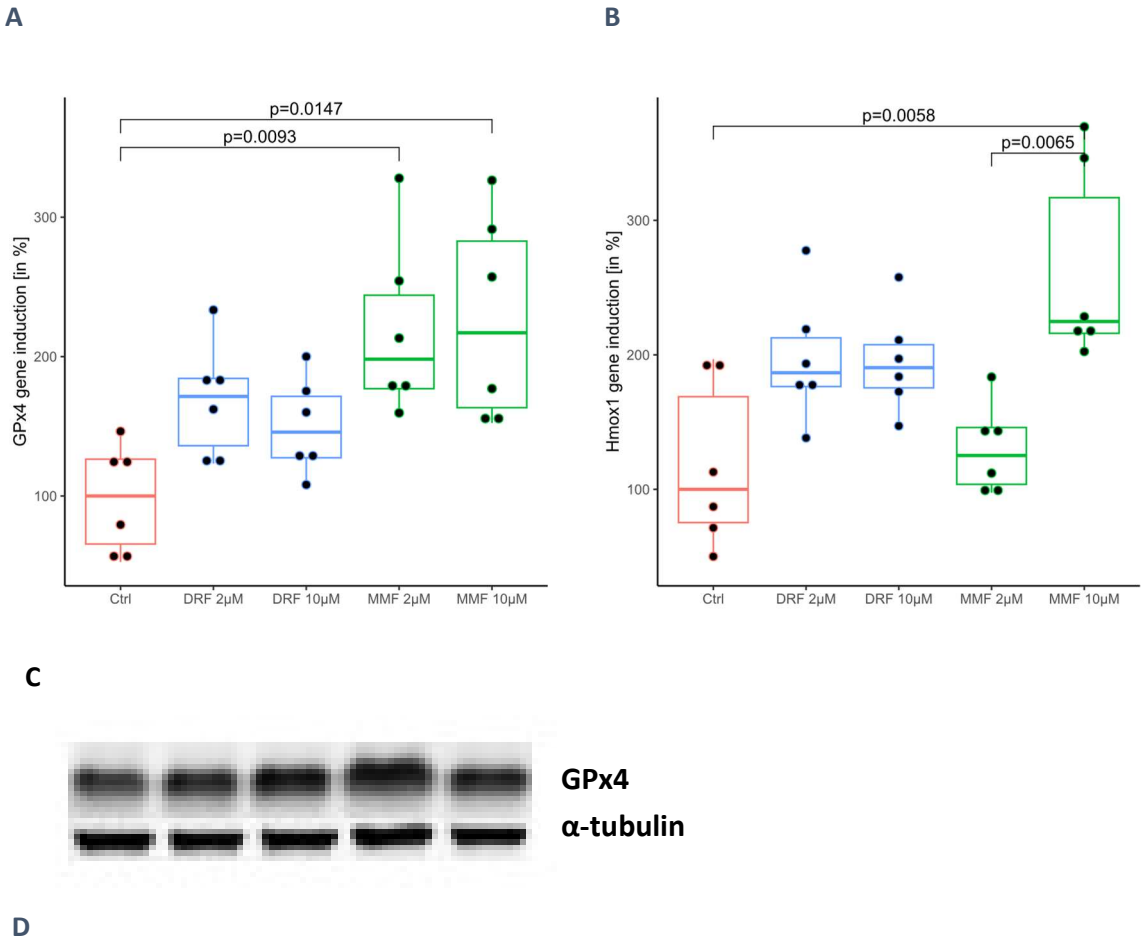

Fig. 10: Gene expression levels of GPx4 (A) and Hmox1 (B) were measured using mRNA isolated from OLN-93 cells treated with fumarates (DRF green, MMF blue) for 24 hours through qPCR analysis. Ct values were determined for the target genes GPx4 and Hmox1, along with the housekeeping genes ß-actin or α-tubulin, used as reference genes to normalize the gene expression data. The levels are presented as percentages relative to the corresponding control, n=3 experiments, 2 replicates each. C) Representative Western blot showing GPx4 and α-tubulin protein levels in OLN-93 cells treated for 24 hours (here α-tubulin was used instead of ß-actin, because of a bubble in a ß-actin band). Uncropped (complete) blot can be found in the supplements. D) Quantification of GPx4 protein level by densitometric analysis of western blot bands normalized to housekeeping protein ß-actin in OLN-93 cells after 24 hours of treatment with fumarates, here presented as percentages relative to the corresponding control, n=5 experiments. Ctrl: Control, DRF: Diroximel fumarate, GPx4: Glutathione peroxidase 4, Hmox1: Heme oxygenase 1, MMF: Monomethyl fumarate, µM: micromolar, mRNA: messenger ribonucleic acid.

3.5 Increased GPx4 Levels in the White Matter of Mouse Brains after DMF Treatment

To translate the cell culture findings to an in vivo model, the GPx4 upregulation in brain tissue from DMF-treated mice was examined. Mice were administered DMF at doses of 15 mg/kg BW or 30 mg/kg BW, with DMSO serving as a control. GPx4 mRNA expression was quantified by qPCR.

Figure 11A shows that GPx4 mRNA expression is upregulated in both gray and white matter after seven days of DMF treatment. The median GPx4 mRNA expression in control white matter tissues (median 100%, IQR: [91%,103%]) increased significantly to a median of 129% (IQR: [119%,148%], p=0.0037) after treatment with 30 mg/kg BW DMF. However, the increase in gray matter GPx4 mRNA expression from a median of 100% (IQR: [83%,102%] to a median of 117% (IQR: [112%,122%]) was not statistically significant (p=0.4320). In the case of Hmox1, after treatment with 30 mg/kg BW DMF, mRNA levels in gray matter increased significantly with a median of 158% (IQR: [150%,163%], p=0.0060) compared to control gray matter (median 100%, IQR: [93%,122%} (Figure 11B). However, Hmox1 mRNA levels in white matter showed no difference compared to control tissue (median 91%, IQR: [81%,133%] versus control (median 100%, IQR: [73%,110%])).

This finding of GPx4 mRNA upregulation in the white matter was confirmed at the protein level using Western blot analysis. Cell extracts were taken from the white and gray matter of six mice treated with 30 mg/kg BW DMF and six control mice previously used for gene expression analysis. White matter samples showed a significant increase in GPx4 protein levels (median 129%, IQR: [112%,135%]) compared to white matter controls (median 97%, IQR: [86%,107%], p=0.0304). Consistent with the gene expression results, gray matter samples did not show elevated GPx4 levels (median 114%, IQR: [99%,119%]) compared to controls (median 112%, IQR: [92%,133%]) (Figure 11C).

In summary, upregulation of GPx4 gene and protein was detected in the brain tissue of DMF-treated mice, with a notable increase in the white matter.

Figure 11 GPx4 and Hmox1 Gene and Protein Induction in Gray and White Matter of Mouse Brains

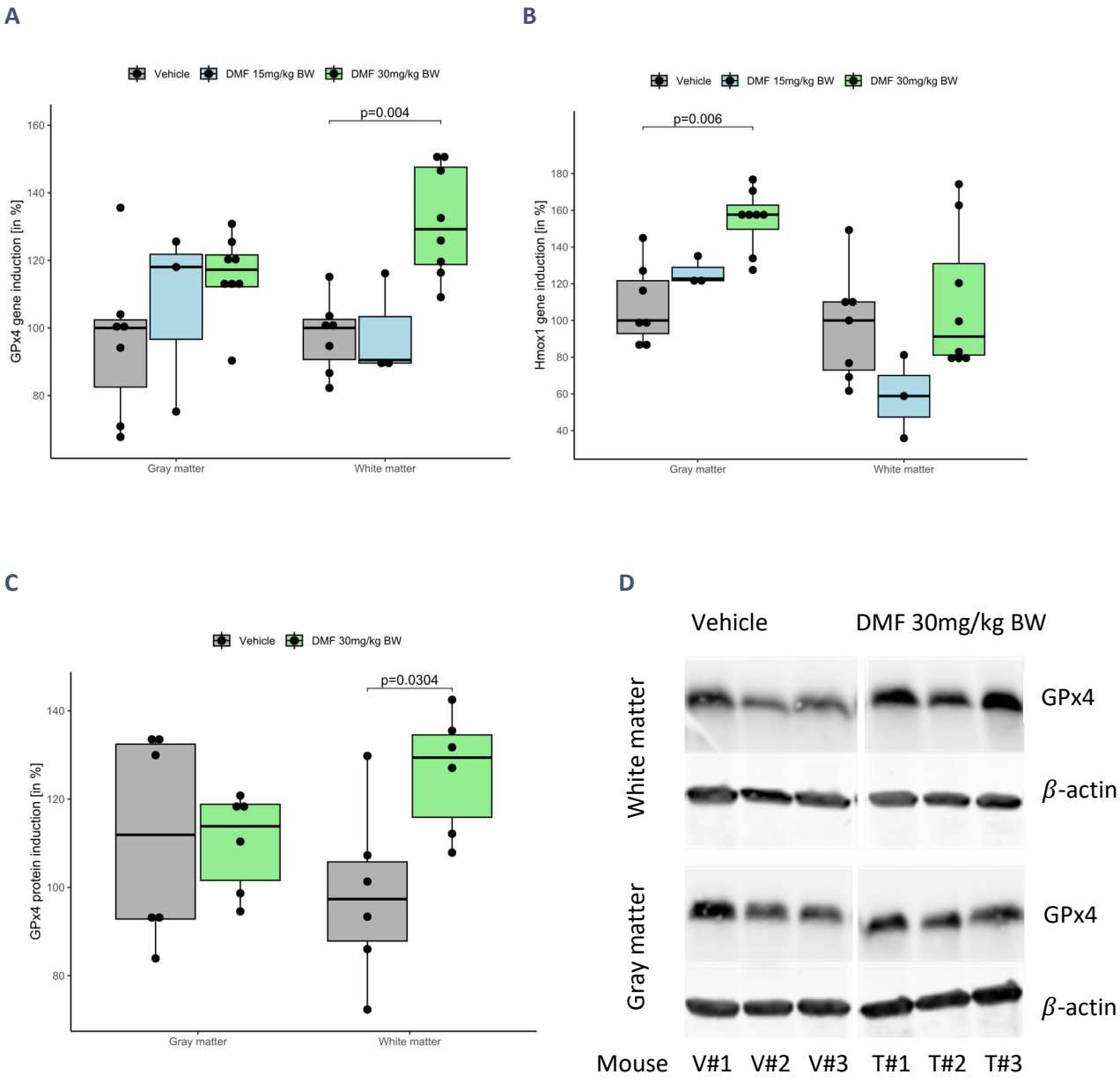

Fig.11: Gene expression levels of GPx4 (A) and Hmox1 (B) in gray and white matter of mouse brain tissue. After treatment with DMF (light blue: 15 mg/kg BW, n=3 mice; light green: 30 mg/kg BW, n=8 mice) for 7 days, mRNA was isolated from cerebellum (white matter) and occipital cortex (gray matter) and measured by qPCR analysis. Ct values were determined for the target genes GPx4 and Hmox1, along with the house-keeping gene Gapdh (as reference gene to normalize the gene expression data). Levels are presented as per-centages relative to the corresponding control (gray, n=7 mice). C) Quantification of GPx4 protein level by densitometric analysis of western blot bands normalized to housekeeping protein β-actin, here presented as percentages relative to the corresponding control, n=6 mice each. Cell extracts were taken from the white and gray matter of six mice treated with 30 mg/kg BW DMF and six control mice previously used for gene expression analysis. D) Representative Western blot showing GPx4 and β-actin protein levels in OLN-93 cells treated for 24 hours. Uncropped (complete) blots can be found in the supplements; V: vehicle, T: treatment, i.e.: V#1 Vehicle mouse number 1, BW: Body weight, DMF: Dimethyl fumarate, Gapdh: Glyceraldehyde 3-phosphate dehydrogenase, GPx4: Glutathione peroxidase 4, Hmox1: Heme oxygenase 1, mg/kg: milligram per kilogram, mRNA: messenger ribonucleic acid.

3.6 Gene Expression in RRMS´ PBMCs

One aim of this study was to investigate the possible deficiency of GPx4 gene expression in vivo, given the GPx4 deficiency observed in postmortem brain tissue studies of patients with MS. The first question was whether there is a deficiency in GPx4 expression in PBMCs, as this cannot be expected uniformly for all GPx4-expressing cells. Furthermore, this study compares GPx4 mRNA-levels in relation to disease duration and severity of MS, as assessed by the EDSS. Additionally, the study investigated whether cellular GPx4 gene expression in MS patients significantly increases after one year of treatment with DMF.

3.6.1 GPx4 and Hmox1 mRNA Expression in PBMCs of RRMS Patients

To investigate a potential deficiency in GPx4 expression in PBMCs of RRMS patients, blood samples were collected prior to scheduled DMF or OCR treatment. The expression levels of GPx4 and Hmox1 mRNA in the isolated cells were subsequently quantified using qPCR.

Comparative analysis revealed a slight decrease in median GPx4 gene expression in MS patients (median 83.8%, IQR: [45.7%, 103.6%]) compared to healthy controls (median 100%, IQR: [68.6%, 202.3%]) (Figure 12A). Moreover, the levels of Hmox1 gene expression were found to be similar between MS patients and healthy volunteers, with median values of 100% (IQR: [66.6%, 136.9%]) for healthy probands and 91% (IQR: [58.4%, 174.5%]) for MS patients (see Figure 12B).

Figure 12 GPx4 and Hmox1 Gene Induction in Patients and Healthy Blood Donors at Baseline

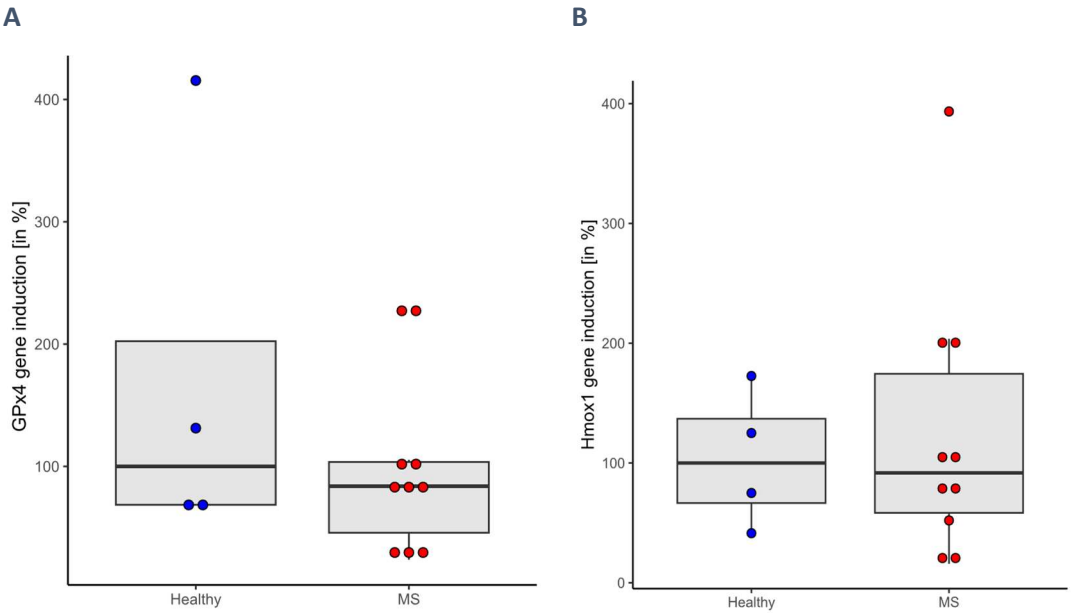

Fig.12: Levels of A) GPx4 mRNA expression and B) Hmox1 mRNA expression in MS patients (n=10) and healthy probands (n=4). Blood from MS patients was collected prior to the scheduled DMF or OCR treatment. The mRNA expression levels were normalized to the median of the corresponding mRNA expression levels of the healthy probands; DMF: Dimethyl fumarate, GPx4: Glutathione peroxidase 4, Hmox1: Heme oxygenase 1, MS: Multiple Sclerosis, mRNA: messenger ribonucleic acid, OCR: Ocrelizumab.

A subgroup analysis of GPx4 and Hmox1 mRNA expression is feasible only to a very limited extent due to the very small number of cases. However, it is conducted to identify potential trends. To explore

potential correlations between demographic factors (age and sex) or clinical parameters (disease duration, AAR, and EDSS) and the gene expression of GPx4 and Hmox1, the data were visualized using scatter plots, dot plots, and box plots.

There was no observable correlation between age and gene expression for GPx4 and Hmox1 in either group (for the MS-patients: Spearman correlation coefficient ρ=0.2 for GPx4 and ρ=-0.21 for Hmox1, Figure 13 A,B). Furthermore, the mRNA levels of both GPx4 and Hmox1 were found to be unaffected by the sex of the probands (Figure 13 C,D).

Figure 13 GPx4 and Hmox1 Gene Induction at Baseline: Correlation Analysis Including Age and Sex

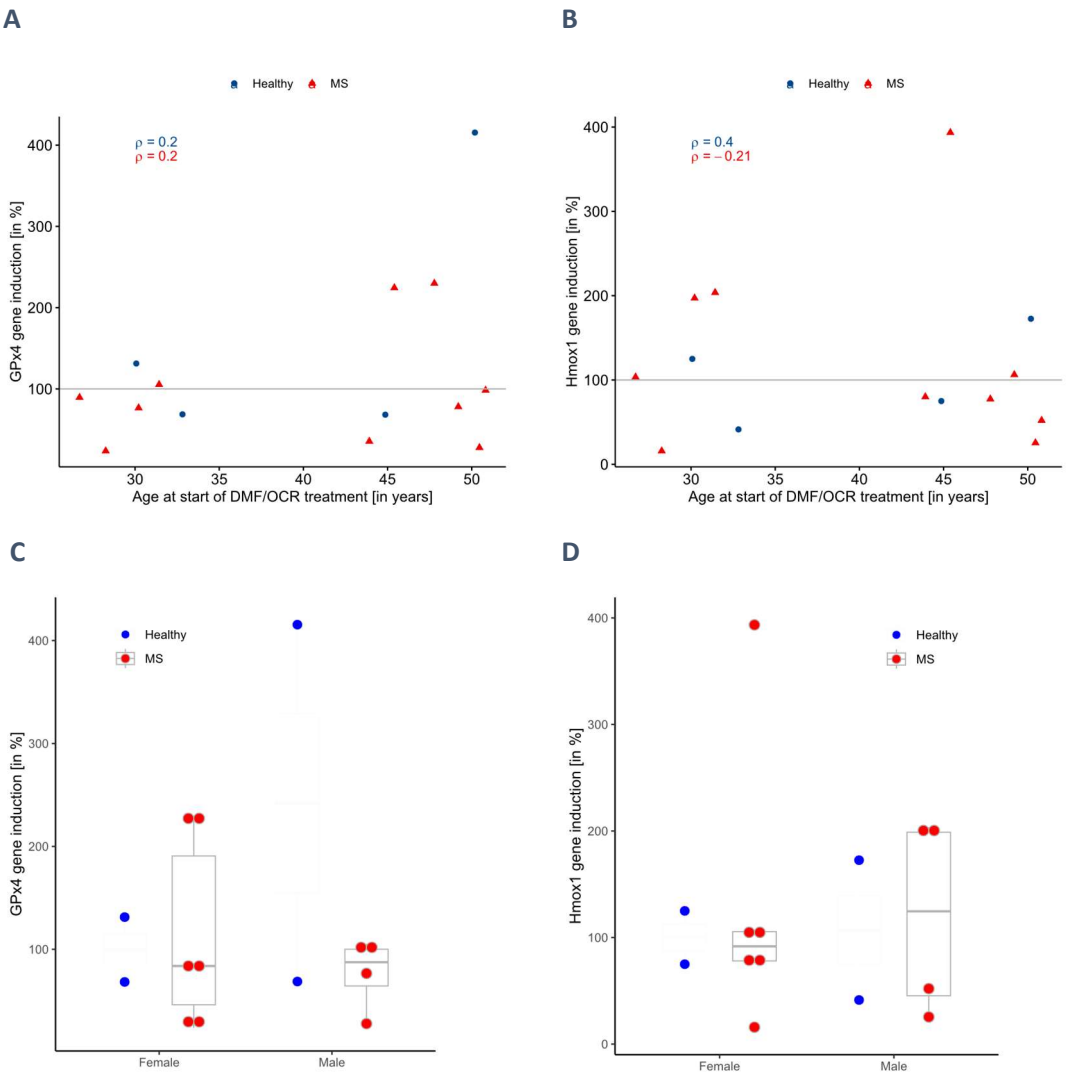

Fig.13: A,B) The scatter plots demonstrate the relationship between the gene expression levels of GPx4 and Hmox1 across various ages in MS patients (red, n=10) and healthy probands (blue, n=4) prior to the initiation of treatment with DMF or OCR. Spearman's correlation coefficients (ρ) were calculated to measure the strength of association between age and gene expression. C,D) The dot and box plots demonstrate the gene expression levels of GPx4 and Hmox1 with respect to sex in MS patients (red, n=10) and healthy probands (blue, n=4) prior to the initiation of treatment with DMF or OCR. All mRNA expression levels were normalized to the median of the corresponding mRNA expression levels of the healthy probands; DMF: Dimethyl fumarate, GPx4: Glutathione peroxidase 4, Hmox1: Heme oxygenase 1, mRNA: messenger ribonucleic acid, MS: Multiple Sclerosis, OCR: Ocrelizumab.

Figure 14 GPx4 and Hmox1 Gene Induction at Baseline: Correlation Analysis Including Disease Duration, AAR, and EDSS

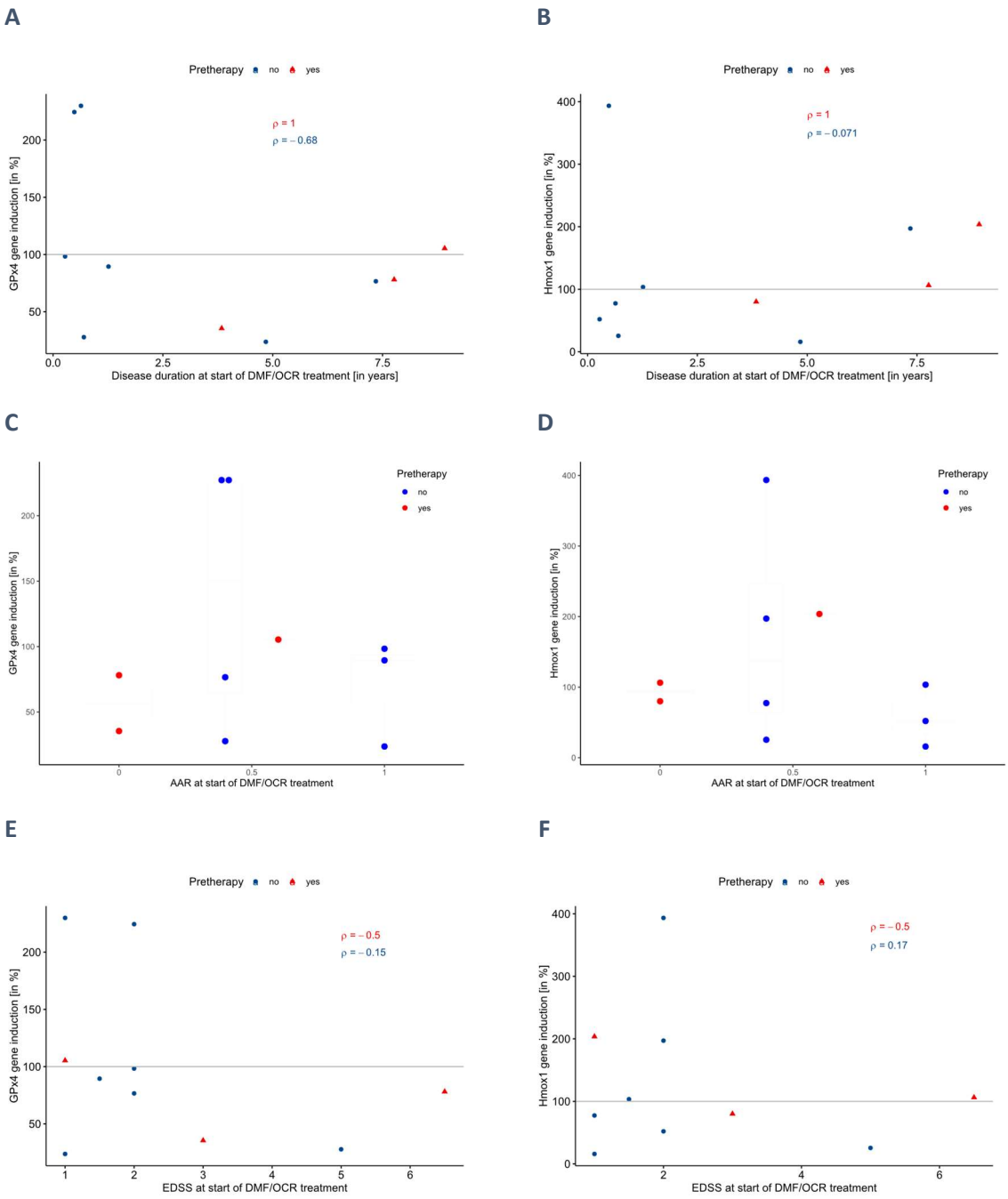

Fig. 14: Visualization of the relationship between the gene expression levels of GPx4 and Hmox1 across various disease duration (A,B), AAR (C,D) and EDSS scores (E,F) in pretreated MS patients (red, n=3) and MS patients without immunotherapy in the last 12 months (blue, n=7; comprising 6 therapy-naïve patients and one patient who underwent immunotherapy 6.5 years ago). Spearman's correlation coefficients (ρ) were calculated to measure the strength of association between disease duration and gene expression, as well as between EDSS scores and gene expression. All mRNA expression levels were normalized to the median of the corresponding mRNA expression levels of the healthy probands; AAR: Annualized Attack Rate, DMF: Dimethyl fumarate, EDSS: Expanded Disability Status Score, GPx4: Glutathione peroxidase 4, Hmox1: Heme oxygenase 1, mRNA: messenger ribonucleic acid, MS: Multiple Sclerosis, OCR: Ocrelizumab.

No relevant statistical trends were observed in the subgroup analysis that examined the correlation between GPx4 and Hmox1 gene expression levels and clinical parameters, such as disease duration and severity quantified by the AAR in the previous two years prior to DMF/OCR initiation and the pre-treatment EDSS score. Since three patients had received immunotherapies prior to the start of OCR treatment, which could potentially influence gene expression values, the data from this subgroup were excluded from the subsequent analysis and merely highlighted in the diagrams. Among the seven remaining patients, six were therapy-naïve, while one patient had received immunotherapy 6.5 years ago prior DMF initiation. In treatment-naïve patients, a slight downward trend in GPx4 mRNA expression was observed with increasing disease duration (Spearman's ρ=-0.68, Figure 14 A). However, no trend was observed for the expression of the Hmox1 gene (Spearman's ρ=-0.07, Figure 14 B). No correlation was observed between AAR and gene expression for GPx4 and Hmox1 (Figure 14 C,D). In addition, the mRNA levels of both GPx4 and Hmox1 were not affected by the EDSS of the patients (for the treatment-naïve patients: Spearman's ρ=-0.15 for GPx4 and ρ=0.17 for Hmox1, Figure 14 E,F).
In summary, there was no clear deficiency of GPx4 detected in PBMCs of RRMS patients.

3.6.2 Gene Expression in RRMS Patients' PBMCs after DMF or OCR Treatment

To assess potential upregulation of GPx4 gene expression in PBMCs from MS patients following one year of DMF or OCR treatment, gene expression ratios were analyzed by comparing 12-month values to baseline measurements.

Following DMF treatment, a clear increase in GPx4 gene expression was observed in only two patients, while one patient remained stable, and there was even a decrease in expression for the other two patients (median 1.01, IQR: [0.80, 2.52]). Remarkably, the patient who experienced an attack during DMF therapy exhibited the highest level of GPx4 mRNA expression in the DMF group (black circle, Figure 15 C). Comparative analysis unveiled a significant difference in median GPx4 gene expression among OCR patients (median 6.70, IQR: [6.37, 8.13], $p<0.01$) compared to DMF patients (Figure 15 A,C). Significant differences were also found in Hmox1 gene expression between DMF and OCR patients, with median values of 1.2 (IQR: [1.2, 1.26]) for DMF patients and 7.96 (IQR: [6.07, 11.39]) for OCR patients ($p<0.01$, see Figure 15 B). However, in four out of five DMF patients, Hmox1 gene expression increased after 12 months compared to the time point before therapy (Figure 15 D).

Figure 15 Alterations of GPx4 and Hmox1 Gene Induction after 12 Months of Treatment: Temporal and Treatment Dependent Effects on Expression Profiles

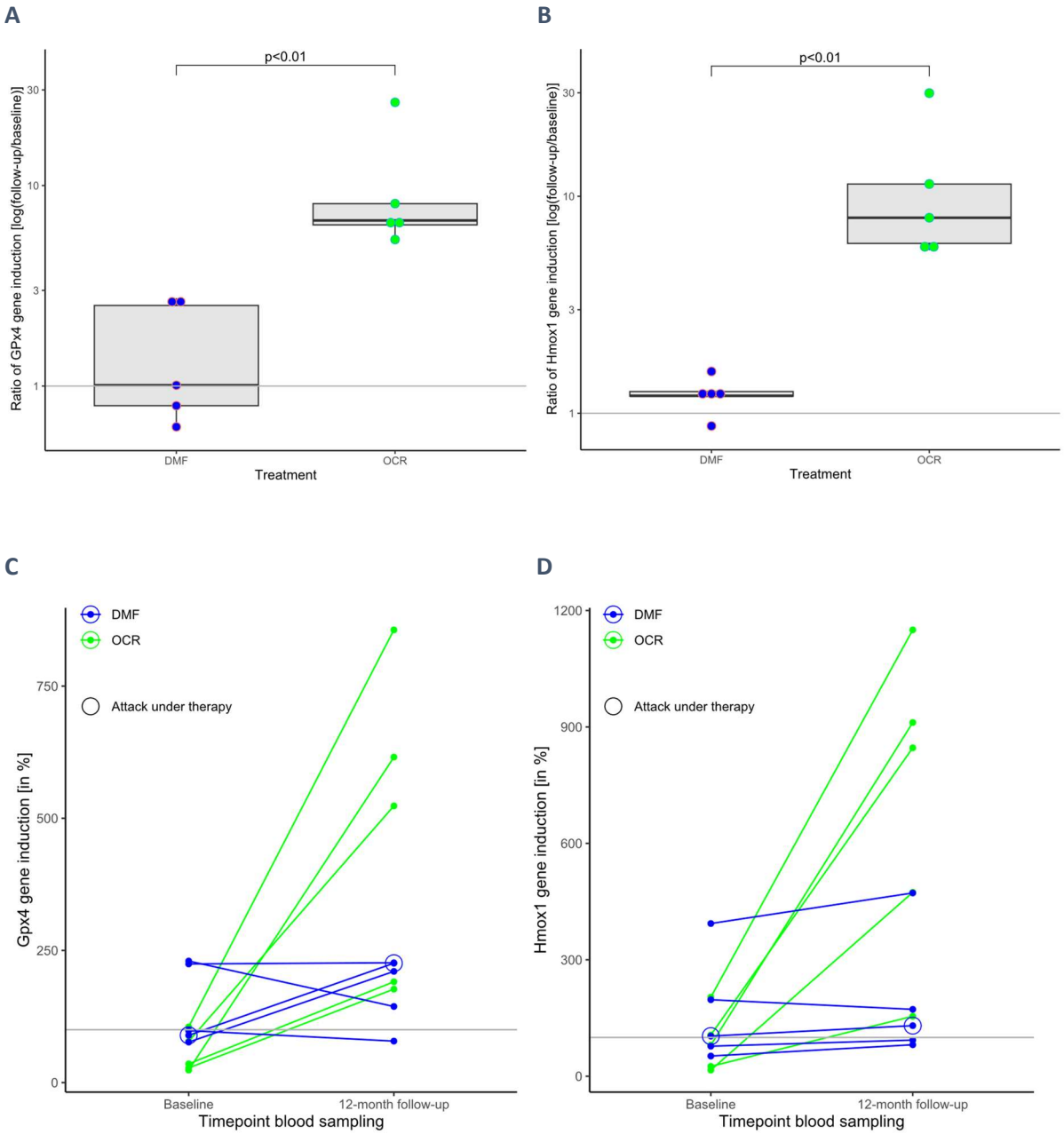

Fig. 15: Ratios (12 months follow-up/baseline) of A) GPx4 and B) Hmox1 mRNA expression in DMF (blue) and OCR (green) patients (n=5 each). Blood was drawn from MS patients before and after 12 months of treatment with DMF or OCR. The horizontal line is positioned at 1 (no difference between pre- and post-12-month therapy). C, D) The individual progressions of gene expression levels are shown in line plots. The mRNA expression values were normalized to the median of the corresponding mRNA expression values of the healthy probands. The horizontal line is positioned at 100% (median value of the healthy probands). The black circles indicate the respective mRNA expression values of the patient who suffered an attack under DMF treatment; DMF: Dimethyl fumarate, GPx4: Glutathione peroxidase 4, Hmox1: Heme oxygenase 1, mRNA: messenger ribonucleic acid, MS: Multiple Sclerosis, OCR: Ocrelizumab.

A subgroup analysis was conducted to identify potential trends related to the change in GPx4 and Hmox1 mRNA expression after 12 months of treatment. To investigate potential correlations between

demographic factors (such as age and sex) or clinical parameters (including disease duration, AAR, and EDSS) and the respective ratios of GPx4 and Hmox1 gene expression, data were visualized using scatter plots and dot plots.

In both groups, the ratio of GPx4 gene expression decreased with increasing age of the patient (ρ = -0.8 for DMF, ρ = -0.7 for OCR; Figure 16 A). This effect was not observed for the ratio of Hmox1 gene expression (ρ = 0.4 for DMF, ρ = -0.4 for OCR; Figure 16 B). With respect to sex, no discernible differences were observed in the ratios of gene expression for any of the treatment groups or genes (Figures 16 C,D).

Figure 16 Alterations of GPx4 and Hmox1 Gene Induction after 12 Months of Treatment: Correlation Analysis Including Age and Sex

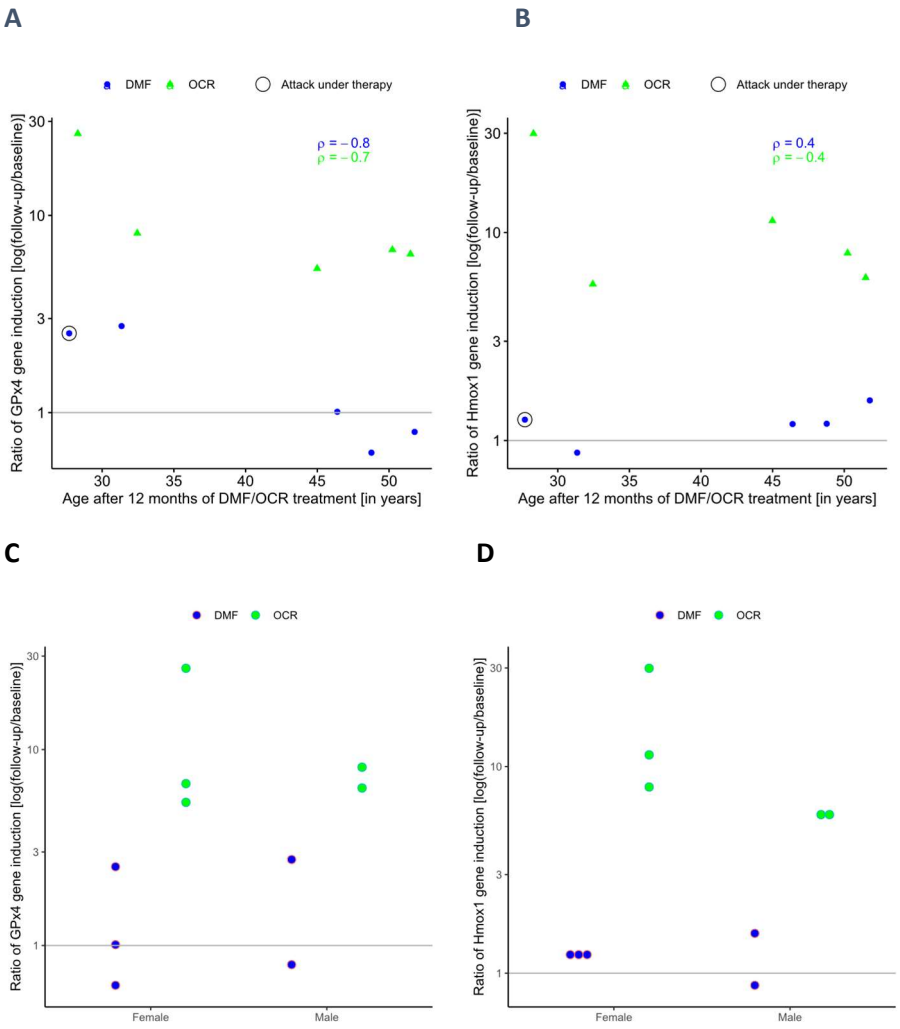

Fig. 16: Ratios (12 months follow-up/baseline) of A, C) GPx4 mRNA expression and B, D) Hmox1 mRNA expression in DMF (blue) and OCR (green) patients (n=5 each) with respect to age and sex of the patients. The horizontal line is positioned at 1 (no difference between pre- and post-12-month therapy). The black circles indicate the ratio of the respective mRNA expression values for the patient who suffered an attack during DNF therapy; DMF: Dimethyl fumarate, GPx4: Glutathione peroxidase 4, Hmox1: Heme oxygenase 1, , mRNA: messenger ribonucleic acid, MS: Multiple Sclerosis, OCR: Ocrelizumab.

Figure 17 Alterations of GPx4 and Hmox1 Gene Induction after 12 Months of Treatment: Correlation Analysis including Disease Duration, AAR, and EDSS.

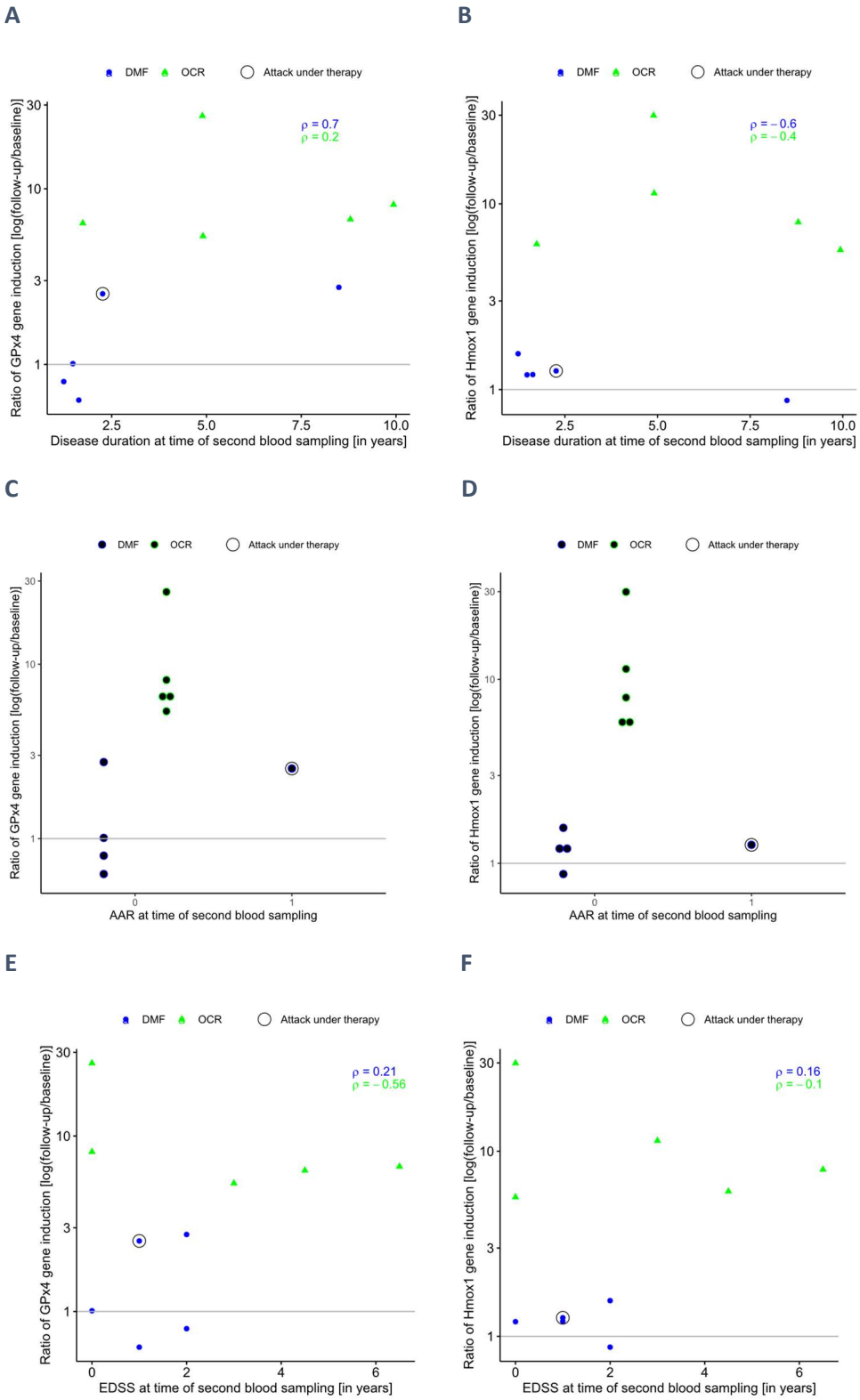

Fig. 17: Ratios (12 months follow-up/baseline) of A, C, E) GPx4 and B, D, F) Hmox1 mRNA expression in DMF (blue) and OCR (green) patients (n=5 each) with respect to disease duration, AAR and EDSS of the patients. The horizontal line is positioned at 1 (no difference between pre- and post-12-month therapy). The black circles indicate the ratio of the patient who suffered an attack during DMF therapy; AAR: Annualized Attack

Rate, DMF: Dimethyl fumarate, EDSS: Expanded Disability Status Score, GPx4: Glutathione peroxidase 4, Hmox1: Heme oxygenase 1, mRNA: messenger ribonucleic acid, MS: Multiple Sclerosis, OCR: Ocrelizumab.

In the subsequent subgroup analysis exploring the potential correlation between GPx4 or Hmox1 gene expression levels and clinical parameters like disease duration and severity (measured by the AAR in the last two years prior to the second blood draw under DMF or OCR therapy, and the current EDSS score), no significant trends were observed based on visual assessment (Figure 17).

In summary, no overall increase in GPx4 mRNA expression was observed in the PBMCs of MS patients after 12 months of DMF treatment. However, a slight rise in Hmox1 mRNA expression was noted. In contrast, the OCR group exhibited a significant increase in both GPx4 and Hmox1 mRNA expression after 12 months of OCR treatment. During both DMF and OCR treatment, the expression levels of GPx4 increased more in younger patients compared to older patients. However, this trend was not evident for Hmox1. Among the DMF cohort, the subject exhibiting the highest GPx4 expression level experienced an attack during DMF therapy.

3.6.3 Changes in GPx4, Hmox1, and TfR mRNA Levels of DMF-Treated RRMS Patients

Finally, in the DMF-treated group, mRNA expression levels of GPx4, Hmox1, and TfR1 were compared, this time after normalization to reference gene β-actin.

The ratios of gene expression levels after 12 months of follow-up to the levels before the start of therapy are shown in Figure 18. Increased GPx4 gene expression was observed in four patients and decreased expression in one patient (median 1.47, IQR: [1.06, 2.62]). Compared to GPx4, Hmox1 mRNA expression showed a higher median expression level after 12 months of DMF treatment (median 1.62, IQR: [1.38, 1.80]). Conversely, TfR1 mRNA levels decreased in three patients, remained stable in one patient, and increased in one patient (median 0.69, IQR: [0.46, 1.02]). Notably, the patient who suffered an attack during DMF had a stable TfR1 expression level (red circle, Figure 18).

In summary, no general increase in GPx4 mRNA expression was observed in the PBMCs of MS patients after 12 months of DMF treatment. A slight overall increase in Hmox1 mRNA expression was observed. A trend towards a decrease in the ferroptosis marker TfR1 was observed after 12 months of treatment.

Figure 18 Alterations of GPx4, Hmox1 and TfR1 Gene Induction after 12 Months of Treatment

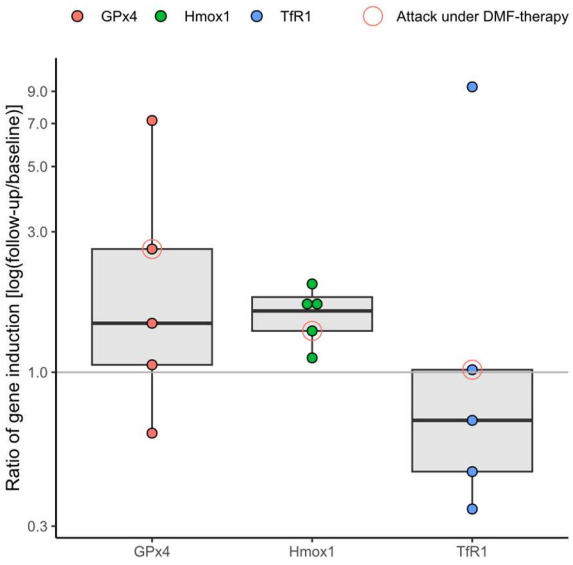

Fig.18: Ratios (12 months follow-up/baseline) of GPx4 (red), Hmox1 (green) and TfR1 (blue) mRNA expression before and after 12 months of treatment in DMF-treated patients (n=5). The horizontal line is positioned at 1 (no difference between pre- and post-12-month therapy). The red circles indicate the ratio of the respective mRNA expression values for the patient who suffered an attack during DMF therapy; DMF: Dimethyl fumarate, GPx4: Glutathione Peroxidase 4, Hmox1: Heme oxygenase 1, TfR1: Transferrin receptor 1, mRNA: messenger ribonucleic acid.

4 Discussion

Ferroptosis has been implicated in the pathogenesis of MS, but its role in the demyelination process and the protective effects of established therapies against ferroptosis remain unclear. This study investigated the effects of ferroptosis on oligodendrocytes and cerebellar myelin, focusing on lipid peroxidation, cell death and demyelination. In addition, the study investigated the potential of fumarates to attenuate cell death and demyelination associated with ferroptosis.

4.1 Cell Survival after Erastin- and Fumarate-Treatment

The susceptibility of oligodendrocytes to ferroptotic cell death was investigated in OLN-93 cells. The survival rate of OLN-93 cells demonstrated a decline with the elevation of ferroptosis inducers Erastin and iron.

In EAE, Hu et al. (2019) did not find GPx4 deficiency in oligodendrocytes, despite a reduced cell number and suggested that neurons are directly affected by ferroptosis, while oligodendrocytes are impacted by various inflammatory mediators. Supporting this, Luoqian et al. (2022) reported that after neurons are damaged by ferroptosis, oligodendrocytes are injured by cytokines expressed by T cells activated by the supernatant of ferroptotic neurons. Nevertheless, the findings of this study suggest a detrimental role, as reflected by the indirect induction of ferroptosis in OLN-93 cells upon Erastin exposure. Whether this process occurs in the pathomechanism of EAE and MS remains unclear.

Furthermore, in vitro pretreatment with the fumarates MMF and DRF increased cell survival when cells were incubated with Erastin, but not when exposed to iron. While treatment with Erastin leads to an intracellular cystine deficiency and a consequent inability for de novo synthesis of the antioxidant GSH, treatment with fumarates causes the expression of over 100 antioxidant proteins via the activation of the Nrf2-pathway, thereby counteracting the deleterious effects of Erastin (Lu et al., 2016). One potential mechanism is the increase in the intracellular recycling rate of pre-existing GSH through the enhanced activation of GSR, thereby increasing GSH availability (Harvey et al., 2009).

Iron was supplied to the cells in the form of ferrous ammonium sulphate. When iron is not bound to proteins such as ferritin or transferrin, as is normally the case physiologically, but is present in free form, it is highly reactive and can potentially cause considerable intra- and extracellular damage through the generation of ROS. This could trigger a cascade of events ranging from membrane and protein damage to DNA damage, disrupted signaling pathways, and ultimately cell damage or cell death (Zuo et al., 2020). Since fumarates mainly act intracellularly via the Nrf2 signaling pathway and could thereby make the cell more resistant to intracellular ROS, the destructive effects originating extracellularly might not be inhibited, which is why fumarates may not be effective in this scenario (Linker et al., 2011; Wang et al., 2024). Furthermore, the incubation process with ferrous ammonium sulphate proved to be a significant challenge due to the rapid precipitation that occurred. To ensure a homogeneous incubation process, the cells were incubated on a horizontal shaker with a rotation speed of 10 rpm. These resulting shear forces may have exerted deleterious effects on cell membranes, potentially leading to additional cell damage and death.

It's important to note that OLN-93 cells display surface antigens similar to those found on primary, late immature oligodendrocytes, including MBP, myelin-associated glycoprotein (MAG), and proteolipid protein (PLP) (Richter-Landsberg & Heinrich, 1996). These cells are positioned between late pre-oligodendrocytes and late immature oligodendrocytes (Buckinx et al., 2009). Consequently, the results

obtained from studies using OLN-93 cells may not be entirely applicable to human oligodendrocytes, whether they are mature cells or at various precursor stages.
Hoshino et al. (2020) demonstrated in MO3.13 cells, another immature oligodendrocyte cell line, that their susceptibility to Erastin-induced ferroptosis decreases with maturation.
In further studies, the susceptibility of primary oligodendrocytes to ferroptotic cell death should be investigated. Given the established vulnerability of OPCs to ferroptosis, it is imperative to investigate the differential susceptibility of primary oligodendrocytes and their progenitors to ferroptosis inducers at varying stages of maturation (Lepka et al., 2017). This approach could provide valuable insights into whether ferroptosis plays a role in remyelination processes, which are often impaired in MS (Gharagozloo et al., 2022).

4.2 Extent of Lipid Peroxidation in Erastin- and Fumarate-Treated OLN-93 Cells

The hypothesis that oligodendrocyte death following Erastin treatment is preceded by lipid peroxidation, indicating ferroptotic cell death, was investigated in OLN-93 cells. Additionally, it was examined whether DRF and MMF could protect cells by reducing lipid peroxidation, suggesting that fumarates can prevent ferroptosis. Cells treated with Erastin for six hours showed an accumulation of lipid peroxidation, while pretreatment with the ferroptosis inhibitor LIP-1 reduced lipid peroxidation as expected. However, protection against lipid peroxidation after fumarate pretreatment could not be demonstrated in OLN-93 cells. Nevertheless, survival assays showed increased cell viability at certain Erastin concentrations when treated with MMF and DRF.
Therefore, the experimental conditions were changed by adjusting several parameters, including the concentrations of fumarates (2-10 µM) and Erastin (IC_{50}- 4x IC_{50}: 2.5-10 µM) as well as the incubation time of the pretreatment (0, 3, 24 hours).
None of these changes in experimental conditions led to a clear confirmation that treatment with fumarates leads to a reduction in lipid peroxidation. However, a trend toward protection against lipid peroxidation was observed at the lowest concentration of Erastin 2.5µM and three hours of pretreatment with fumarates, especially in the presence of 2µM MMF.
It is notable that treatment with fumarates alone resulted in a reduction in lipid peroxidation compared to the untreated control cells. In accordance with the experimental conditions, all cells were incubated in serum-free medium, which has been demonstrated to induce oxidative stress. These findings suggest that fumarates may provide some protection against oxidative stress following a single pretreatment and an incubation period of 24 hours. However, this effect may not be sufficient to reduce lipid peroxidation when cells are exposed to Erastin.
One potential explanation for the absence of a reduction in lipid peroxidation is that the antioxidant gene products of the Nrf2 pathway, including GPx4, FSP1, and GSR, which are activated by fumarates, may exhibit diminished efficacy in OLN-93 cells and necessitate a period exceeding six hours to neutralize lipid peroxides.
The most efficient cellular strategy for preventing ferroptosis involve upregulating the GSH/GPx4 system, primarily via the Nrf2 pathway (Seiler et al., 2008; Yang et al., 2014; Yoo et al., 2012). However, given that GSH levels in oligodendrocytes are naturally low and decline further under oxidative conditions, the GSH/GPx4 system in these cells, including OLN-93 cells, may be insufficient to prevent the accumulation of reactive oxygen products and lipid peroxides (Fan et al., 2021; Lassmann & van Horssen, 2016). Although Hu et al. (2019) demonstrated that GPx4 reduction has a greater impact on the

oxidative/antioxidant balance than GSH reduction in EAE when peroxides accumulate, it can be postulated that this GSH deficiency may play a more significant role in oligodendrocytes. Moreover, while the de novo synthesis of GSH is part of the Nrf2 pathway, the subsequent blocking of the Xc- system by Erastin may have a more significant impact on intracellular GSH levels. Increasing antioxidant enzymes such as GPx4 can improve GSH recycling, but the effect is diminished when GSH levels are inadequate.

Moreover, the current understanding of the regulation of the GSH/GPx4 system, particularly in the context of oligodendrocytes, remains relatively limited. In addition to Nrf2, other transcription factors have been identified as regulators of GPx4 gene expression. These include TFAP2c and Sp1 in neurons and p53 in endothelial cells (Alim et al., 2019; Chen et al., 2021; Lan et al., 2023). Although it has been demonstrated that GPx4 is upregulated via the Nrf2 pathway (see 3.4 and 4.4), an alternative pathway of GPx4 gene expression that is not targeted by fumarates may prove to be a more effective approach in oligodendrocytes.

Moreover, it remains unclear whether GPx4 and other antioxidant enzymes can be adequately stabilized despite the observed upregulation of their gene expression. Post-translational modifications play a pivotal role in the stabilization of GPx4. The precise mechanism by which this occurs remains to be fully elucidated (Lan et al., 2023). Recently, the linear ubiquitin chain assembly complex has been proposed as an important stabilizer for GPx4 (Dong et al., 2022).

Furthermore, the quantity of gene products may be inadequate following a single pretreatment with fumarates prior to Erastin treatment. Accordingly, repeated treatment with fumarates or higher dosing prior to Erastin exposure may be necessary to induce higher expression of antioxidant genes, including genes involved in GSH synthesis, and thus provide better protection against the effects of Erastin. Brennan et al. (2016) reported that after administering a single oral dose of DMF at 100 mg/kg BW to wild-type mice, they detected MMF in the brain tissue at a concentration of 100 µM. At this dosage, our own cell survival assays have demonstrated approximately 80% cell survival after MMF treatment (Fig. 3C). In contrast, DMF and DRF exhibited increasing toxicity at such high doses in cell culture experiments (Fig. 3C), (Majkutewicz, 2022). Given that MMF is the primary metabolite of both DRF and DMF, and MMF is the only metabolite detectable in blood plasma following their ingestion, experiments involving the brain or its cellular components should be conducted exclusively with MMF to accurately reflect the in vivo conditions.

It is important to note that the inhibition of ferroptosis and its regulation vary between different cell types and diseases (Lan et al., 2023). Thus, it remains unclear whether oligodendrocytes possess an alternative, more efficient protective mechanism against ferroptosis than the GPx4/GSH system, such as the GSH-independent enzyme FSP1, which is also targeted by Nrf2. Supporting the idea that the GPx4/GSH system is not the major protection mechanism is the observation by Hu et al. (2019) that oligodendrocyte GPx4 levels remained stable while the number of oligodendrocytes decreased. It is also conceivable that no intrinsic effective protective mechanism exists, rendering oligodendrocytes particularly vulnerable to oxidative stress. Nonetheless, artificial upregulation of GPx4/GSH or FSP1 can still provide a protective antioxidant effect in oligodendrocytes. However, the kinetics of FSP1 in OLN-93 cells, similar to GPx4, have not been examined.

However, since membrane damage caused by lipid peroxides likely increases only after significantly more than six hours, subsequent neutralization could still protect the cells from death. This would be consistent with the results presented in Chapter 3.1.

On the other hand, treatment with LIP-1 proved to be much more effective in eliminating lipid peroxidation. In contrast to fumarates, LIP-1 intervenes more rapidly, preventing the formation of lipid peroxides by directly inhibiting the oxidation of polyunsaturated fatty acids in the bilayers, thereby more efficiently preventing the accumulation of lipid peroxides and restoring the activity of GSH, GPx4 and FSP1 (Fan et al., 2021).
In conclusion, the precise mechanism by which fumarate exerts its protective effect against ferroptotic cell death remains uncertain. The hypothesis that it reduces the accumulation of lipid peroxidation was not confirmed after a single pretreatment and concurrent treatment with fumarates. Further studies with repeated applications of fumarates to OLN-93 cells should be conducted.

4.3 Demyelination and Protection in Organotypic Slice Cultures

The impact of Erastin- and iron-induced ferroptosis on demyelination and axonal degeneration was analyzed, along with the effectiveness of DRF and MMF in protecting against ferroptosis-induced demyelination. Cerebellar OSCs from C57BL/6 wild-type mouse brains (P9-P11) were used, as OSC is a well-established in vitro model representing all major CNS cell types and their interactions, excluding peripheral immune cell migration.
Erastin primarily caused myelin damage, while iron affected both myelin and axons. In the experiments of this thesis, the amount of healthy myelin and axons were assessed after 24 hours incubation with ferroptosis inducers Erastin and iron. The results indicate that the stablished ferroptosis inhibitor LIP-1, DRF, and MMF equally attenuated Erastin-induced myelin damage. For iron-treated slices, the iron chelator SIH offered the best protection against both demyelination and axonal damage.
As observed in cell culture experiments, treatment with fumarates alone resulted in higher healthy myelin in OSCs compared to untreated control slices. Under experimental conditions, all slices were incubated in serum-free medium, which can induce oxidative stress. This suggests that fumarates may offer some protection against oxidative stress after two treatments, as observed in OLN-93 cells in cell culture experiments.
The results of the iron experiments are only partially conclusive due to the difficulty in distinguishing between mechanical and iron-induced ferroptotic damage. As previously stated in chapter 4.1, the incubation process with ferrous ammonium sulphate proved to be challenging due to its rapid precipitation. To ensure uniform incubation conditions, cells were shaken horizontally at 10 rpm, which may have resulted in shear forces that potentially caused additional cell damage. Moreover, the persistent precipitation despite shaking probably required higher iron concentrations than necessary to induce visible damage.
As already described in Birgbauer et al. (2004), the results of the Erastin-treated slices also indicate that the initial consequence of ferroptosis induction is demyelination, namely damage to oligodendrocytes, before axons are targeted. This is supported by the observation that oligodendrocytes are particularly susceptible to ferroptosis, and that they can undergo direct ferroptotic cell death, as previously discussed in Chapter 1.3.4.
While the results for fumarate appear promising with regard to protection against demyelination following Erastin treatment, it is important to consider that this is merely an artificial ferroptosis induction. Given the evidence suggesting that a pro-inflammatory environment likely promotes ferroptosis in MS pathogenesis (Fischer et al., 2012; Lucchinetti et al., 2011),

future studies should investigate demyelination in cerebellar slice cultures following induced neuroinflammation, as well as the potential inhibitory effects of fumarate treatment on this process. To simulate MS-related processes, it is proposed to introduce CD4+ T cells, including CNS-specific Th1 and Th17 cells, into the cerebellar slices. Th1 cells exacerbate pathology by activating local macrophages and microglia via granulocyte-macrophage colony-stimulating factor (GM-CSF), which impairs the survival and differentiation of OPCs (Charabati et al., 2023; Murphy et al., 2010). Proinflammatory microglia have also been demonstrated to play a pivotal role in the initiation of ferroptosis (Ryan et al., 2023). Furthermore, within the CNS, GM-CSF has been observed to promote the differentiation of pathogenic astrocyte subsets while simultaneously inhibiting the functions of anti-inflammatory astrocyte subsets (Charabati et al., 2023). This results in the creation of an additional pro-inflammatory environment. Another approach to induce neuroinflammation in slice cultures would be to add T cells specific to PLP and ovalbumin to brain slices. Nitsch et al. (2004) demonstrated that these cells exhibit a Th1-like profile, predominantly secreting IFN-γ and TNF-α with minimal IL-4 production. In slice cultures, these T cells directly interacted with neurons in an MHC-independent manner, inducing calcium oscillations. Prolonged T cell contact ultimately resulted in lethal increases in neuronal calcium levels.

The precise role of ferroptosis in MS remains uncertain. Does it represent an initial mechanism of neuroinflammation and demyelination, or does it serve as an amplification mechanism in the context of secondary demyelination? The role of ferroptosis in the progression of MS has been previously investigated by Van San et al. (2023). Further studies are required to assess the development of myelin and axon degeneration and regeneration over time, with a longer incubation period or multiple administrations of ferroptosis inducers. It is imperative to assess the activity of oligodendrocyte precursor cells (OPCs) in this context, as it is well-established that OPCs are highly susceptible to ferroptotic cell death (Lepka et al., 2017; Wu et al., 2024).

4.4 Fumarate Treatment Elevates GPx4 Levels in OLN-93 Cells

It is established that treatment with fumarates results in the activation of the Nrf2 pathway and the transcription of antioxidant genes, thereby maintaining intracellular redox homeostasis. The extent to which the Nrf2 signaling pathway also regulates GPx4 is still discussed in the literature (Berndt et al., 2024).

To elucidate the regulation of GPx4, the gene expression of GPx4 and the established Nrf2 target gene Hmox1 in OLN-93 cells following 24 hours of treatment with DRF and MMF was quantified using qPCR. This suggests that GPx4 regulation in oligodendrocytes, particularly in OLN-93 cells, is at least partially mediated by the Nrf2 pathway. However, it is imperative to assess the expression levels of additional known Nrf2 target genes following a 24-hour exposure to fumarates. Nevertheless, it is conceivable that an alternative signaling pathway activated by fumarates could be involved in the regulation of GPx4.

The gene expression results for GPx4 were validated at the protein level through Western blotting of OLN-93 cell extracts. The results showed a consistent upregulation of GPx4 in all cases, regardless of concentration (2 or 10µM) or substance (MMF or DRF), although specific levels could not be determined due to high variability in the data of expression levels.

Since GPx4 gene expression levels are increased after 3 hours of incubation compared to 24 hours, it is recommended to repeat the experiments in this specific case (Tim Prozorovski, 2024, data unpublished). Nevertheless, it is still unclear which quantity of GPx4 is sufficient for optimal protection

against lipid peroxidation. Repeated administration of fumarates may be necessary to achieve an effective level that protects against the accumulation of lipid peroxidation and ferroptotic cell damage. In addition, the same experiments could be repeated with FSP1 as the investigated anti-ferroptotic enzyme, considering that the FSP1 system may be the main protective mechanism against oxidative stress in oligodendrocytes.
The combined findings suggest that DRF and MMF treatments may confer antioxidant protection in oligodendrocytes through the activation of the Nrf2 pathway, which subsequently leads to the upregulation of antioxidant protein expression.

4.5 Fumarate Treatment Elevates GPx4 Levels in Mouse Brain White Matter

The study aimed to validate cell culture findings by examining GPx4 upregulation in brain tissue from DMF-treated mice, while also comparing GPx4 gene expression and protein levels between gray and white matter in different brain regions.
DMF treatment, especially at high doses, significantly increased GPx4 gene and protein expression in mouse brain tissue, with the enhanced effect likely due to repeated administration over seven days. Whether this amount of GPx4 would better protect against the accumulation of lipid peroxidation should be tested in a new experiment by inducing ferroptosis with e.g. Erastin on brain slices from the treated mice and observing them for demyelination and remyelination.
In addition, a significant increase in white matter compared to gray matter was observed in the experiments for this thesis. However, since GPx4 gene expression was not significantly upregulated in gray matter in the experiments for this thesis despite Nrf2 activation by fumarates, this suggests that neuronal GPx4, at least in the cerebrum, is not primarily regulated by Nrf2. Instead, it is likely that GPx4 in neurons is regulated by another transcription factor that is not activated via fumarates. For example, it could be regulated by the TFAP2c/Sp1 system, as demonstrated in the context of stroke by Alim et al. (2019). TFAP2c and Sp1 were shown to be dysregulated in MS according to the microarray gene expression study conducted by Islam et al. (2019).
In EAE, Hu et al. (2019) did not find GPx4 deficiency in oligodendrocytes, despite a reduced cell number. However, the results in section 3.5 show a marked increase in GPx4 expression at the gene and protein levels in the white matter of the cerebellum, which is primarily composed of oligodendrocytes and axons. This suggests that while the GPx4/GSH system in oligodendrocytes plays a minor role in the physiological protection against ferroptosis, it can be artificially upregulated to exhibit some antioxidant effects.

4.6 Gene Expression Levels in PBMCs of RRMS Patients

This experiment investigated the potential absence of GPx4 gene expression in vivo, given the GPx4 deficiency observed in postmortem brain tissue samples from MS patients. It also evaluated whether one year of DMF treatment significantly increased GPx4 gene expression in PBMCs from RRMS patients.
The study used PBMCs due to material availability, as CSF was not collected at the required timepoints. While CSF better reflects CNS processes, PBMC gene expression can indicate disease relapses (Brynedal et al., 2010). However, former findings on GPx activity in PBMCs remained inconclusive (Carvalho et al., 2014).

A major limitation of the study is the small and heterogeneous sample size, with only five patients per group and four healthy volunteers, which precludes statistically significant results and meaningful subgroup analyses, especially for widely scattered gene expression levels. These factors limit the statistical power of the study and the generalizability of the results. Consequently, only descriptive trends can be cautiously discussed. In addition, differences in disease activity levels prior to treatment switching and different pretreatment histories between the ocrelizumab and dimethyl fumarate groups may have influenced baseline gene expression, although no such differences were observed. Similarly, no differences in GPx4 gene expression were found between MS patients and healthy probands. Given the disease state-dependent gene expression patterns and the fact that all patients were in remission at the time of blood sampling, it was expected that patients in remission would not show significant differences.

After 12 months of DMF therapy, hardly any change in GPx4 mRNA expression was observed in the PBMCs of MS patients. Only in two patients a slight upregulation was observed. In addition, a slight increase in Hmox1 mRNA expression was observed, which may indicate activation of the Nrf2 signaling pathway in PBMCs by DMF. A trend towards a decrease in TfR1, a marker for ferroptosis, was also observed, which may indicate the general potential of DMF to inhibit ferroptosis.

Disease activity remained stable in all but one patient, as measured by AAR. In the patient who relapsed one month before the last blood draw, TfR1 levels did not change compared to the first examination, while GPx4 and Hmox1 levels increased slightly. However, as gene expression can change rapidly in relation to disease activity, the gene expression values at the time of relapse are not clear. A limitation of this study is that TfR gene expression was only measured in the PBMCs of DMF-treated patients.

In contrast, the OCR group showed a change in both GPx4 and Hmox1 mRNA expression after 12 months of treatment. The precise mechanism of action of ocrelizumab remains to be fully elucidated. Ocrelizumab exerts its effects through immunomodulation, specifically by reducing the number and function of CD20+ B cells (Flynn & Gerriets, 2024). B cells are implicated in the pathogenesis of MS via mechanisms including antigen presentation, autoantibody production, cytokine regulation, and the formation of ectopic lymphoid aggregates in the meninges, potentially leading to cortical demyelination and neurodegeneration (Hauser et al., 2017; Li et al., 2015; Michel et al., 2015). In RRMS, the migration of activated B cell populations between the CNS and peripheral circulation has been observed (Palanichamy et al., 2014). Disruption of this migratory pathway may underlie the clinical efficacy of ocrelizumab (Hauser et al., 2017). In the OPERA trials, ocrelizumab demonstrated superior efficacy compared to interferon beta-1a, with significantly reduced disability progression at both 12 and 24 weeks, and greater disability improvement at 12 weeks (Hauser et al., 2017). In this patient cohort, we observed elevated GPx4 levels in PBMCs. This finding may suggest that certain migrating immune cells, such as monocytes, T cells, and B cells, could potentially be shifting towards an anti-inflammatory and anti-oxidative phenotype. While further research is needed, these changes might play a role in modulating ferroptosis, though the exact mechanisms require additional investigation. Given that ferroptosis may be important in the pathogenesis of progressive MS (Van San et al., 2023), the inhibition of ferroptosis may explain ocrelizumab's protective effect on disease progression (Hauser et al., 2017).

This study doesn't clarify if GPx4 expression also increases in oligodendrocytes. If Ocrelizumab reaches sufficient concentrations in the CNS (currently unproven), it could potentially increase GPx4 in glial cells and their precursors, potentially protecting them from ferroptotic cell death. The relationship

between Ocrelizumab, GPx4 expression, and ferroptosis in MS is an area that warrants additional investigation.

Further studies with larger sample sizes are needed to gain a more comprehensive understanding of the subject matter. Additionally, evaluating gene expression levels in PBMCs during or shortly after relapse is crucial, as these cells undergo significant compositional changes during that time (Brynedal et al., 2010).

5 Conclusion

Ferroptosis has been implicated in the pathogenesis of MS, although its precise role in the demyelinating process remains unclear. This study suggests that ferroptosis has a detrimental effect on oligodendrocytes and myelin, as demonstrated by Erastin-induced damage in the oligodendroglial cell line OLN-93. Pretreatment with fumarates enhanced cell viability following Erastin exposure. However, it did not mitigate the accumulation of lipid peroxides in OLN-93 cells. These results suggest that the current dosage and incubation regimen may need to be further optimized to accelerate the relevant biochemical processes, reduce the lipid peroxides produced and enhance the protective mechanisms. In OSCs, Erastin-induced ferroptosis primarily targeted myelin, with oligodendrocyte damage preceding axonal injury. The comparable efficacy of an established ferroptosis inhibitor and fumarates in attenuating ferroptosis-associated myelin damage suggests that inhibition of ferroptotic glial cell death may be a part of the mechanism of action of fumarates. This effect may occurs via upregulation of GPx4 through Nrf2 activation.

In conclusion, this study highlights the need for further investigation into the complex relationship between neuroinflammation and ferroptosis-induced demyelination. Future research should focus on long-term dynamics of myelin and axon degeneration and, the role of oligodendrocyte progenitor cells in ferroptosis, as well as possible modulation by fumarates. Recent clinical and MRI evidence suggests that in advanced stages of RRMS, paramagnetic rim lesions (PRLs), reflecting iron-related pathological processes, contribute to the gradual progression of demyelination and axonal degeneration, potentially facilitating the transition to progressive MS. Given that ferroptosis may be the underlying mechanism driving this process, it is crucial to investigate the optimal dosage of fumarates for preventing ferroptosis in MS patients. Notably, a controlled, randomized study found that DMF had no effect on disease progression in patients with PPMS (Hojsgaard Chow et al., 2021), suggesting that the current standard doses of DMF may be insufficient to inhibit ferroptosis. These investigations may provide crucial insights into MS pathogenesis and inform the development of more effective therapeutic strategies.

6 References

Absinta, M., Sati, P., Masuzzo, F., Nair, G., Sethi, V., Kolb, H., Ohayon, J., Wu, T., Cortese, I. C. M., & Reich, D. S. (2019). Association of Chronic Active Multiple Sclerosis Lesions With Disability In Vivo. *JAMA Neurol*, *76*(12), 1474-1483. https://doi.org/10.1001/jamaneurol.2019.2399

Aggarwal, S., Yurlova, L., & Simons, M. (2011). Central nervous system myelin: structure, synthesis and assembly. *Trends in Cell Biology*, *21*(10), 585-593. https://doi.org/10.1016/j.tcb.2011.06.004

Aktas, O., Kury, P., Kieseier, B., & Hartung, H. P. (2010). Fingolimod is a potential novel therapy for multiple sclerosis. *Nature Reviews: Neurology*, *6*(7), 373-382. https://doi.org/10.1038/nrneurol.2010.76

Aktas, O., Smorodchenko, A., Brocke, S., Infante-Duarte, C., Schulze Topphoff, U., Vogt, J., Prozorovski, T., Meier, S., Osmanova, V., Pohl, E., Bechmann, I., Nitsch, R., & Zipp, F. (2005). Neuronal damage in autoimmune neuroinflammation mediated by the death ligand TRAIL. *Neuron*, *46*(3), 421-432. https://doi.org/10.1016/j.neuron.2005.03.018

Alim, I., Caulfield, J. T., Chen, Y., Swarup, V., Geschwind, D. H., Ivanova, E., Seravalli, J., Ai, Y., Sansing, L. H., Ste Marie, E. J., Hondal, R. J., Mukherjee, S., Cave, J. W., Sagdullaev, B. T., Karuppagounder, S. S., & Ratan, R. R. (2019). Selenium Drives a Transcriptional Adaptive Program to Block Ferroptosis and Treat Stroke. *Cell*, *177*(5), 1262-1279 e1225. https://doi.org/10.1016/j.cell.2019.03.032

Atlas of MS. (2023). *https://www.atlasofms.org*. MS International Federation.

Barnes-Velez, J. A., Aksoy Yasar, F. B., & Hu, J. (2023). Myelin lipid metabolism and its role in myelination and myelin maintenance. *Innovation (Camb)*, *4*(1), 100360. https://doi.org/10.1016/j.xinn.2022.100360

Baud, O., Greene, A. E., Li, J., Wang, H., Volpe, J. J., & Rosenberg, P. A. (2004). Glutathione peroxidase-catalase cooperativity is required for resistance to hydrogen peroxide by mature rat oligodendrocytes. *Journal of Neuroscience*, *24*(7), 1531-1540. https://doi.org/10.1523/JNEUROSCI.3989-03.2004

Berndt, C., Alborzinia, H., Amen, V. S., Ayton, S., Barayeu, U., Bartelt, A., Bayir, H., Bebber, C. M., Birsoy, K., Bottcher, J. P., Brabletz, S., Brabletz, T., Brown, A. R., Brune, B., Bulli, G., Bruneau, A., Chen, Q., DeNicola, G. M., Dick, T. P., . . . Conrad, M. (2024). Ferroptosis in health and disease. *Redox Biol*, *75*, 103211. https://doi.org/10.1016/j.redox.2024.103211

Berndt, C., Kurz, T., Selenius, M., Fernandes, A. P., Edgren, M. R., & Brunk, U. T. (2010). Chelation of lysosomal iron protects against ionizing radiation. *Biochemical Journal*, *432*(2), 295-301. https://doi.org/10.1042/BJ20100996

Bierhansl, L., Hartung, H. P., Aktas, O., Ruck, T., Roden, M., & Meuth, S. G. (2022). Thinking outside the box: non-canonical targets in multiple sclerosis. *Nat Rev Drug Discov*, *21*(8), 578-600. https://doi.org/10.1038/s41573-022-00477-5

Birgbauer, E., Rao, T. S., & Webb, M. (2004). Lysolecithin induces demyelination in vitro in a cerebellar slice culture system. *Journal of Neuroscience Research*, *78*(2), 157-166. https://doi.org/10.1002/jnr.20248

Bittner, S., Ruck, T., Wiendl, H., Grauer, O. M., & Meuth, S. G. (2017). Targeting B cells in relapsing-remitting multiple sclerosis: from pathophysiology to optimal clinical management. *Therapeutic Advances in Neurological Disorders*, *10*(1), 51-66. https://doi.org/10.1177/1756285616666741

Bizzozero, O. A., DeJesus, G., Callahan, K., & Pastuszyn, A. (2005). Elevated protein carbonylation in the brain white matter and gray matter of patients with multiple sclerosis. *Journal of Neuroscience Research*, *81*(5), 687-695. https://doi.org/10.1002/jnr.20587

Blauth, K., Owens, G. P., & Bennett, J. L. (2015). The Ins and Outs of B Cells in Multiple Sclerosis. *Frontiers in Immunology*, *6*, 565. https://doi.org/10.3389/fimmu.2015.00565

Brennan, M. S., Patel, H., Allaire, N., Thai, A., Cullen, P., Ryan, S., Lukashev, M., Bista, P., Huang, R., Rhodes, K. J., & Scannevin, R. H. (2016). Pharmacodynamics of Dimethyl Fumarate Are Tissue

Specific and Involve NRF2-Dependent and -Independent Mechanisms. *Antioxid Redox Signal*, *24*(18), 1058-1071. https://doi.org/10.1089/ars.2015.6622

Brynedal, B., Khademi, M., Wallstrom, E., Hillert, J., Olsson, T., & Duvefelt, K. (2010). Gene expression profiling in multiple sclerosis: a disease of the central nervous system, but with relapses triggered in the periphery? *Neurobiology of Disease*, *37*(3), 613-621. https://doi.org/10.1016/j.nbd.2009.11.014

Buckinx, R., Smolders, I., Sahebali, S., Janssen, D., Smets, I., Ameloot, M., & Rigo, J. M. (2009). Morphological changes do not reflect biochemical and functional differentiation in OLN-93 oligodendroglial cells. *Journal of Neuroscience Methods*, *184*(1), 1-9. https://doi.org/10.1016/j.jneumeth.2009.07.004

Calabrese, V., Raffaele, R., Cosentino, E., & Rizza, V. (1994). Changes in cerebrospinal fluid levels of malondialdehyde and glutathione reductase activity in multiple sclerosis. *International Journal of Clinical Pharmacology Research*, *14*(4), 119-123. https://www.ncbi.nlm.nih.gov/pubmed/7607784

Calabrese, V., Scapagnini, G., Ravagna, A., Bella, R., Foresti, R., Bates, T. E., Giuffrida Stella, A. M., & Pennisi, G. (2002). Nitric oxide synthase is present in the cerebrospinal fluid of patients with active multiple sclerosis and is associated with increases in cerebrospinal fluid protein nitrotyrosine and S-nitrosothiols and with changes in glutathione levels. *Journal of Neuroscience Research*, *70*(4), 580-587. https://doi.org/10.1002/jnr.10408

Cao, Y., Li, Y., He, C., Yan, F., Li, J. R., Xu, H. Z., Zhuang, J. F., Zhou, H., Peng, Y. C., Fu, X. J., Lu, X. Y., Yao, Y., Wei, Y. Y., Tong, Y., Zhou, Y. F., & Wang, L. (2021). Selective Ferroptosis Inhibitor Liproxstatin-1 Attenuates Neurological Deficits and Neuroinflammation After Subarachnoid Hemorrhage. *Neuroscience Bulletin*, *37*(4), 535-549. https://doi.org/10.1007/s12264-020-00620-5

Carvalho, A. N., Lim, J. L., Nijland, P. G., Witte, M. E., & Van Horssen, J. (2014). Glutathione in multiple sclerosis: more than just an antioxidant? *Multiple Sclerosis*, *20*(11), 1425-1431. https://doi.org/10.1177/1352458514533400

Charabati, M., Wheeler, M. A., Weiner, H. L., & Quintana, F. J. (2023). Multiple sclerosis: Neuroimmune crosstalk and therapeutic targeting. *Cell*, *186*(7), 1309-1327. https://doi.org/10.1016/j.cell.2023.03.008

Cheff, D. M., Huang, C., Scholzen, K. C., Gencheva, R., Ronzetti, M. H., Cheng, Q., Hall, M. D., & Arner, E. S. J. (2023). The ferroptosis inducing compounds RSL3 and ML162 are not direct inhibitors of GPX4 but of TXNRD1. *Redox Biol*, *62*, 102703. https://doi.org/10.1016/j.redox.2023.102703

Cheli, V. T., Correale, J., Paez, P. M., & Pasquini, J. M. (2020). Iron Metabolism in Oligodendrocytes and Astrocytes, Implications for Myelination and Remyelination. *ASN Neuro*, *12*, 1759091420962681. https://doi.org/10.1177/1759091420962681

Cheli, V. T., Santiago Gonzalez, D. A., Marziali, L. N., Zamora, N. N., Guitart, M. E., Spreuer, V., Pasquini, J. M., & Paez, P. M. (2018). The Divalent Metal Transporter 1 (DMT1) Is Required for Iron Uptake and Normal Development of Oligodendrocyte Progenitor Cells. *Journal of Neuroscience*, *38*(43), 9142-9159. https://doi.org/10.1523/JNEUROSCI.1447-18.2018

Chen, C., Huang, Y., Xia, P., Zhang, F., Li, L., Wang, E., Guo, Q., & Ye, Z. (2021). Long noncoding RNA Meg3 mediates ferroptosis induced by oxygen and glucose deprivation combined with hyperglycemia in rat brain microvascular endothelial cells, through modulating the p53/GPX4 axis. *European Journal of Histochemistry*, *65*(3). https://doi.org/10.4081/ejh.2021.3224

Clarke, M. A., Cheek, R., Kazimuddin, H. F., Hernandez, B., Clarke, R., McKnight, C. D., Derwenskus, J., Eaton, J., Irlmeier, R., Ye, F., O'Grady, K. P., Rogers, B., Smith, S. A., & Bagnato, F. (2024). Paramagnetic rim lesions and the central vein sign: Characterizing multiple sclerosis imaging markers. *Journal of Neuroimaging*, *34*(1), 86-94. https://doi.org/10.1111/jon.13173

Connor, J. R., & Menzies, S. L. (1996). Relationship of iron to oligodendrocytes and myelination. *Glia*, *17*(2), 83-93. https://doi.org/10.1002/(SICI)1098-1136(199606)17:2<83::AID-GLIA1>3.0.CO;2-7

Corazza, M., Odorici, G., Conti, A., Di Lernia, V., Motolese, A., Bardazzi, F., Di Nuzzo, S., Monti, A., Arginelli, F., Filippi, F., Valpiani, G., Morotti, C., & Borghi, A. (2021). Dimethyl fumarate treatment for psoriasis in a real-life setting: A multicentric retrospective study. *Dermatologic Therapy*, *34*(5), e15066. https://doi.org/10.1111/dth.15066

Cortese, M., Munger, K. L., Martinez-Lapiscina, E. H., Barro, C., Edan, G., Freedman, M. S., Hartung, H. P., Montalban, X., Foley, F. W., Penner, I. K., Hemmer, B., Fox, E. J., Schippling, S., Wicklein, E. M., Kappos, L., Kuhle, J., Ascherio, A., & Group, B. S. (2020). Vitamin D, smoking, EBV, and long-term cognitive performance in MS: 11-year follow-up of BENEFIT. *Neurology*, *94*(18), e1950-e1960. https://doi.org/10.1212/WNL.0000000000009371

Dal-Bianco, A., Grabner, G., Kronnerwetter, C., Weber, M., Hoftberger, R., Berger, T., Auff, E., Leutmezer, F., Trattnig, S., Lassmann, H., Bagnato, F., & Hametner, S. (2017). Slow expansion of multiple sclerosis iron rim lesions: pathology and 7 T magnetic resonance imaging. *Acta Neuropathologica*, *133*(1), 25-42. https://doi.org/10.1007/s00401-016-1636-z

Dal-Bianco, A., Grabner, G., Kronnerwetter, C., Weber, M., Kornek, B., Kasprian, G., Berger, T., Leutmezer, F., Rommer, P. S., Trattnig, S., Lassmann, H., & Hametner, S. (2021). Long-term evolution of multiple sclerosis iron rim lesions in 7 T MRI. *Brain*, *144*(3), 833-847. https://doi.org/10.1093/brain/awaa436

Dietrich, M., Hecker, C., Nasiri, M., Samsam, S., Issberner, A., Kohne, Z., Hartung, H. P., & Albrecht, P. (2020). Neuroprotective Properties of Dimethyl Fumarate Measured by Optical Coherence Tomography in Non-inflammatory Animal Models. *Frontiers in Neurology*, *11*, 601628. https://doi.org/10.3389/fneur.2020.601628

Dixon, S. J., Lemberg, K. M., Lamprecht, M. R., Skouta, R., Zaitsev, E. M., Gleason, C. E., Patel, D. N., Bauer, A. J., Cantley, A. M., Yang, W. S., Morrison, B., 3rd, & Stockwell, B. R. (2012). Ferroptosis: an iron-dependent form of nonapoptotic cell death. *Cell*, *149*(5), 1060-1072. https://doi.org/10.1016/j.cell.2012.03.042

Dodson, M., Castro-Portuguez, R., & Zhang, D. D. (2019). NRF2 plays a critical role in mitigating lipid peroxidation and ferroptosis. *Redox Biol*, *23*, 101107. https://doi.org/10.1016/j.redox.2019.101107

Dong, K., Wei, R., Jin, T., Zhang, M., Shen, J., Xiang, H., Shan, B., Yuan, J., & Li, Y. (2022). HOIP modulates the stability of GPx4 by linear ubiquitination. *Proceedings of the National Academy of Sciences of the United States of America*, *119*(44), e2214227119. https://doi.org/10.1073/pnas.2214227119

Duarte-Silva, E., Meuth, S. G., & Peixoto, C. A. (2023). The role of iron metabolism in the pathogenesis and treatment of multiple sclerosis. *Frontiers in Immunology*, *14*, 1137635. https://doi.org/10.3389/fimmu.2023.1137635

Duffy, S. S., Lees, J. G., & Moalem-Taylor, G. (2014). The contribution of immune and glial cell types in experimental autoimmune encephalomyelitis and multiple sclerosis. *Multiple Sclerosis International*, *2014*, 285245. https://doi.org/10.1155/2014/285245

Fagnart, O. C., Sindic, C. J., & Laterre, C. (1988). Free kappa and lambda light chain levels in the cerebrospinal fluid of patients with multiple sclerosis and other neurological diseases. *Journal of Neuroimmunology*, *19*(1-2), 119-132. https://doi.org/10.1016/0165-5728(88)90041-0

Faiss, J. (2020). *Multiple Sklerose. In P. Berlit (Hrsg.). Klinische Neurologie.* (Vol. 4). Springer-Verlag GmbH Deutschland, 1063-1123. https://doi.org/10.1007/978-3-662-60676-6_157

Fan, B. Y., Pang, Y. L., Li, W. X., Zhao, C. X., Zhang, Y., Wang, X., Ning, G. Z., Kong, X. H., Liu, C., Yao, X., & Feng, S. Q. (2021). Liproxstatin-1 is an effective inhibitor of oligodendrocyte ferroptosis induced by inhibition of glutathione peroxidase 4. *Neural Regen Res*, *16*(3), 561-566. https://doi.org/10.4103/1673-5374.293157

Fischer, M. T., Sharma, R., Lim, J. L., Haider, L., Frischer, J. M., Drexhage, J., Mahad, D., Bradl, M., van Horssen, J., & Lassmann, H. (2012). NADPH oxidase expression in active multiple sclerosis lesions in relation to oxidative tissue damage and mitochondrial injury. *Brain*, *135*(Pt 3), 886-899. https://doi.org/10.1093/brain/aws012

Fischer, M. T., Wimmer, I., Hoftberger, R., Gerlach, S., Haider, L., Zrzavy, T., Hametner, S., Mahad, D., Binder, C. J., Krumbholz, M., Bauer, J., Bradl, M., & Lassmann, H. (2013). Disease-specific molecular events in cortical multiple sclerosis lesions. *Brain*, *136*(Pt 6), 1799-1815. https://doi.org/10.1093/brain/awt110

Flynn, J. P., & Gerriets, V. (2024). Ocrelizumab. In *StatPearls*. https://www.ncbi.nlm.nih.gov/pubmed/31613530

Gale, C. R., & Martyn, C. N. (1995). Migrant studies in multiple sclerosis. *Progress in Neurobiology*, *47*(4-5), 425-448. https://www.ncbi.nlm.nih.gov/pubmed/8966212

https://www.sciencedirect.com/science/article/abs/pii/030100829580008V?via%3Dihub

Gao, W., Guo, L., Yang, Y., Wang, Y., Xia, S., Gong, H., Zhang, B. K., & Yan, M. (2021). Dissecting the Crosstalk Between Nrf2 and NF-kappaB Response Pathways in Drug-Induced Toxicity. *Front Cell Dev Biol*, *9*, 809952. https://doi.org/10.3389/fcell.2021.809952

Gharagozloo, M., Bannon, R., & Calabresi, P. A. (2022). Breaking the barriers to remyelination in multiple sclerosis. *Current Opinion in Pharmacology*, *63*, 102194. https://doi.org/10.1016/j.coph.2022.102194

Girotti, A. W. (1985). Mechanisms of lipid peroxidation. *Journal of Free Radicals in Biology and Medicine*, *1*(2), 87-95. https://doi.org/10.1016/0748-5514(85)90011-x

Graf, J., Albrecht, P., Goebels, N., Aktas, O., & Hartung, H. P. (2020). [Ocrelizumab for treatment of multiple sclerosis]. *Nervenarzt*, *91*(8), 722-734. https://doi.org/10.1007/s00115-020-00937-6 (Ocrelizumab zur Behandlung der Multiplen Sklerose.)

Gray, E., Thomas, T. L., Betmouni, S., Scolding, N., & Love, S. (2008). Elevated activity and microglial expression of myeloperoxidase in demyelinated cerebral cortex in multiple sclerosis. *Brain Pathology*, *18*(1), 86-95. https://doi.org/10.1111/j.1750-3639.2007.00110.x

Gross, C. C., Schulte-Mecklenbeck, A., Klinsing, S., Posevitz-Fejfar, A., Wiendl, H., & Klotz, L. (2016). Dimethyl fumarate treatment alters circulating T helper cell subsets in multiple sclerosis. *Neurol Neuroimmunol Neuroinflamm*, *3*(1), e183. https://doi.org/10.1212/NXI.0000000000000183

Hametner, S., Wimmer, I., Haider, L., Pfeifenbring, S., Bruck, W., & Lassmann, H. (2013). Iron and neurodegeneration in the multiple sclerosis brain. *Annals of Neurology*, *74*(6), 848-861. https://doi.org/10.1002/ana.23974

Hartung, H. P., Aktas, O., & Boyko, A. N. (2015). Alemtuzumab: a new therapy for active relapsing-remitting multiple sclerosis. *Multiple Sclerosis*, *21*(1), 22-34. https://doi.org/10.1177/1352458514549398

Harvey, C. J., Thimmulappa, R. K., Singh, A., Blake, D. J., Ling, G., Wakabayashi, N., Fujii, J., Myers, A., & Biswal, S. (2009). Nrf2-regulated glutathione recycling independent of biosynthesis is critical for cell survival during oxidative stress. *Free Radical Biology and Medicine*, *46*(4), 443-453. https://doi.org/10.1016/j.freeradbiomed.2008.10.040

Hauser, S. L., Bar-Or, A., Comi, G., Giovannoni, G., Hartung, H. P., Hemmer, B., Lublin, F., Montalban, X., Rammohan, K. W., Selmaj, K., Traboulsee, A., Wolinsky, J. S., Arnold, D. L., Klingelschmitt, G., Masterman, D., Fontoura, P., Belachew, S., Chin, P., Mairon, N., . . . Investigators, O. I. C. (2017). Ocrelizumab versus Interferon Beta-1a in Relapsing Multiple Sclerosis. *New England Journal of Medicine*, *376*(3), 221-234. https://doi.org/10.1056/NEJMoa1601277

He, A., Merkel, B., Brown, J. W. L., Zhovits Ryerson, L., Kister, I., Malpas, C. B., Sharmin, S., Horakova, D., Kubala Havrdova, E., Spelman, T., Izquierdo, G., Eichau, S., Trojano, M., Lugaresi, A., Hupperts, R., Sola, P., Ferraro, D., Lycke, J., Grand'Maison, F., . . . group, M. S. s. (2020). Timing of high-efficacy therapy for multiple sclerosis: a retrospective observational cohort study. *Lancet Neurology*, *19*(4), 307-316. https://doi.org/10.1016/S1474-4422(20)30067-3

Hohlfeld, R., Dornmair, K., Meinl, E., & Wekerle, H. (2016). The search for the target antigens of multiple sclerosis, part 1: autoreactive CD4+ T lymphocytes as pathogenic effectors and therapeutic targets. *Lancet Neurology*, *15*(2), 198-209. https://doi.org/10.1016/S1474-4422(15)00334-8

Hojsgaard Chow, H., Talbot, J., Lundell, H., Gobel Madsen, C., Marstrand, L., Lange, T., Mahler, M. R., Buhelt, S., Holm Hansen, R., Blinkenberg, M., Romme Christensen, J., Soelberg Sorensen, P., Rode von Essen, M., Siebner, H. R., & Sellebjerg, F. (2021). Dimethyl Fumarate Treatment in Patients With Primary Progressive Multiple Sclerosis: A Randomized, Controlled Trial. *Neurol Neuroimmunol Neuroinflamm*, *8*(5). https://doi.org/10.1212/NXI.0000000000001037

Hoshino, T., Yamakado, H., Takahashi, R., & Matsuzawa, S. I. (2020). Susceptibility to erastin-induced ferroptosis decreases during maturation in a human oligodendrocyte cell line. *FEBS Open Bio*, *10*(9), 1758-1764. https://doi.org/10.1002/2211-5463.12923

Hu, C. L., Nydes, M., Shanley, K. L., Morales Pantoja, I. E., Howard, T. A., & Bizzozero, O. A. (2019). Reduced expression of the ferroptosis inhibitor glutathione peroxidase-4 in multiple sclerosis and experimental autoimmune encephalomyelitis. *Journal of Neurochemistry*, *148*(3), 426-439. https://doi.org/10.1111/jnc.14604

Hufschmidt, A., Lücking, C.H., Rauer, S., Glocker, F.X. (2020). *Neurologie compact* (Vol. 8). Thieme, 269-287.

Ingwersen, J., Aktas, O., Kuery, P., Kieseier, B., Boyko, A., & Hartung, H. P. (2012). Fingolimod in multiple sclerosis: mechanisms of action and clinical efficacy. *Clinical Immunology*, *142*(1), 15-24. https://doi.org/10.1016/j.clim.2011.05.005

Interchim. (2023). *BC Assay Protein Quantitation Kit – User Manual* *https://www.interchim.fr/ft/4/40840A.pdf*.

Islam, T., Rahman, R., Karim, R., Huq, F., Quinn, J. M. W., & Moni, M. A. (2019). Detection of Multiple Sclerosis using Blood and Brain Cells Transcript Profiles: Insights from Comprehensive Bioinformatics Approach. *Informatics in Medicine Unlocked*, *16*. https://doi.org/10.1016/j.imu.2019.100201

Jack, C., Ruffini, F., Bar-Or, A., & Antel, J. P. (2005). Microglia and multiple sclerosis. *Journal of Neuroscience Research*, *81*(3), 363-373. https://doi.org/10.1002/jnr.20482

Jakimovski, D., Bittner, S., Zivadinov, R., Morrow, S. A., Benedict, R. H., Zipp, F., & Weinstock-Guttman, B. (2024). Multiple sclerosis. *Lancet*, *403*(10422), 183-202. https://doi.org/10.1016/S0140-6736(23)01473-3

Jelcic, I., Al Nimer, F., Wang, J., Lentsch, V., Planas, R., Jelcic, I., Madjovski, A., Ruhrmann, S., Faigle, W., Frauenknecht, K., Pinilla, C., Santos, R., Hammer, C., Ortiz, Y., Opitz, L., Gronlund, H., Rogler, G., Boyman, O., Reynolds, R., . . . Martin, R. (2018). Memory B Cells Activate Brain-Homing, Autoreactive CD4(+) T Cells in Multiple Sclerosis. *Cell*, *175*(1), 85-100 e123. https://doi.org/10.1016/j.cell.2018.08.011

Kocur, M., Schneider, R., Pulm, A. K., Bauer, J., Kropp, S., Gliem, M., Ingwersen, J., Goebels, N., Alferink, J., Prozorovski, T., Aktas, O., & Scheu, S. (2015). IFNbeta secreted by microglia mediates clearance of myelin debris in CNS autoimmunity. *Acta Neuropathol Commun*, *3*, 20. https://doi.org/10.1186/s40478-015-0192-4

Kraft, V. A. N., Bezjian, C. T., Pfeiffer, S., Ringelstetter, L., Muller, C., Zandkarimi, F., Merl-Pham, J., Bao, X., Anastasov, N., Kossl, J., Brandner, S., Daniels, J. D., Schmitt-Kopplin, P., Hauck, S. M., Stockwell, B. R., Hadian, K., & Schick, J. A. (2020). GTP Cyclohydrolase 1/Tetrahydrobiopterin Counteract Ferroptosis through Lipid Remodeling. *ACS Cent Sci*, *6*(1), 41-53. https://doi.org/10.1021/acscentsci.9b01063

Kuhlmann, T., Moccia, M., Coetzee, T., Cohen, J. A., Correale, J., Graves, J., Marrie, R. A., Montalban, X., Yong, V. W., Thompson, A. J., Reich, D. S., & International Advisory Committee on Clinical Trials in Multiple, S. (2023). Multiple sclerosis progression: time for a new mechanism-driven framework. *Lancet Neurology*, *22*(1), 78-88. https://doi.org/10.1016/S1474-4422(22)00289-7

La Rosa, F., Wynen, M., Al-Louzi, O., Beck, E. S., Huelnhagen, T., Maggi, P., Thiran, J. P., Kober, T., Shinohara, R. T., Sati, P., Reich, D. S., Granziera, C., Absinta, M., & Bach Cuadra, M. (2022). Cortical lesions, central vein sign, and paramagnetic rim lesions in multiple sclerosis: Emerging machine learning techniques and future avenues. *Neuroimage Clin*, *36*, 103205. https://doi.org/10.1016/j.nicl.2022.103205

Lan, T., Sun, T. T., Wei, C., Cheng, T., Yang, F., Zhang, J. N., & Li, Q. (2023). Epigenetic Regulation of Ferroptosis in Central Nervous System Diseases. *Molecular Neurobiology*, *60*(7), 3584-3599. https://doi.org/10.1007/s12035-023-03267-1

Lassmann, H. (2020). Pathology of inflammatory diseases of the nervous system: Human disease versus animal models. *Glia*, *68*(4), 830-844. https://doi.org/10.1002/glia.23726

Lassmann, H. (2022). The contribution of neuropathology to multiple sclerosis research. *European Journal of Neurology*, *29*(9), 2869-2877. https://doi.org/10.1111/ene.15360

Lassmann, H., & van Horssen, J. (2016). Oxidative stress and its impact on neurons and glia in multiple sclerosis lesions. *Biochimica et Biophysica Acta*, *1862*(3), 506-510. https://doi.org/10.1016/j.bbadis.2015.09.018

Lepka, K., Volbracht, K., Bill, E., Schneider, R., Rios, N., Hildebrandt, T., Ingwersen, J., Prozorovski, T., Lillig, C. H., van Horssen, J., Steinman, L., Hartung, H. P., Radi, R., Holmgren, A., Aktas, O., & Berndt, C. (2017). Iron-sulfur glutaredoxin 2 protects oligodendrocytes against damage induced by nitric oxide release from activated microglia. *Glia*, *65*(9), 1521-1534. https://doi.org/10.1002/glia.23178

Levraut, M., Laurent-Chabalier, S., Ayrignac, X., Bigaut, K., Rival, M., Squalli, S., Zephir, H., Alberto, T., Pekar, J. D., Ciron, J., Biotti, D., Puissant-Lubrano, B., Camdessanche, J. P., Tholance, Y., Casez, O., Toussaint, B., Marion, J., Moreau, T., Lakomy, D., . . . Societe Francophone de la Sclerose En, P. (2023). Kappa Free Light Chain Biomarkers Are Efficient for the Diagnosis of Multiple Sclerosis: A Large Multicenter Cohort Study. *Neurol Neuroimmunol Neuroinflamm*, *10*(1). https://doi.org/10.1212/NXI.0000000000200049

Li, R., Rezk, A., Miyazaki, Y., Hilgenberg, E., Touil, H., Shen, P., Moore, C. S., Michel, L., Althekair, F., Rajasekharan, S., Gommerman, J. L., Prat, A., Fillatreau, S., Bar-Or, A., & Canadian, B. c. i. M. S. T. (2015). Proinflammatory GM-CSF-producing B cells in multiple sclerosis and B cell depletion therapy. *Science Translational Medicine*, *7*(310), 310ra166. https://doi.org/10.1126/scitranslmed.aab4176

Li, S., He, Y., Chen, K., Sun, J., Zhang, L., He, Y., Yu, H., & Li, Q. (2021). RSL3 Drives Ferroptosis through NF-kappaB Pathway Activation and GPX4 Depletion in Glioblastoma. *Oxidative Medicine and Cellular Longevity*, *2021*, 2915019. https://doi.org/10.1155/2021/2915019

Li, Y., Wang, B., Yang, J., Liu, R., Xie, J., & Wang, J. (2023). Iron Overload Causes Ferroptosis But Not Apoptosis in MO3.13 Oligodendrocytes. *Neurochemical Research*, *48*(3), 830-838. https://doi.org/10.1007/s11064-022-03807-6

Linker, R. A., & Gold, R. (2013). Dimethyl fumarate for treatment of multiple sclerosis: mechanism of action, effectiveness, and side effects. *Current Neurology and Neuroscience Reports*, *13*(11), 394. https://doi.org/10.1007/s11910-013-0394-8

Linker, R. A., Lee, D. H., Ryan, S., van Dam, A. M., Conrad, R., Bista, P., Zeng, W., Hronowsky, X., Buko, A., Chollate, S., Ellrichmann, G., Bruck, W., Dawson, K., Goelz, S., Wiese, S., Scannevin, R. H., Lukashev, M., & Gold, R. (2011). Fumaric acid esters exert neuroprotective effects in neuroinflammation via activation of the Nrf2 antioxidant pathway. *Brain*, *134*(Pt 3), 678-692. https://doi.org/10.1093/brain/awq386

Lu, M. C., Ji, J. A., Jiang, Z. Y., & You, Q. D. (2016). The Keap1-Nrf2-ARE Pathway As a Potential Preventive and Therapeutic Target: An Update. *Medicinal Research Reviews*, *36*(5), 924-963. https://doi.org/10.1002/med.21396

Lublin, F. D. (2014). New multiple sclerosis phenotypic classification. *European Neurology*, *72 Suppl 1*, 1-5. https://doi.org/10.1159/000367614

Lucchinetti, C. F., Popescu, B. F., Bunyan, R. F., Moll, N. M., Roemer, S. F., Lassmann, H., Bruck, W., Parisi, J. E., Scheithauer, B. W., Giannini, C., Weigand, S. D., Mandrekar, J., & Ransohoff, R. M. (2011). Inflammatory cortical demyelination in early multiple sclerosis. *New England Journal of Medicine*, *365*(23), 2188-2197. https://doi.org/10.1056/NEJMoa1100648

Luoqian, J., Yang, W., Ding, X., Tuo, Q. Z., Xiang, Z., Zheng, Z., Guo, Y. J., Li, L., Guan, P., Ayton, S., Dong, B., Zhang, H., Hu, H., & Lei, P. (2022). Ferroptosis promotes T-cell activation-induced neurodegeneration in multiple sclerosis. *Cellular & Molecular Immunology*, *19*(8), 913-924. https://doi.org/10.1038/s41423-022-00883-0

Mahad, D. H., Trapp, B. D., & Lassmann, H. (2015). Pathological mechanisms in progressive multiple sclerosis. *Lancet Neurology*, *14*(2), 183-193. https://doi.org/10.1016/S1474-4422(14)70256-X

Mahad, D. J., Ziabreva, I., Campbell, G., Lax, N., White, K., Hanson, P. S., Lassmann, H., & Turnbull, D. M. (2009). Mitochondrial changes within axons in multiple sclerosis. *Brain*, *132*(Pt 5), 1161-1174. https://doi.org/10.1093/brain/awp046

Majkutewicz, I. (2022). Dimethyl fumarate: A review of preclinical efficacy in models of neurodegenerative diseases. *European Journal of Pharmacology*, *926*, 175025. https://doi.org/10.1016/j.ejphar.2022.175025

Marrie, R. A. (2011). Demographic, genetic, and environmental factors that modify disease course. *Neurologic Clinics*, *29*(2), 323-341. https://doi.org/10.1016/j.ncl.2010.12.004

Marti, Z., Ruder, J., Thomas, O. G., Bronge, M., De La Parra Soto, L., Gronlund, H., Olsson, T., & Martin, R. (2024). Enhanced and cross-reactive in vitro memory B cell response against Epstein-Barr virus nuclear antigen 1 in multiple sclerosis. *Frontiers in Immunology*, *15*, 1334720. https://doi.org/10.3389/fimmu.2024.1334720

Martinez, A. M., Kim, A., & Yang, W. S. (2020). Detection of Ferroptosis by BODIPY 581/591 C11. *Methods in Molecular Biology*, *2108*, 125-130. https://doi.org/10.1007/978-1-0716-0247-8_11

McDonald, W. I., Compston, A., Edan, G., Goodkin, D., Hartung, H. P., Lublin, F. D., McFarland, H. F., Paty, D. W., Polman, C. H., Reingold, S. C., Sandberg-Wollheim, M., Sibley, W., Thompson, A., van den Noort, S., Weinshenker, B. Y., & Wolinsky, J. S. (2001). Recommended diagnostic criteria for multiple sclerosis: guidelines from the International Panel on the diagnosis of multiple sclerosis. *Annals of Neurology*, *50*(1), 121-127. https://doi.org/10.1002/ana.1032

Michel, L., Touil, H., Pikor, N. B., Gommerman, J. L., Prat, A., & Bar-Or, A. (2015). B Cells in the Multiple Sclerosis Central Nervous System: Trafficking and Contribution to CNS-Compartmentalized Inflammation. *Frontiers in Immunology*, *6*, 636. https://doi.org/10.3389/fimmu.2015.00636

Mitchell, K. M., Dotson, A. L., Cool, K. M., Chakrabarty, A., Benedict, S. H., & LeVine, S. M. (2007). Deferiprone, an orally deliverable iron chelator, ameliorates experimental autoimmune encephalomyelitis. *Multiple Sclerosis*, *13*(9), 1118-1126. https://doi.org/10.1177/1352458507078916

Moharregh-Khiabani, D., Linker, R. A., Gold, R., & Stangel, M. (2009). Fumaric Acid and its esters: an emerging treatment for multiple sclerosis. *Current Neuropharmacology*, *7*(1), 60-64. https://doi.org/10.2174/157015909787602788

Moutsianas, L., Jostins, L., Beecham, A. H., Dilthey, A. T., Xifara, D. K., Ban, M., Shah, T. S., Patsopoulos, N. A., Alfredsson, L., Anderson, C. A., Attfield, K. E., Baranzini, S. E., Barrett, J., Binder, T. M. C., Booth, D., Buck, D., Celius, E. G., Cotsapas, C., D'Alfonso, S., . . . McVean, G. (2015). Class II HLA interactions modulate genetic risk for multiple sclerosis. *Nature Genetics*, *47*(10), 1107-1113. https://doi.org/10.1038/ng.3395

Murphy, A. C., Lalor, S. J., Lynch, M. A., & Mills, K. H. (2010). Infiltration of Th1 and Th17 cells and activation of microglia in the CNS during the course of experimental autoimmune encephalomyelitis. *Brain, Behavior, and Immunity*, *24*(4), 641-651. https://doi.org/10.1016/j.bbi.2010.01.014

Naismith, R. T., Wundes, A., Ziemssen, T., Jasinska, E., Freedman, M. S., Lembo, A. J., Selmaj, K., Bidollari, I., Chen, H., Hanna, J., Leigh-Pemberton, R., Lopez-Bresnahan, M., Lyons, J., Miller, C., Rezendes, D., Wolinsky, J. S., & Group, E.-M.-S. (2020). Diroximel Fumarate Demonstrates an Improved Gastrointestinal Tolerability Profile Compared with Dimethyl Fumarate in Patients with Relapsing-Remitting Multiple Sclerosis: Results from the Randomized, Double-Blind, Phase III EVOLVE-MS-2 Study. *CNS Drugs*, *34*(2), 185-196. https://doi.org/10.1007/s40263-020-00700-0

Nitsch, R., Pohl, E. E., Smorodchenko, A., Infante-Duarte, C., Aktas, O., & Zipp, F. (2004). Direct impact of T cells on neurons revealed by two-photon microscopy in living brain tissue. *Journal of Neuroscience*, *24*(10), 2458-2464. https://doi.org/10.1523/JNEUROSCI.4703-03.2004

O'Sullivan, S. A., & Dev, K. K. (2017). The chemokine fractalkine (CX3CL1) attenuates H(2)O(2)-induced demyelination in cerebellar slices. *Journal of Neuroinflammation*, *14*(1), 159. https://doi.org/10.1186/s12974-017-0932-4

Osburn, W. O., Wakabayashi, N., Misra, V., Nilles, T., Biswal, S., Trush, M. A., & Kensler, T. W. (2006). Nrf2 regulates an adaptive response protecting against oxidative damage following diquat-mediated formation of superoxide anion. *Archives of Biochemistry and Biophysics*, *454*(1), 7-15. https://doi.org/10.1016/j.abb.2006.08.005

Ou, M., Jiang, Y., Ji, Y., Zhou, Q., Du, Z., Zhu, H., & Zhou, Z. (2022). Role and mechanism of ferroptosis in neurological diseases. *Mol Metab*, *61*, 101502. https://doi.org/10.1016/j.molmet.2022.101502

Paez, P. M., Marta, C. B., Moreno, M. B., Soto, E. F., & Pasquini, J. M. (2002). Apotransferrin decreases migration and enhances differentiation of oligodendroglial progenitor cells in an in vitro system. *Developmental Neuroscience*, *24*(1), 47-58. https://doi.org/10.1159/000064945

Palanichamy, A., Apeltsin, L., Kuo, T. C., Sirota, M., Wang, S., Pitts, S. J., Sundar, P. D., Telman, D., Zhao, L. Z., Derstine, M., Abounasr, A., Hauser, S. L., & von Budingen, H. C. (2014). Immunoglobulin class-switched B cells form an active immune axis between CNS and periphery in multiple sclerosis. *Science Translational Medicine*, *6*(248), 248ra106. https://doi.org/10.1126/scitranslmed.3008930

Palte, M. J., Wehr, A., Tawa, M., Perkin, K., Leigh-Pemberton, R., Hanna, J., Miller, C., & Penner, N. (2019). Improving the Gastrointestinal Tolerability of Fumaric Acid Esters: Early Findings on Gastrointestinal Events with Diroximel Fumarate in Patients with Relapsing-Remitting Multiple Sclerosis from the Phase 3, Open-Label EVOLVE-MS-1 Study. *Advances in Therapy*, *36*(11), 3154-3165. https://doi.org/10.1007/s12325-019-01085-3

Papadopoulou, A., D'Souza, M., Kappos, L., & Yaldizli, O. (2010). Dimethyl fumarate for multiple sclerosis. *Expert Opin Investig Drugs*, *19*(12), 1603-1612. https://doi.org/10.1517/13543784.2010.534778

Parodi, B., Rossi, S., Morando, S., Cordano, C., Bragoni, A., Motta, C., Usai, C., Wipke, B. T., Scannevin, R. H., Mancardi, G. L., Centonze, D., Kerlero de Rosbo, N., & Uccelli, A. (2015). Fumarates modulate microglia activation through a novel HCAR2 signaling pathway and rescue synaptic dysregulation in inflamed CNS. *Acta Neuropathologica*, *130*(2), 279-295. https://doi.org/10.1007/s00401-015-1422-3

Pedchenko, T. V., & LeVine, S. M. (1998). Desferrioxamine suppresses experimental allergic encephalomyelitis induced by MBP in SJL mice. *Journal of Neuroimmunology*, *84*(2), 188-197. https://doi.org/10.1016/s0165-5728(97)00256-7

Pipek, L. Z., Mahler, J. V., Nascimento, R. F. V., Apostolos-Pereira, S. L., Silva, G. D., & Callegaro, D. (2023). Cost, efficacy, and safety comparison between early intensive and escalating strategies for multiple sclerosis: A systematic review and meta-analysis. *Mult Scler Relat Disord*, *71*, 104581. https://doi.org/10.1016/j.msard.2023.104581

Promega. (2023). *CellTiter-Blue® Cell Viability Assay, Technical Bulletin #TB317,* *https://www.promega.com/-/media/files/resources/protocols/technical-bulletins/101/celltiter-blue-cell-viability-assay-protocol.pdf*.

Reinert, A., Morawski, M., Seeger, J., Arendt, T., & Reinert, T. (2019). Iron concentrations in neurons and glial cells with estimates on ferritin concentrations. *BMC Neuroscience*, *20*(1), 25. https://doi.org/10.1186/s12868-019-0507-7

Ren, J. X., Sun, X., Yan, X. L., Guo, Z. N., & Yang, Y. (2020). Ferroptosis in Neurological Diseases. *Frontiers in Cellular Neuroscience*, *14*, 218. https://doi.org/10.3389/fncel.2020.00218

Richter-Landsberg, C., & Heinrich, M. (1996). OLN-93: a new permanent oligodendroglia cell line derived from primary rat brain glial cultures. *Journal of Neuroscience Research*, *45*(2), 161-173. https://doi.org/10.1002/(SICI)1097-4547(19960715)45:2<161::AID-JNR8>3.0.CO;2-8

Ropele, S., Enzinger, C., & Fazekas, F. (2017). Iron Mapping in Multiple Sclerosis. *Neuroimaging Clinics of North America*, *27*(2), 335-342. https://doi.org/10.1016/j.nic.2016.12.003

Ryan, S. K., Zelic, M., Han, Y., Teeple, E., Chen, L., Sadeghi, M., Shankara, S., Guo, L., Li, C., Pontarelli, F., Jensen, E. H., Comer, A. L., Kumar, D., Zhang, M., Gans, J., Zhang, B., Proto, J. D., Saleh, J., Dodge, J. C., . . . Hammond, T. R. (2023). Microglia ferroptosis is regulated by SEC24B and contributes to neurodegeneration. *Nature Neuroscience*, *26*(1), 12-26. https://doi.org/10.1038/s41593-022-01221-3

Salazar, M., Rojo, A. I., Velasco, D., de Sagarra, R. M., & Cuadrado, A. (2006). Glycogen synthase kinase-3beta inhibits the xenobiotic and antioxidant cell response by direct phosphorylation and nuclear exclusion of the transcription factor Nrf2. *Journal of Biological Chemistry*, *281*(21), 14841-14851. https://doi.org/10.1074/jbc.M513737200

Saleh, M. C., Espinosa de los Monteros, A., de Arriba Zerpa, G. A., Fontaine, I., Piaud, O., Djordjijevic, D., Baroukh, N., Garcia Otin, A. L., Ortiz, E., Lewis, S., Fiette, L., Santambrogio, P., Belzung, C., Connor, J. R., de Vellis, J., Pasquini, J. M., Zakin, M. M., Baron, B., & Guillou, F. (2003). Myelination and motor coordination are increased in transferrin transgenic mice. *Journal of Neuroscience Research*, *72*(5), 587-594. https://doi.org/10.1002/jnr.10619

Satoh, T., & Lipton, S. (2017). Recent advances in understanding NRF2 as a druggable target: development of pro-electrophilic and non-covalent NRF2 activators to overcome systemic side effects of electrophilic drugs like dimethyl fumarate. *F1000Res*, *6*, 2138. https://doi.org/10.12688/f1000research.12111.1

Scannevin, R. H., Chollate, S., Jung, M. Y., Shackett, M., Patel, H., Bista, P., Zeng, W., Ryan, S., Yamamoto, M., Lukashev, M., & Rhodes, K. J. (2012). Fumarates promote cytoprotection of central nervous system cells against oxidative stress via the nuclear factor (erythroid-derived 2)-like 2 pathway. *Journal of Pharmacology and Experimental Therapeutics*, *341*(1), 274-284. https://doi.org/10.1124/jpet.111.190132

Schulz, K., Kroner, A., & David, S. (2012). Iron efflux from astrocytes plays a role in remyelination. *Journal of Neuroscience*, *32*(14), 4841-4847. https://doi.org/10.1523/JNEUROSCI.5328-11.2012

Schulze-Topphoff, U., Varrin-Doyer, M., Pekarek, K., Spencer, C. M., Shetty, A., Sagan, S. A., Cree, B. A., Sobel, R. A., Wipke, B. T., Steinman, L., Scannevin, R. H., & Zamvil, S. S. (2016). Dimethyl fumarate treatment induces adaptive and innate immune modulation independent of Nrf2. *Proceedings of the National Academy of Sciences of the United States of America*, *113*(17), 4777-4782. https://doi.org/10.1073/pnas.1603907113

Seiler, A., Schneider, M., Forster, H., Roth, S., Wirth, E. K., Culmsee, C., Plesnila, N., Kremmer, E., Radmark, O., Wurst, W., Bornkamm, G. W., Schweizer, U., & Conrad, M. (2008). Glutathione peroxidase 4 senses and translates oxidative stress into 12/15-lipoxygenase dependent- and AIF-mediated cell death. *Cell Metabolism*, *8*(3), 237-248. https://doi.org/10.1016/j.cmet.2008.07.005

Sendtner, M., Dittrich, F., Hughes, R. A., & Thoenen, H. (1994). Actions of CNTF and neurotrophins on degenerating motoneurons: preclinical studies and clinical implications. *Journal of the Neurological Sciences*, *124 Suppl*, 77-83. https://doi.org/10.1016/0022-510x(94)90187-2

Shah, R., Margison, K., & Pratt, D. A. (2017). The Potency of Diarylamine Radical-Trapping Antioxidants as Inhibitors of Ferroptosis Underscores the Role of Autoxidation in the Mechanism of Cell Death. *ACS Chemical Biology*, *12*(10), 2538-2545. https://doi.org/10.1021/acschembio.7b00730

Singer, B. A., Feng, J., & Chiong-Rivero, H. (2024). Early use of high-efficacy therapies in multiple sclerosis in the United States: benefits, barriers, and strategies for encouraging adoption. *Journal of Neurology*, *271*(6), 3116-3130. https://doi.org/10.1007/s00415-024-12305-4

Skrzypczak-Wiercioch, A., & Salat, K. (2022). Lipopolysaccharide-Induced Model of Neuroinflammation: Mechanisms of Action, Research Application and Future Directions for Its Use. *Molecules*, *27*(17). https://doi.org/10.3390/molecules27175481

Spelman, T., Magyari, M., Piehl, F., Svenningsson, A., Rasmussen, P. V., Kant, M., Sellebjerg, F., Joensen, H., Hillert, J., & Lycke, J. (2021). Treatment Escalation vs Immediate Initiation of Highly Effective Treatment for Patients With Relapsing-Remitting Multiple Sclerosis: Data From 2 Different National Strategies. *JAMA Neurol*, *78*(10), 1197-1204. https://doi.org/10.1001/jamaneurol.2021.2738

Stephenson, E., Nathoo, N., Mahjoub, Y., Dunn, J. F., & Yong, V. W. (2014). Iron in multiple sclerosis: roles in neurodegeneration and repair. *Nature Reviews: Neurology*, *10*(8), 459-468. https://doi.org/10.1038/nrneurol.2014.118

Stoppini, L., Buchs, P. A., & Muller, D. (1991). A simple method for organotypic cultures of nervous tissue. *Journal of Neuroscience Methods*, *37*(2), 173-182. https://doi.org/10.1016/0165-0270(91)90128-m

Tang, D., Chen, X., Kang, R., & Kroemer, G. (2021). Ferroptosis: molecular mechanisms and health implications. *Cell Research*, *31*(2), 107-125. https://doi.org/10.1038/s41422-020-00441-1

Thermo Fisher Invitrogen™. (2012). *BODIPY™ 581/591 C11: Product describtion, https://www.thermofisher.com/order/catalog/product/D3861*.

Thompson, A. J., Banwell, B. L., Barkhof, F., Carroll, W. M., Coetzee, T., Comi, G., Correale, J., Fazekas, F., Filippi, M., Freedman, M. S., Fujihara, K., Galetta, S. L., Hartung, H. P., Kappos, L., Lublin, F. D., Marrie, R. A., Miller, A. E., Miller, D. H., Montalban, X., . . . Cohen, J. A. (2018). Diagnosis of multiple sclerosis: 2017 revisions of the McDonald criteria. *Lancet Neurology*, *17*(2), 162-173. https://doi.org/10.1016/S1474-4422(17)30470-2

Tuo, Q. Z., Liu, Y., Xiang, Z., Yan, H. F., Zou, T., Shu, Y., Ding, X. L., Zou, J. J., Xu, S., Tang, F., Gong, Y. Q., Li, X. L., Guo, Y. J., Zheng, Z. Y., Deng, A. P., Yang, Z. Z., Li, W. J., Zhang, S. T., Ayton, S., . . . Lei, P. (2022). Thrombin induces ACSL4-dependent ferroptosis during cerebral ischemia/reperfusion. *Signal Transduct Target Ther*, *7*(1), 59. https://doi.org/10.1038/s41392-022-00917-z

Ufer, C., Wang, C. C., Fahling, M., Schiebel, H., Thiele, B. J., Billett, E. E., Kuhn, H., & Borchert, A. (2008). Translational regulation of glutathione peroxidase 4 expression through guanine-rich sequence-binding factor 1 is essential for embryonic brain development. *Genes and Development*, *22*(13), 1838-1850. https://doi.org/10.1101/gad.466308

van Horssen, J., Witte, M. E., Schreibelt, G., & de Vries, H. E. (2011). Radical changes in multiple sclerosis pathogenesis. *Biochimica et Biophysica Acta*, *1812*(2), 141-150. https://doi.org/10.1016/j.bbadis.2010.06.011

Van San, E., Debruyne, A. C., Veeckmans, G., Tyurina, Y. Y., Tyurin, V. A., Zheng, H., Choi, S. M., Augustyns, K., van Loo, G., Michalke, B., Venkataramani, V., Toyokuni, S., Bayir, H., Vandenabeele, P., Hassannia, B., & Vanden Berghe, T. (2023). Ferroptosis contributes to multiple sclerosis and its pharmacological targeting suppresses experimental disease progression. *Cell Death and Differentiation*, *30*(9), 2092-2103. https://doi.org/10.1038/s41418-023-01195-0

Volpe, E., Sambucci, M., Battistini, L., & Borsellino, G. (2016). Fas-Fas Ligand: Checkpoint of T Cell Functions in Multiple Sclerosis. *Frontiers in Immunology*, *7*, 382. https://doi.org/10.3389/fimmu.2016.00382

Waiczies, S., Weber, A., Lunemann, J. D., Aktas, O., Zschenderlein, R., & Zipp, F. (2002). Elevated Bcl-X(L) levels correlate with T cell survival in multiple sclerosis. *Journal of Neuroimmunology*, *126*(1-2), 213-220. https://doi.org/10.1016/s0165-5728(02)00067-x

Walton, C., King, R., Rechtman, L., Kaye, W., Leray, E., Marrie, R. A., Robertson, N., La Rocca, N., Uitdehaag, B., van der Mei, I., Wallin, M., Helme, A., Angood Napier, C., Rijke, N., & Baneke, P. (2020). Rising prevalence of multiple sclerosis worldwide: Insights from the Atlas of MS, third edition. *Multiple Sclerosis*, *26*(14), 1816-1821. https://doi.org/10.1177/1352458520970841

Wandinger, K. P., Lunemann, J. D., Wengert, O., Bellmann-Strobl, J., Aktas, O., Weber, A., Grundstrom, E., Ehrlich, S., Wernecke, K. D., Volk, H. D., & Zipp, F. (2003). TNF-related apoptosis inducing ligand (TRAIL) as a potential response marker for interferon-beta treatment in multiple sclerosis. *Lancet*, *361*(9374), 2036-2043. https://doi.org/10.1016/S0140-6736(03)13641-0

Wang, J., Cao, Y., Lu, Y., Zhu, H., Zhang, J., Che, J., Zhuang, R., & Shao, J. (2024). Recent progress and applications of small molecule inhibitors of Keap1-Nrf2 axis for neurodegenerative diseases. *European Journal of Medicinal Chemistry*, *264*, 115998. https://doi.org/10.1016/j.ejmech.2023.115998

Warnke, C., Leussink, V. I., Goebels, N., Aktas, O., Boyko, A., Kieseier, B. C., & Hartung, H. P. (2012). Cladribine as a therapeutic option in multiple sclerosis. *Clinical Immunology*, *142*(1), 68-75. https://doi.org/10.1016/j.clim.2011.05.009

White, A. R. (2023). Ferroptosis drives immune-mediated neurodegeneration in multiple sclerosis. *Cellular & Molecular Immunology*, *20*(1), 112-113. https://doi.org/10.1038/s41423-022-00941-7

Wicks, P., Rasouliyan, L., Katic, B., Nafees, B., Flood, E., & Sasane, R. (2016). The real-world patient experience of fingolimod and dimethyl fumarate for multiple sclerosis. *BMC Research Notes*, *9*(1), 434. https://doi.org/10.1186/s13104-016-2243-8

Wiendl, H., Gold, R., Berger, T., Derfuss, T., Linker, R., Maurer, M., Aktas, O., Baum, K., Berghoff, M., Bittner, S., Chan, A., Czaplinski, A., Deisenhammer, F., Di Pauli, F., Du Pasquier, R., Enzinger, C., Fertl, E., Gass, A., Gehring, K., . . . Multiple Sclerosis Therapy Consensus, G. (2021). Multiple Sclerosis Therapy Consensus Group (MSTCG): position statement on disease-modifying therapies for multiple sclerosis (white paper). *Therapeutic Advances in Neurological Disorders*, *14*, 17562864211039648. https://doi.org/10.1177/17562864211039648

Wu, W., Luo, Z., Shen, D., Lan, T., Xiao, Z., Liu, M., Hu, L., Sun, T., Wang, Y., Zhang, J. N., Zhang, C., Wang, P., Lu, Y., Yang, F., & Li, Q. (2024). IL-10 protects against OPC ferroptosis by regulating lipid reactive oxygen species levels post stroke. *Redox Biol*, *69*, 102982. https://doi.org/10.1016/j.redox.2023.102982

Yan, H. F., Zou, T., Tuo, Q. Z., Xu, S., Li, H., Belaidi, A. A., & Lei, P. (2021). Ferroptosis: mechanisms and links with diseases. *Signal Transduct Target Ther*, *6*(1), 49. https://doi.org/10.1038/s41392-020-00428-9

Yang, W. S., SriRamaratnam, R., Welsch, M. E., Shimada, K., Skouta, R., Viswanathan, V. S., Cheah, J. H., Clemons, P. A., Shamji, A. F., Clish, C. B., Brown, L. M., Girotti, A. W., Cornish, V. W., Schreiber, S. L., & Stockwell, B. R. (2014). Regulation of ferroptotic cancer cell death by GPX4. *Cell*, *156*(1-2), 317-331. https://doi.org/10.1016/j.cell.2013.12.010

Yang, W. S., & Stockwell, B. R. (2008). Synthetic lethal screening identifies compounds activating iron-dependent, nonapoptotic cell death in oncogenic-RAS-harboring cancer cells. *Chemistry and Biology*, *15*(3), 234-245. https://doi.org/10.1016/j.chembiol.2008.02.010

Yoo, S. E., Chen, L., Na, R., Liu, Y., Rios, C., Van Remmen, H., Richardson, A., & Ran, Q. (2012). Gpx4 ablation in adult mice results in a lethal phenotype accompanied by neuronal loss in brain. *Free Radical Biology and Medicine*, *52*(9), 1820-1827. https://doi.org/10.1016/j.freeradbiomed.2012.02.043

Zhang, X., Haaf, M., Todorich, B., Grosstephan, E., Schieremberg, H., Surguladze, N., & Connor, J. R. (2005). Cytokine toxicity to oligodendrocyte precursors is mediated by iron. *Glia*, *52*(3), 199-208. https://doi.org/10.1002/glia.20235

Zhang, X., Surguladze, N., Slagle-Webb, B., Cozzi, A., & Connor, J. R. (2006). Cellular iron status influences the functional relationship between microglia and oligodendrocytes. *Glia*, *54*(8), 795-804. https://doi.org/10.1002/glia.20416

Zhao, Y., Li, Y., Zhang, R., Wang, F., Wang, T., & Jiao, Y. (2020). The Role of Erastin in Ferroptosis and Its Prospects in Cancer Therapy. *OncoTargets and Therapy*, *13*, 5429-5441. https://doi.org/10.2147/OTT.S254995

Ziemssen, T., Bhan, V., Chataway, J., Chitnis, T., Campbell Cree, B. A., Havrdova, E. K., Kappos, L., Labauge, P., Miller, A., Nakahara, J., Oreja-Guevara, C., Palace, J., Singer, B., Trojano, M., Patil, A., Rauser, B., & Hach, T. (2023). Secondary Progressive Multiple Sclerosis: A Review of Clinical Characteristics, Definition, Prognostic Tools, and Disease-Modifying Therapies. *Neurol Neuroimmunol Neuroinflamm*, *10*(1). https://doi.org/10.1212/NXI.0000000000200064

Zilka, O., Shah, R., Li, B., Friedmann Angeli, J. P., Griesser, M., Conrad, M., & Pratt, D. A. (2017). On the Mechanism of Cytoprotection by Ferrostatin-1 and Liproxstatin-1 and the Role of Lipid Peroxidation in Ferroptotic Cell Death. *ACS Cent Sci*, *3*(3), 232-243. https://doi.org/10.1021/acscentsci.7b00028

Zuo, S., Yu, J., Pan, H., & Lu, L. (2020). Novel insights on targeting ferroptosis in cancer therapy. *Biomark Res*, *8*, 50. https://doi.org/10.1186/s40364-020-00229-w

7 Supplements

Figure 19 GPx4 Protein Expression in OLN-93 Cells

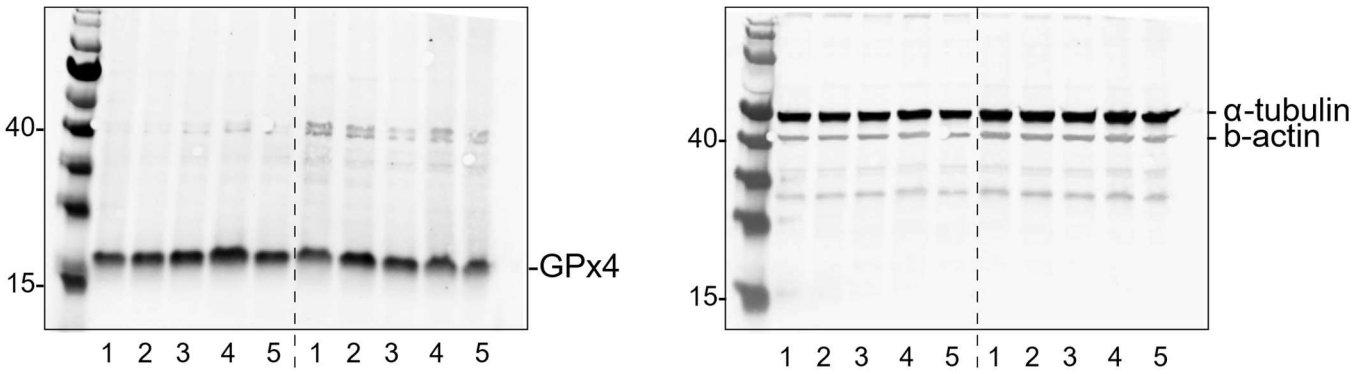

Fig. 19: The GPx4 bands on the left plot correspond to the β-actin bands on the right plot, respectively. It is the same blot, but images were acquired separately for each protein. Normally, GPx4 was normalized to β-actin, in this experiment it was normalized to α-tubulin due to a bubble in the bands of β-actin. 1: control, 2: 2µM DRF, 3: 10µM DRF, 4: 2µM MMF, 5: 10µM MMF. Molecular masses of proteins: GPx4: 22 kDa, α-tubulin: 52 kDa, β-actin: 42 kDa; DRF: Diroximel fumarate, GPx4: Glutathione Peroxidase 4, kDa: Kilodalton, MMF: Monomethyl fumarate.

Figure 20 GPx4 Protein Expression in White and Gray Matter of DMF-Treated Mice

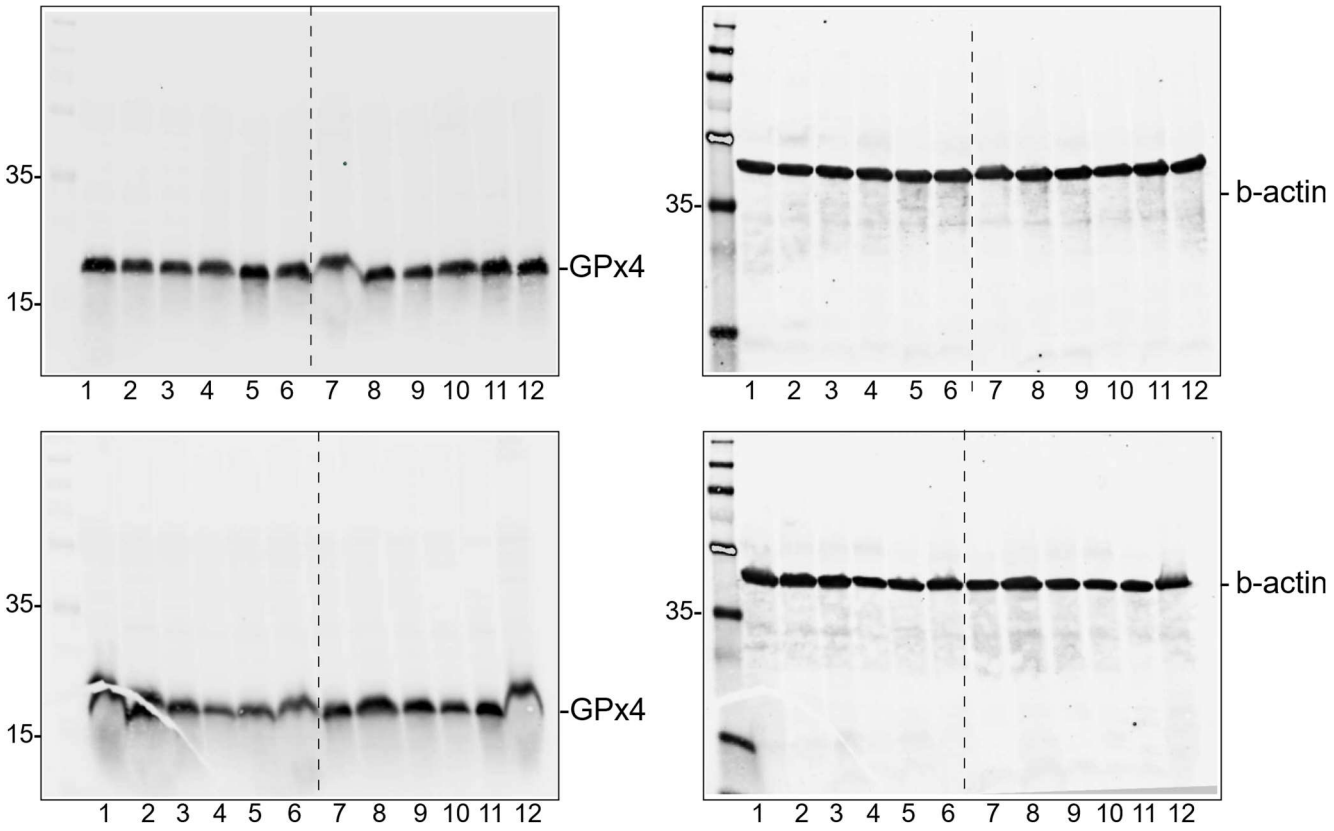

Fig. 20: The GPx4 bands on the left plot correspond to the β-actin bands on the right plot, respectively. It is the same blot in each case, but images were acquired separately for each protein. Mouse 1 to 6: control mice, mouse 7 to 12: mice treated with DMF. Molecular masses of proteins: GPx4: 22 kDa, β-actin: 42 kDa; DMF: Dimethyl fumarate, GPx4: Glutathione Peroxidase 4, kDa: Kilodalton.

Danksagung

Mein aufrichtiger Dank gilt zunächst meinem Doktorvater, Prof. Dr. Orhan Aktas, für die Überlassung des spannenden Themas dieser Arbeit. Seine stete Bereitschaft, bei Problemen zur Seite zu stehen und wertvolle Anregungen zu erteilen, hat maßgeblich zum Gelingen dieser Arbeit beigetragen. Besonders möchte ich auch meinem Betreuer, PD Dr. Carsten Berndt, für die vielen interessanten Ideen und unsere Diskussionen danken, die diese Arbeit bereichert haben. Herrn Dr. Tim Prozorovski und Frau Mary Bayer gebührt mein herzlicher Dank für ihre geduldige Hilfe bei den experimentellen Arbeiten und die Beantwortung unzähliger Fragen, die den Fortschritt meiner Forschung erheblich vorangetrieben haben. Dem gesamten Laborteam danke ich für die vielfältigen Hilfestellungen und die Bereitschaft, jederzeit meine Fragen zu beantworten. Eure Unterstützung war von unschätzbarem Wert.

Herrn Tim Lohoff möchte ich für seine geduldige mentale Unterstützung während des gesamten Promotionsprozesses danken. Deine Ermutigung und dein Verständnis haben mir Kraft gegeben, auch in schwierigen Phasen durchzuhalten. Nicht zuletzt gilt mein tiefer Dank meiner Familie und meinen Freunden für ihre unerschütterliche Unterstützung, ihre Geduld und ihren Zuspruch während meines gesamten Studiums und der Arbeit an dieser Dissertation.